Used Fuel Disposition Campaign

Baseline Studies for Ring Compression Testing of High-Burnup Fuel Cladding

Fuel Cycle Research & Development

Prepared for
U.S. Department of Energy
Used Fuel Disposition Campaign

M.C. Billone, T.A. Burtseva,
and Y.Y. Liu

Argonne National Laboratory
November 23, 2012
FCRD-USED-2013-000040
ANL-12/58

Reviewed by:

(accepted via email – signature on file)

Hanchung Tsai (Argonne National Laboratory)
Technical Reviewer

Submitted by:

2012.12.07 10:44:24 -06'00'

Yung Y. Liu (Argonne National Laboratory)

Work Package Manager for ST Storage and Transportation Experiments

This page intentionally blank.

SUMMARY

Structural analyses of high-burnup fuel require cladding mechanical properties and failure limits to assess fuel behavior during long-term dry cask storage and transportation. Pre-storage drying-transfer operations and early stage storage subject cladding to higher temperatures and much higher pressure-induced tensile hoop stresses relative to in-reactor operation and pool storage. Under these conditions, radial hydrides may precipitate during slow cooling and provide an additional embrittlement mechanism as the cladding temperature decreases below the ductile-to-brittle transition temperature (DBTT). On the basis of previous test results, susceptibility to radial-hydride precipitation depends on cladding material, microstructure, and pre-drying distribution of hydrides across the cladding wall, as well as peak hoop stresses and temperatures during drying operations and storage. Susceptibility to embrittlement depends on the extent of radial-hydride precipitation and the thickness of the outer-surface hydride rim.

Consistent with the Argonne Test Plan (December 31, 2011), baseline studies were conducted with as-irradiated cladding to determine hydrogen distribution and hydride morphology across the cladding wall; strain-rate sensitivity; and temperature sensitivity of high-burnup M5®, ZIRLO™, and Zircaloy-4 (Zry-4) cladding subjected to ring compression test (RCT) loading. The results also serve as the baseline for high-burnup cladding exposed to drying-storage conditions that do not lead to radial-hydride precipitation.

Baseline mechanical properties and failure limits for irradiated M5® and ZIRLO™ are particularly important because they are not publicly available. Cladding samples used for baseline studies were from sibling high-burnup rods irradiated to high-burnup in the same assembly as cladding samples used to study radial-hydride-induced embrittlement. RCT displacement rates were 0.05–50 mm/s (1000-fold increase in elastic strain rate). High-burnup M5® with <100-wppm hydrogen exhibited high strength (based on maximum load) and high ductility (>10%, based on offset strain) with relatively low strain-rate and temperature (20–90°C) sensitivity. High-burnup ZIRLO™ samples had 530-wppm hydrogen, a well-developed hydride rim, and only 140-wppm hydrogen within the inner two-thirds of the cladding wall. This ZIRLO™ also exhibited low strain-rate and temperature sensitivity. Cracking initiated in the hydride rim. Room-temperature (RT) offset strains were 7±1% for the three displacement rates. Offset strains increased from 7% to >10% with the 20–150°C increase in RCT temperature. High-burnup Zry-4 samples had 640-wppm hydrogen, a well-developed hydride rim, and 250-wppm hydrogen within the inner two-thirds of the cladding wall. Based on maximum load, the material appeared to have low strain-rate sensitivity. However, offset strains were too low (<2%) to assess strain-rate and temperature (20–90°C) effects on ductility. Cracking within the outer half of the cladding wall occurred concurrently with plastic deformation within the inner half of the cladding wall.

The strength and ductility of as-irradiated M5®, ZIRLO™, and Zry-4 samples were compared to values obtained previously for the same materials exposed to simulated peak drying-storage hoop stresses of 140 MPa and 110 MPa at 400°C and subjected to RCTs. For radial-hydride-treated (RHT) M5®, the DBTT was about 75°C for the two RHT stress levels. At 60°C RCT temperature, failure of RHT (140 MPa) M5® occurred in the elastic deformation regime at 50% of the strength for as-irradiated M5® tested at RT. The ductility decreased from >10% to 0% following RHT. Similar results were obtained for high-burnup ZIRLO™ for which the DBTT is ≈185°C following RHT at 140 MPa and 400°C. At 150°C, failure of RHT (140 MPa) ZIRLO™ occurred at 40% of the strength for as-irradiated ZIRLO™ tested at RT. The ductility decreased from 7% to 0%.

These results highlight the importance of determining the DBTT for high-burnup cladding as a function of peak drying-storage temperatures and stresses and including the relevant mechanical properties in cask structural analyses. Additional testing is needed at lower (and perhaps more realistic) peak drying-storage temperatures and stresses, for which the DBTT is expected to decrease.

This page intentionally blank.

CONTENTS

FIGURES

FIGURES (Cont.)

FIGURES (Cont.)

FIGURES (Cont.)

FIGURES (Cont.)

TABLES

This page intentionally blank.

1. INTRODUCTION

Structural analyses of high-burnup fuel rods require cladding mechanical properties and failure limits to assess fuel behavior during long-term dry-cask storage, post-storage retrieval and transportation, and post-transport retrieval. License applications for high-burnup transport casks use properties and failure limits for as-irradiated cladding [see Ref. 1 for Zircaloy-4 (Zry-4)]. The Zry-4 properties and limits in Ref. 1 were based primarily on axial tensile tests. Isotropic correlations were developed for stress vs. strain and failure limits. Pre-storage drying-transfer operations and early stage storage subject cladding to higher temperatures and higher pressure-induced tensile hoop stresses relative to in-reactor operation and pool storage. Under these conditions, radial hydrides may precipitate during slow cooling and provide an additional embrittlement mechanism as the cladding temperature decreases below the ductile-to-brittle transition temperature (DBTT).

In Interim Staff Guidance – 11, Revision 3 (ISG-11 Rev. 3), the Nuclear Regulatory Commission (NRC) recommends a peak cladding temperature limit of 400°C for drying-transfer operations, storage, and transport in casks containing high-burnup fuel [2]. Limits are also placed on the number of drying cycles and the temperature drop per cycle. One concern for high-burnup cladding is the possible precipitation of radial hydrides, which could embrittle cladding in response to tensile hoop stresses caused by internal pressure loading and "pinch-type" loading during transport. Limits established in ISG-11 Rev. 3 relied on data available before 2002, which were primarily for low-burnup and non-irradiated/pre-hydrided Zircaloy-4. At the time ISG-11 Rev. 3 was issued (2003), NRC recognized that data for high-burnup cladding alloys were needed to determine the extent of radial-hydride embrittlement under conditions relevant to drying-transfer operations and storage. Data generated since 2002, mostly at Argonne, indicate that limits imposed by ISG-11 Rev. 3 do not protect high-burnup cladding from embrittlement due to radial hydrides. Recent NRC reviews of applications for license renewal of the Prairie Island ISFSI and Amendment 5 of the CoC for Transnuclear MP-197 have raised concerns for the long-term storage and transportation of high-burnup fuel. The issues are summarized in "Compatibility of Requirements for Storage and Transportation of Spent Nuclear Fuel (Retrievability, Cladding Integrity, and Safe Handling)," a summary paper presented at the NRC Public Meeting to obtain stakeholder feedback on enhancements to the licensing and inspection programs for spent fuel storage and transportation under 10 CFR Parts 71 and 72 [3]. A major concern is whether or not high-burnup fuel will maintain cladding integrity and be readily retrievable after more than 20 years of storage. License approvals for the transport of high-burnup fuel have been delayed because of a lack of data for high-burnup fuel cladding after more than 20 years of storage, which corresponds to peak cladding temperatures of ≈200°C or less.

Argonne has developed a test protocol for studying high-burnup cladding embrittlement that has been approved by NRC. Experimentally, the protocol involves two steps: (1) radial-hydride treatment (RHT), during which high-burnup cladding is exposed to simulated drying-storage temperature and hoop stress conditions, including slow cooling with decreasing stress, followed by (2) ring compression testing, in which rings sectioned from RHT high-burnup cladding are compressed to determine strength and ductility as a function of test temperature. The ring compression test (RCT) is used as a ductility screening test, and the RCT loading simulates pinch-type loading on high-burnup cladding that occurs during normal cask transport and drop accidents. The protocol was used to generate DBTT data for high-burnup ZIRLO™ [4,5,6] and Zry-4 [5,6] (both NRC sponsored) and high-burnup M5® (DOE sponsored) [7]. Under DOE-sponsored research, Argonne has also generated baseline properties for the strength and ductility of as-irradiated Zry-4, ZIRLO™, and M5® that are important not only for determining the degrading effects of drying and early stage storage, but also for serving as reference properties for future evaluations of the effects of drying-storage studies on these cladding alloys.

Characteristics of high-burnup fuel cladding, experimental methods for exposing cladding to simulated drying-storage conditions (referred to as RHT), and RCT conduct and data interpretation are well described in Ref. 7, as well as Refs. 4–6. Reference 5 contains the full dataset generated for NRC.

In addition to the Argonne datasets for PWR cladding alloys, Aomi et al. [8] have generated data for Zry-2 and Zry-4 by using test methods similar to the ones used by Argonne. However, RHT samples were cooled under constant stress (vs. decreasing stress, as used by Argonne), and RCTs were conducted only at room temperature (RT) and a slow displacement rate (0.033 vs. 5 mm/s at Argonne). Their results are very interesting and relevant in evaluating the effects of hydrogen content and thermo-mechanical treatment (TMT) on the susceptibility of cladding alloys to radial-hydride formation. Table 1 summarizes the cladding alloys tested, their fuel burnups and hydrogen contents, and simulated drying-storage conditions for tests conducted by Argonne and Aomi et al. Test results indicate that susceptibility to radial-hydride precipitation during cooling is dependent on cladding alloy, TMT, total hydrogen content, hydrogen content below the hydride rim, and peak RHT temperature and hoop stress. The combination of recrystallized-annealed (RXA) microstructure and low hydrogen content (above the inner liner for Zry-2) makes M5® and Zry-2 highly susceptible to precipitation of long radial hydrides during cooling. For cold-worked, stress-relieved annealed (CWSRA) alloys, ZIRLO™ was found to be more susceptible to radial-hydride precipitation than Zry-4. It has been speculated that differences in distribution of hydrides across the cladding wall (lower for ZIRLO™ below the hydride rim) may be responsible for this behavior [6].

Table 1. Summary of cladding materials and simulated drying-storage (RHT) conditions for radial-hydride precipitation and ring-compression ductility studies.

Cladding Alloy	TMT	Burnup, GWd/MTU	Hydrogen Content, wppm	Peak RHT T, °C	Peak RHT Stress, MPa	References
M5®	RXA	63	94±4	400	140	7
		68	72±10	400	110	7
ZIRLO™	CWSRA	70	650±190	400	140	4-6
		70	425±63	400	110	4-6
		70	350±80	400	110	5-6
Zry-4	CWSRA	67	615±82	400	140	5-6
		67	520±90	400	110	5-6
Zry-4	CWSRA	40–55	Not Reported	250–340	85–130	8
Zry-2	RXA	30–59	Not Reported	250–400	16–100	8

In the current work, baseline-studies results are reported for as-irradiated cladding samples. These samples were from fuel rods irradiated in the same assemblies as rods used to fabricate cladding samples for the Argonne RHT studies. Characterization for ZIRLO™ and Zry-4 included measurement of the total hydrogen content and the hydrogen content within the inner two-thirds of the cladding wall to enhance our understanding of the higher susceptibility of high-burnup ZIRLO™ to radial-hydride precipitation. For RCTs, the displacement rate was varied over a factor of 1000 (0.05 to 50 mm/s) at RT to study the strain-rate sensitivity of high-burnup cladding alloys. The metrics used to determine strain-rate effects were maximum RCT load (measure of strength) and offset strain (measure of ductility). At the reference displacement rate (5 mm/s), RCTs were conducted at 20–150°C to determine the effects of test temperature on maximum load and offset strain. RCT results for as-irradiated cladding were compared to those for RHT cladding to determine degradation in strength and ductility due to radial hydrides. The baseline results are very useful for establishing stress-strain properties and failure limits for materials-modeling and structural-analyses codes.

2. CLADDING CHARACTERIZATION

2.1 As-Irradiated High-Burnup M5®

M5® segment 652E6 was selected for baseline studies from a fuel rod irradiated to about 70 GWd/MTU in the same assembly as the fuel rod used to fabricate the 651E5 cladding rodlet for the RHT study [7]. It was also from the same axial elevation as the 651E5 sample. Figure 1 shows the 652E6 sectioning diagram used to identify samples for metallographic examination (G), hydrogen analysis (F and H), and RCTs (B–E and J–L). The corrosion layer thickness (h_{ox}) was 8±1 μm and the hydrogen content (C_H) was 76±5 wppm. These values are typical for high-burnup M5® and are essentially the same as the values measured for 651E5 (8±1 μm and 72±10 wppm). Also, both cladding segments were exposed to the same fast-fluence level. Other measurements important to the assessment of RCT data are the cladding metal outer diameter (D_{mo}) and the metal wall thickness (h_m): 9.51 mm and 0.56 mm, respectively.

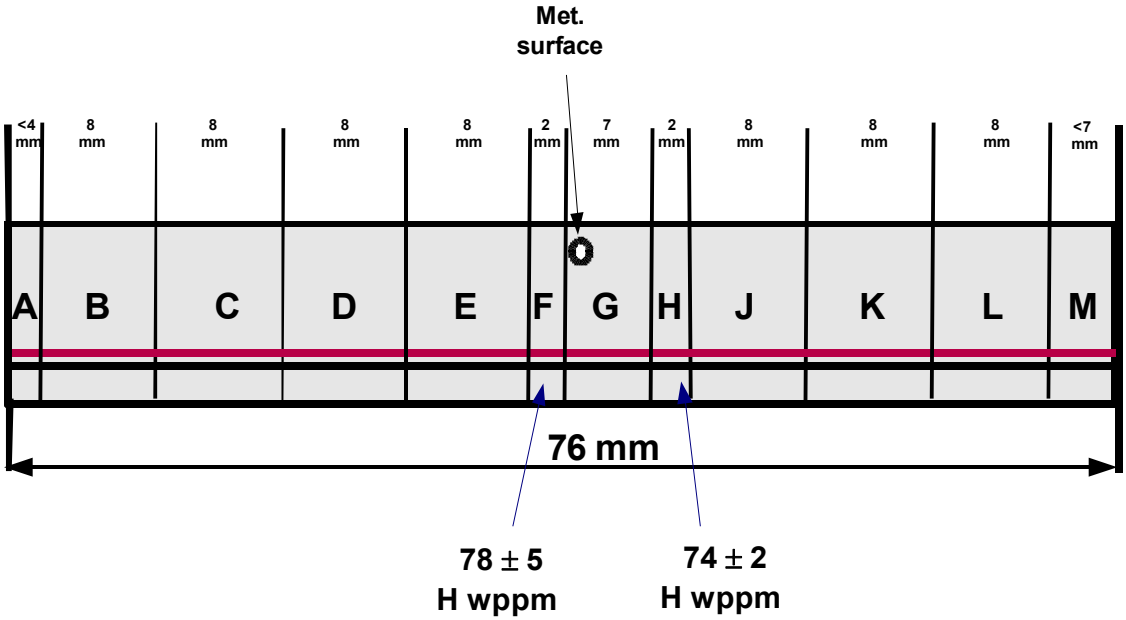

Figure 1. Sectioning diagram for as-irradiated M5® segment 652E6 used for baseline studies.

Figure 2 shows the hydride orientation and distribution for the cross section of ring G indicated in Fig. 1. As expected for an RXA microstructure and the low C_H of irradiated M5®, both circumferential (predominant) and radial hydrides were observed. However, given the low C_H, the relatively short length of radial hydrides, and the location of these hydrides, the strength and ductility of irradiated M5® are not anticipated to be degraded as a result of the presence of these radial hydrides.

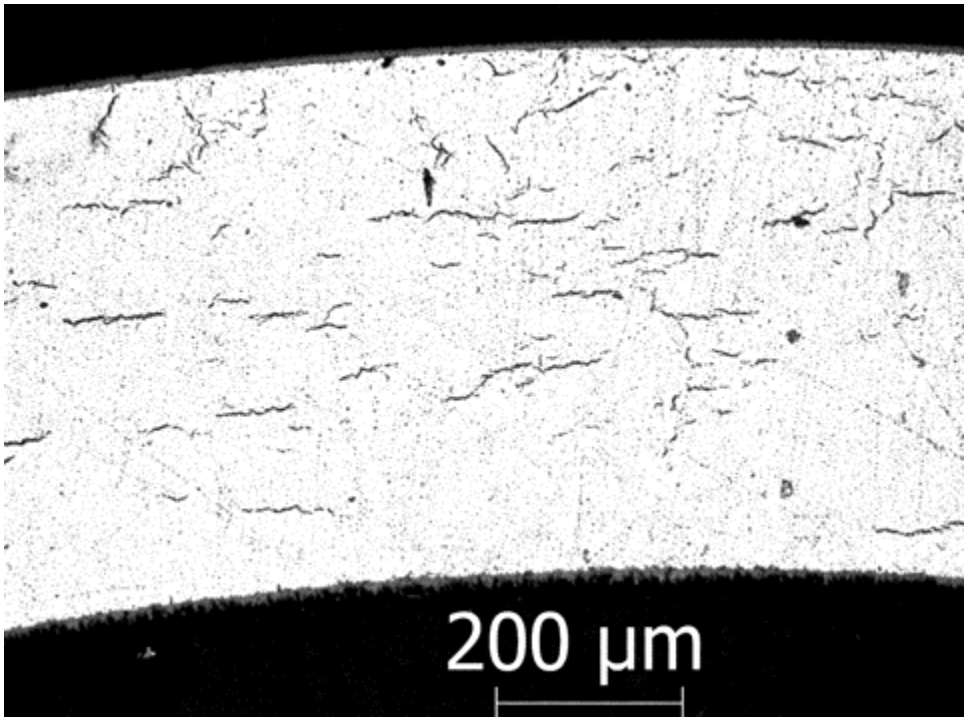

(a)

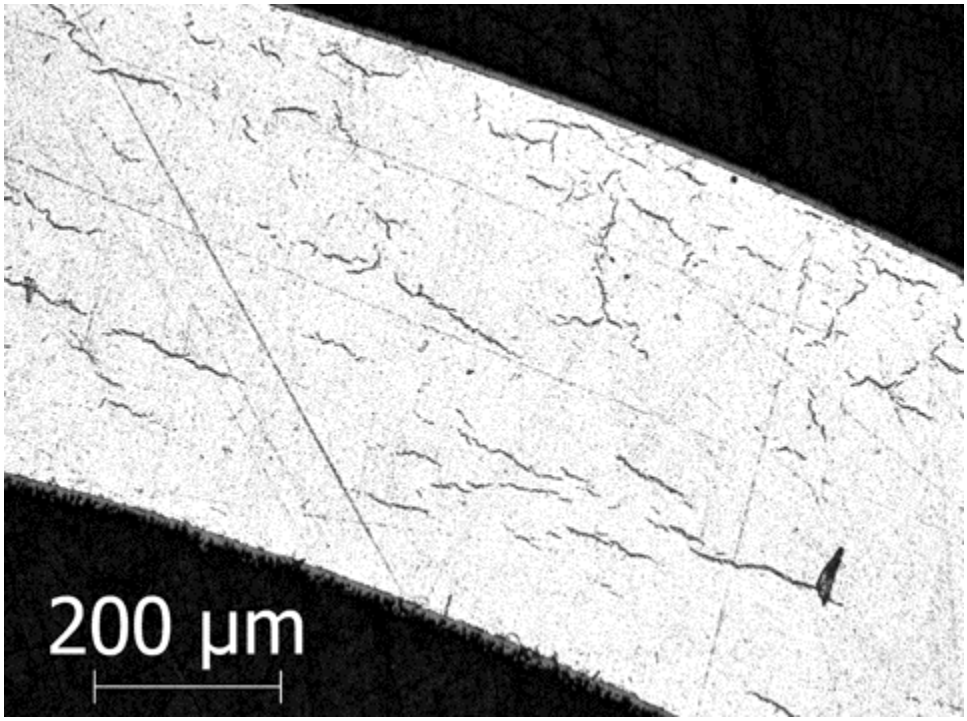

(b)

Figure 2. Hydride orientation and distribution for as-irradiated M5® ring 652E6G: (a) 12 o'clock position and (b) 1 o'clock position. C_H was 78±5 wppm for adjacent ring F.

2.2 As-Irradiated High-Burnup ZIRLO™

The high-burnup ZIRLO™ segment (105A) selected for baseline studies was from a fuel rod that was a sibling to the fuel rod from which cladding was sectioned for RHT studies [4–6]. On the basis of previous observations of the hydrides in high-burnup ZIRLO™ with 300–600 wppm hydrogen [4,9,10], the primary difference in hydride distribution is in the thickness of the outer-surface hydride rim. Hydrides below the rim, particularly within the inner two thirds of the cladding wall, were sparsely distributed circumferential hydrides, and the C_H values within this region appeared to be low. The susceptibility to radial-hydride precipitation increases with decreasing C_H below the hydride rim (high susceptibility at <200 wppm for 400°C peak drying temperature). An important part of the baseline studies was to measure the hydrogen content below the hydride rim. Figure 3 shows the sectioning diagram for ZIRLO™ segment 105A.

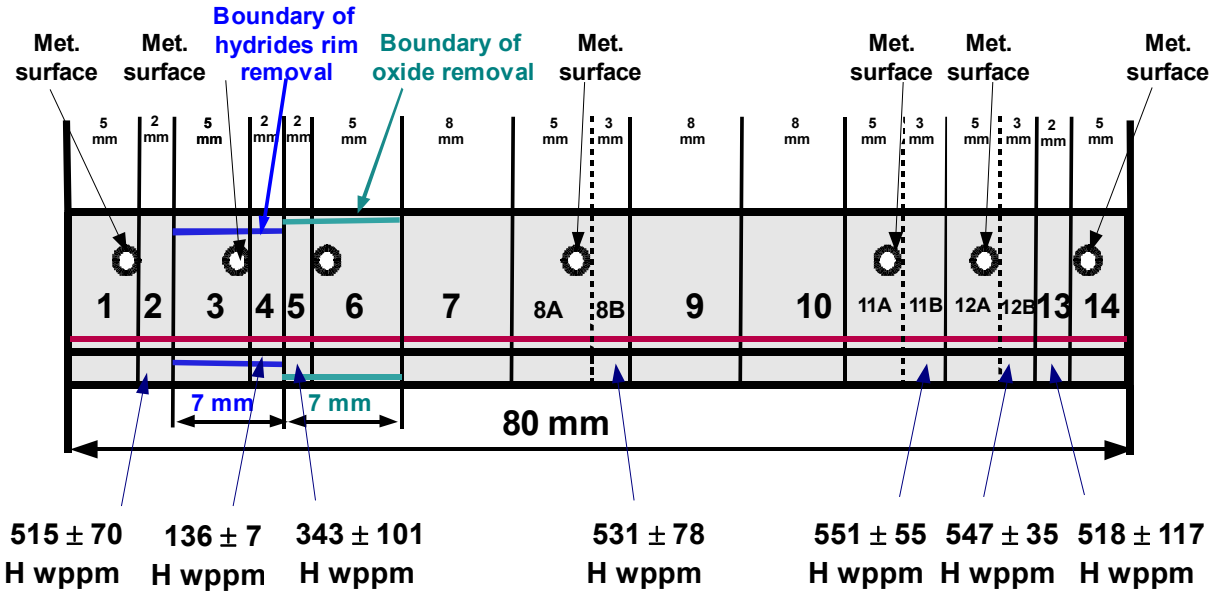

Figure 3. Sectioning diagram for as-irradiated ZIRLO™ segment 105A used for baseline studies.

Metallographic examinations were performed for rings 1 and 14 to determine h_{ox}, h_m, and hydride morphology. Adjacent rings 2 and 13 were used for measurement of C_H for corroded cladding. Rings 7–12 were subjected to RCTs. Post-RCT metallographic analysis and C_H measurements were performed for rings 8, 11, and 12, as indicated in Fig. 3. For as-irradiated cladding, C_H was 530±70 wppm (based on five rings), h_{ox} was 47±11 μm, D_{mo} was 9.44 mm, and h_m was 0.54 mm.

After sectioning rings 1 and 2, h_{ox} was removed by mechanical means from the segment labeled rings 3–6 in Fig. 3. Figure 4 shows a photograph of the segment after h_{ox} removal (region 5–6) and after oxide-rim-metal removal (region 3–4). The purpose of removing h_{ox}, which adds mass and some hydrogen to the cladding, was to obtain a more accurate measure of C_H in the cladding metal. However, as the cladding has both ovality and variation in h_{ox}, it is difficult to remove the oxide layer without removing some of the hydride rim at the oxide/rim boundary. The decrease in C_H from 515 wppm (ring 2) to 343 wppm (ring 5) was apparently due to partial removal of the hydride rim. This result is important for mechanical-property samples with gauge sections cut by electro-discharge machining (EDM wire cutter). As EDM requires electrical conductivity, h_{ox} must be removed prior to cutting. During this removal, some hydrogen will be lost from the rim region. Thus, it is important to measure and report the posttest C_H for the gauge sections for use in mechanical-property models and correlations.

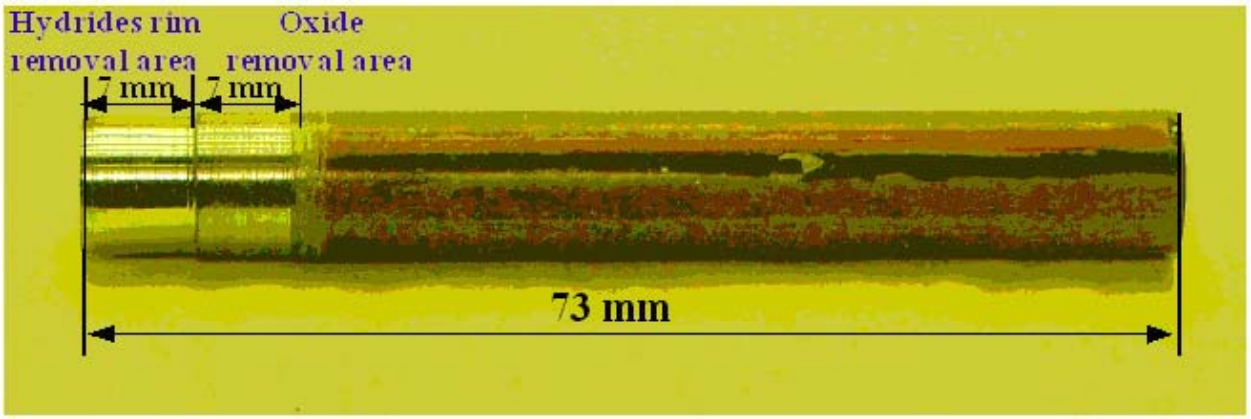

Figure 4. As-irradiated ZIRLO™ segment 105A after oxide and hydride-rim/metal removal in short regions on the left side of the photograph. The black line along the corroded section was inscribed on the segment to maintain orientation.

After removal of h_{ox}, about one-third (36%) of the cladding metal was removed by mechanical means from the region spanned by rings 3–4. The low C_H value (136±7 wppm ≈ 140 wppm) measured for ring 4 was consistent with the low density of hydrides observed in metallographic images of the ring 3 cross section. These results are significant for two reasons:

Circumferential hydrides within the inner two-thirds of the cladding would all go into solution during drying-storage at peak temperatures >360°C, and the dissolved hydrogen would be available for precipitation as long radial hydrides during cooling under stress, and

For hydride reorientation studies using non-irradiated, pre-hydrided cladding, it is very important to simulate the distribution of hydrides across the wall for high-burnup cladding (i.e., hydride rim with low concentration of hydrogen from the inner-rim surface to the cladding inner surface).

Figure 5 shows metallographic images at two circumferential locations for ring 1: (a) 12 o'clock position with circumferential hydrides and (b) 7 o'clock position with a few radial hydrides among the predominantly circumferential hydrides. With regard to the observed radial hydride in Fig. 5b, it is not expected to result in crack initiation, which would occur at the more highly stressed and brittle outer surface of the hydride rim during RCT loading. However, it could participate in crack propagation from the rim to the thin circumferential hydride below the rim. Even with the presence of a few radial hydrides, the material should behave in a ductile manner, especially within the inner two-thirds of the cladding wall.

Figure 6 shows the hydride distribution and orientation for ring 6 with h_{ox} removed and ring 3 with h_{ox} and 36% of the cladding metal removed. A pronounced radial hydride is observed in Fig. 6a within the inner-third of the cladding wall. It is unlikely that a few isolated radial hydrides within the inner-third of the cladding wall would contribute to crack initiation or propagation, especially if they do not extend to the cladding inner surface.

Isolated radial hydrides may have precipitated in high-burnup ZIRLO™ during reactor cooldown as a result of residual stresses from pellet-cladding mechanical interaction. However, radial hydrides of this length have not been observed in high-burnup Zry-4 cladding, which has been examined at multiple elevations of seven different rods irradiated in the same assembly. It is not clear if the presence and length of such radial hydrides in high-burnup ZIRLO™ is due to differences in cladding material or operating conditions relative to high-burnup Zry-4.

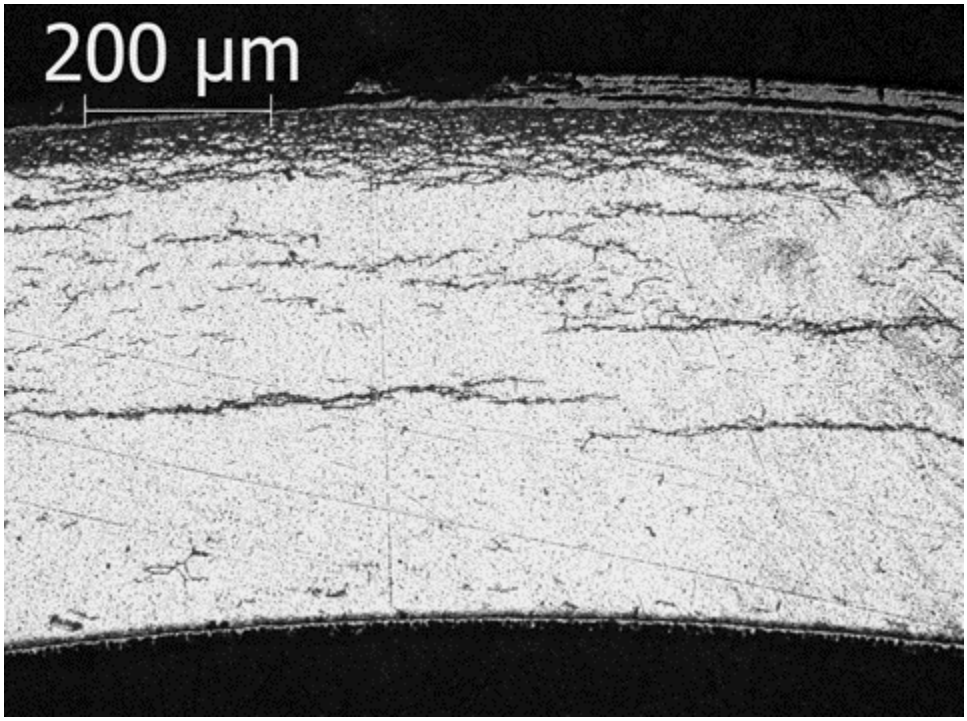

(a)

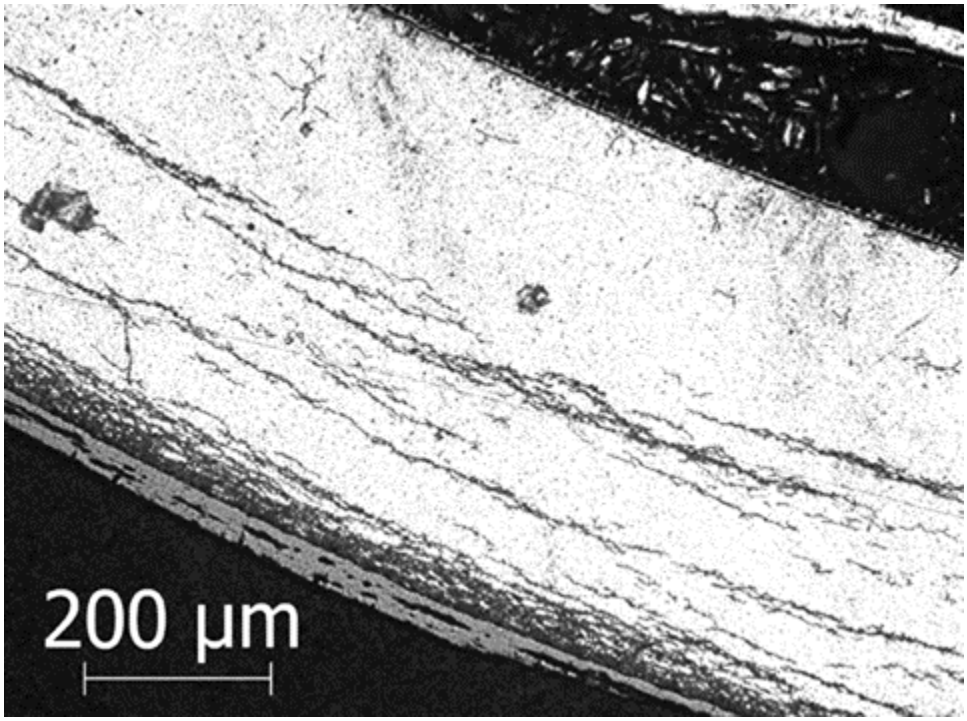

(b)

Figure 5. Hydride orientation and distribution for as-irradiated ZIRLO™ ring 105A1: (a) 12 o'clock position with circumferential hydrides and (b) 7 o'clock position with a few radial hydrides among the predominantly circumferential hydrides. C_H was 515±70 wppm for adjacent ring 2.

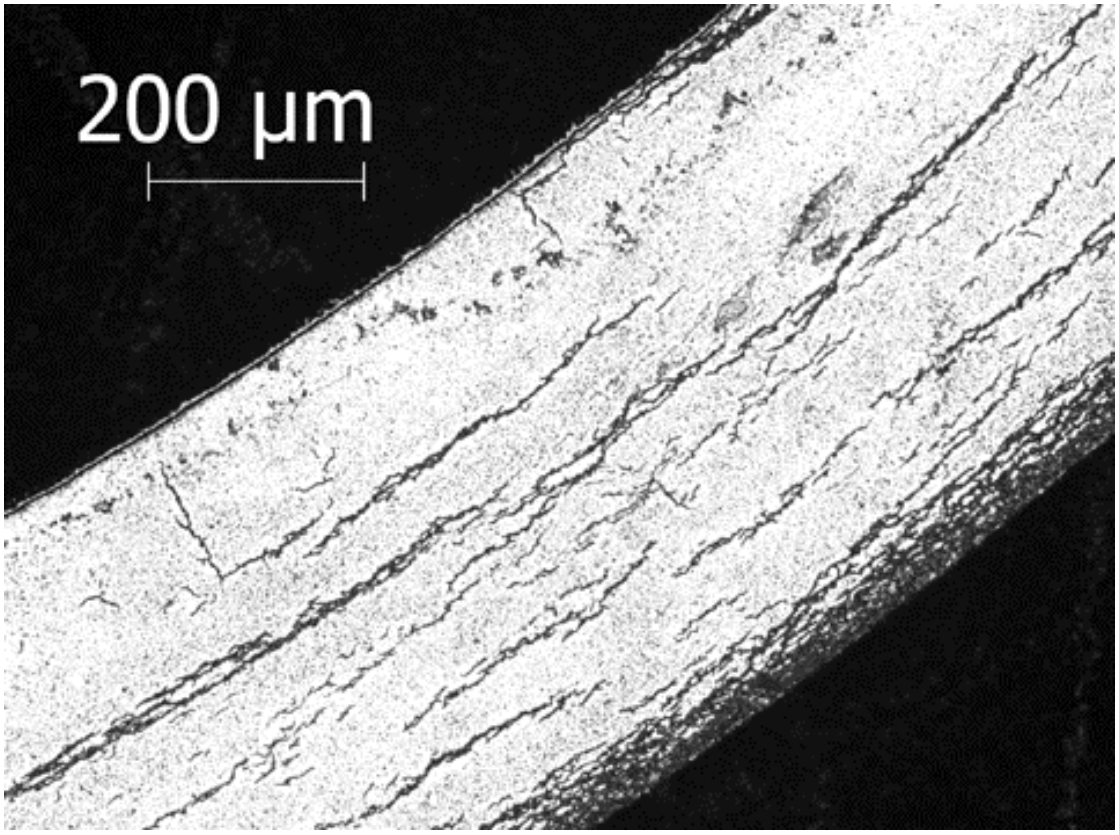

(a)

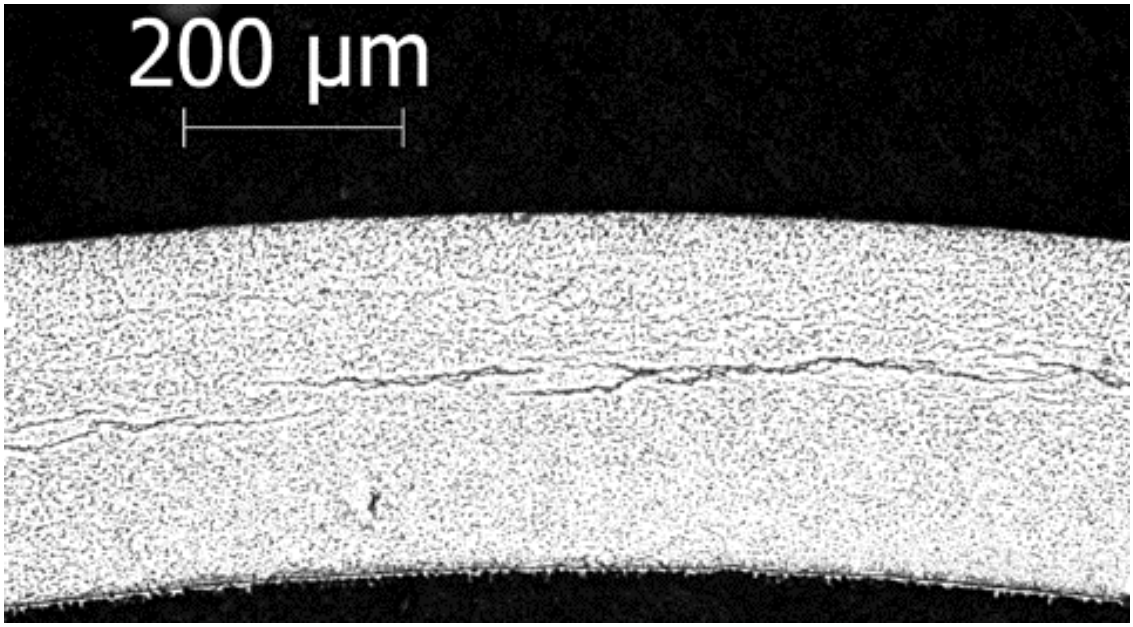

(b)

Figure 6. Hydride orientation and distribution for as-irradiated ZIRLO™: (a) sector of ring 105A6 after removal of h_{ox} and (b) sector of ring 105A3 after removal of h_{ox} and 36% of cladding metal (including the hydride rim).

2.3 As-Irradiated High-Burnup Zry-4

Baseline studies were conducted by using a Zry-4 segment (606C2) from a high-burnup rod irradiated in the same assembly as the rod used to fabricate the segment (605C2) for RHT studies at 400°C and 140-MPa peak hoop stress. The axial elevations of segments 606C2 and 605C2 were the same. Characterization of high-burnup Zry-4 paralleled ZIRLO™ characterization, as both materials had high C_H and pronounced hydride rims. Figure 7 shows the sectioning diagram for high-burnup Zry-4 baseline studies.

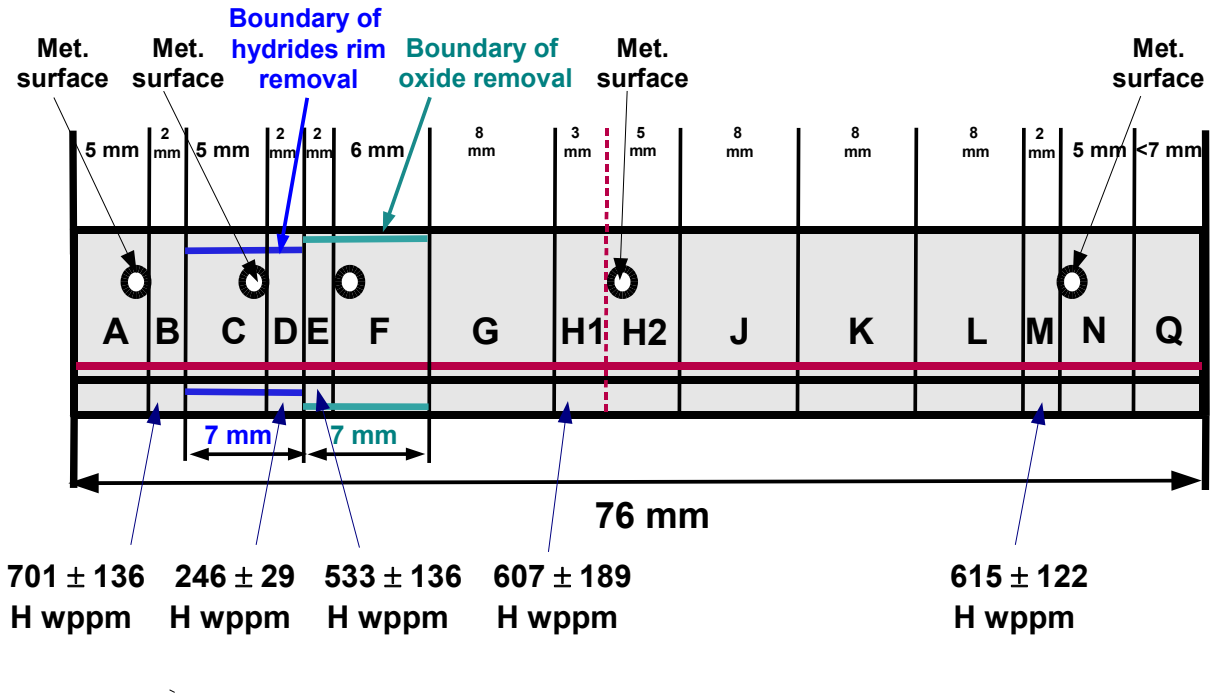

Figure 7. Sectioning diagram for as-irradiated Zry-4 segment 606C2 used for baseline studies.

Rings A and N were used for pre-RCT metallographic examination, and ring H2 was used for post-RCT metallography to image crack patterns and depths. The region spanning rings C–F was used for metallographic examination and hydrogen determination after (a) removal of the oxide layer and (b) removal of the oxide layer and 34% of the cladding wall. Data for corroded rings A and N were used to determine h_{ox} (95±5 µm), D_{mo} (10.56 mm), and h_m (0.69 mm). On the basis of data for rings B, H1, and M (0.9 g total mass), C_H was 640±140 wppm for the corroded cladding.

Figure 8 shows local regions (180° apart) from the cross section of ring A with relatively (a) high C_H and (b) low C_H. For adjacent ring B, C_H was 701±136 wppm (see Fig. 7) on the basis of quarter-ring measurements of 589, 818, 778, and 543 wppm. It is reasonable to assume that the local C_H shown in Fig. 8a is >820 wppm, while the local C_H shown in Fig. 8b is <540 wppm. Compared to high-burnup ZIRLO™, the high-burnup Zry-4 hydride rim was more diffuse, and the decrease in hydride density across the wall was more gradual.

Figure 9 shows local regions of rings F (h_{ox} removed) and C (h_{ox} -metal removed). For the region of ring F in Fig. 9a, a thin oxide layer can be observed on the outer side of about half the arc length. As a result of partial removal of the hydride rim, C_H was 533±136 wppm for adjacent E. For the region of ring C shown in Fig. 9b, C_H was 246±29 wppm (about 250 wppm) for adjacent ring D. At 400°C, about 50 wppm of hydrogen would be present as circumferential hydrides, which would make the cladding less susceptible to the precipitation of long radial-hydrides during cooling under stress.

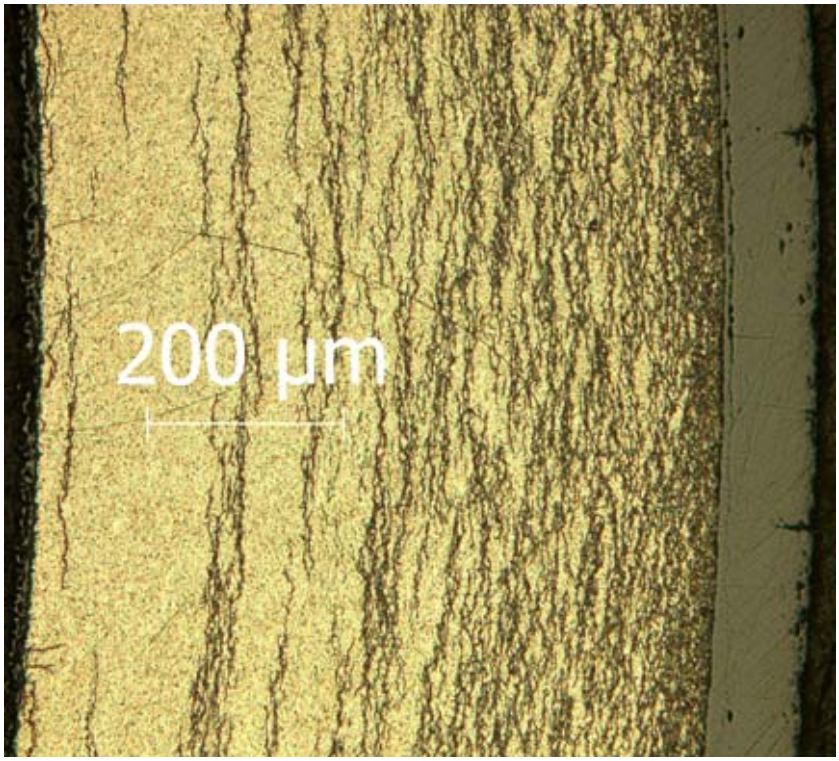

(a)

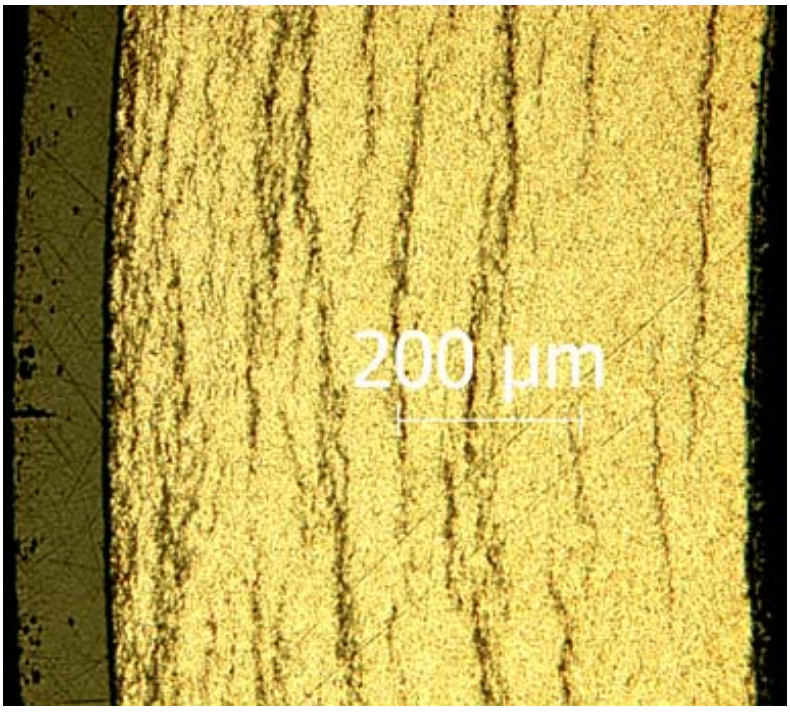

(b)

Figure 8. Hydride orientation and distribution for as-irradiated Zry-4 ring 606C2A at locations with relatively (a) high C_H and (b) low C_H. C_H was 701±136 wppm (543 to 818 wppm) for adjacent ring B.

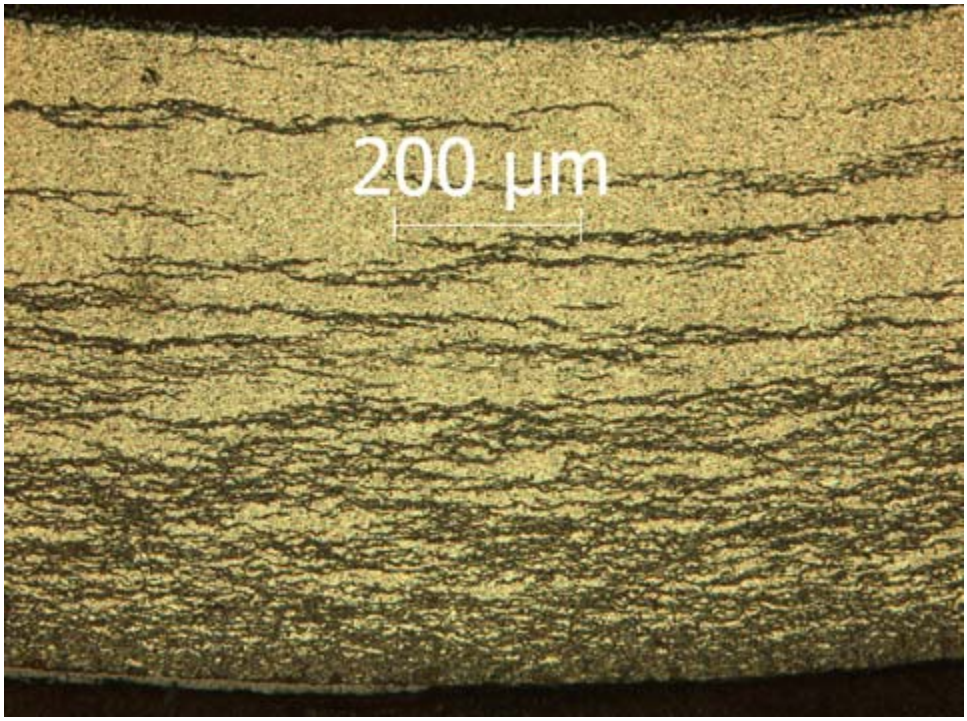

(a)

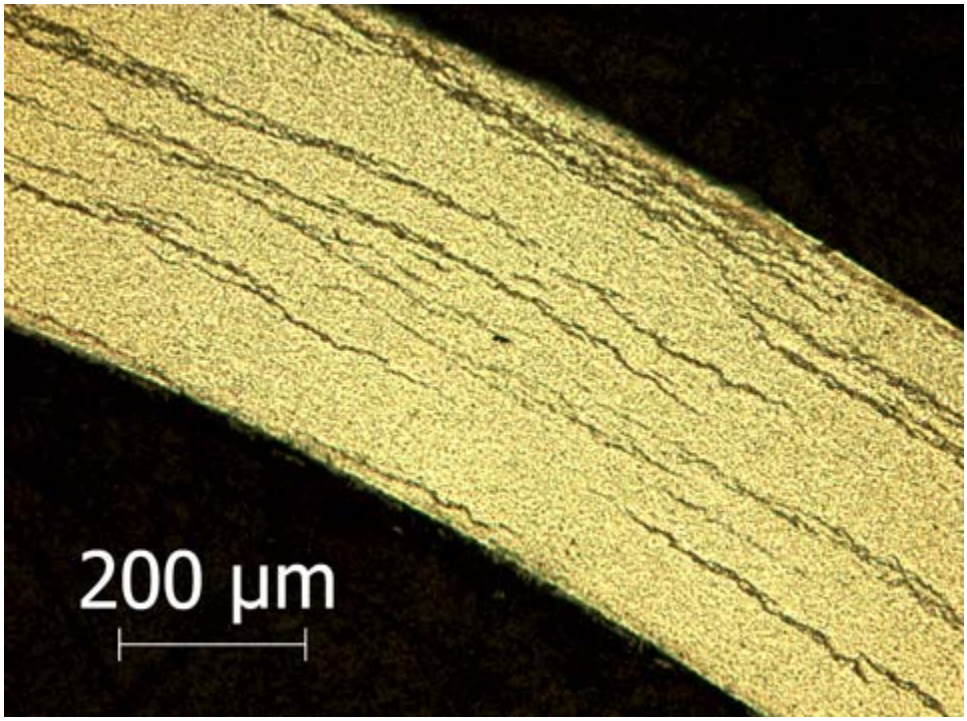

(b)

Figure 9. Hydride orientation and distribution for as-irradiated Zry-4 rings: (a) 606C2F following h_{ox} removal and (b) 606C2C following h_{ox}-rim-metal removal. For adjacent rings, corresponding C_H values were 533±136 wppm and 246±29 wppm, respectively.

2.4 Summary of As-Irradiated Cladding Characterization Results

Table 2 summarizes the characterization results for the as-irradiated, high-burnup cladding used in the baseline studies.

Table 2. Characterization results for high-burnup cladding segments used in baseline studies. D_o is the average outer diameter of the corroded cladding.

Parameter	17×17 M5®	17×17 ZIRLO™	15×15 Zry-4
Burnup, GWd/MTU	72	68	67
ANL Segment ID	652E6	105A	606C2
D_o, mm	9.53	9.53	10.75
h_{ox}, μm	8±1	47±11	95±5
D_{mo}, mm	9.51	9.44	10.56
h_m, mm	0.55	0.54	0.69
Corroded Cladding C_H, wppm	76±5	530±70	640±140
Inner Two-Thirds of Cladding C_H, wppm	≈76	136±7	246±29

3. RCT RESULTS

The experimental procedure for conducting RCTs and the methodology used to extract ductility data from load-displacement curves are described in Refs. 4–7. Additional details have been provided by Billone [11]. In previous experimental work with RHT cladding, RCT parameters were fixed at a crosshead displacement (δ) rate of 5 mm/s and a total displacement of 1.7 mm. The nominal length of RCT samples was 8 mm. Actual lengths were in the range of 7.0–8.6 mm. The load cell measured load (P) and the output formed the basis for the load-displacement curve (P vs. δ). Tests were conducted by using 3–4 rings sectioned from each cladding segment at temperatures ranging from 20 to 200°C to determine ductility vs. temperature curves and the DBTT as a function of peak RHT hoop stress.

In the current work, RCTs were conducted with rings from as-irradiated cladding to determine maximum strength (P_{max}) and ductility (d_p/D_{mo} or δ_p/D_{mo}) as a function of displacement rate and test temperature. Pre- and posttest micrometer measurements of the cladding outer diameter were used to determine the permanent displacement (d_p). Load-displacement curves were used to determine the offset displacement (δ_p). These displacements were normalized to the cladding metal outer diameter to determine offset and permanent "strains." By doing so, these strains represent relative changes in the RCT ring when treated as a spring. Neither permanent nor offset strains represent local or average strains in the cladding material. However, with materials modeling coupled with FEA, local stresses and strains can be calculated. Although d_p is the more accurate measure of plastic displacement of the ring, it can only be determined accurately for rings that do not experience significant cracking. Thus, δ_p is reported for all tests conducted, while d_p is only reported for ring samples that do not have significant cracks.

3.1 RCT Results for As-Irradiated High-Burnup M5®

Room-temperature RCTs were conducted at 0.05, 5, and 50 mm/s to determine the sensitivity of the mechanical behavior of high-burnup M5® to displacement rate. Sample lengths varied from 7.7 mm to 8.0 mm. The measured loads were normalized to 8 mm to generate the results shown in Fig. 10. The normalized maximum load increased by <11% with the 1000-fold increase in displacement rate. Note that none of the rings tested developed any cracks. Thus, ductility values determined from the load-displacement curves and micrometer measurements represent lower-bound values. Corrected offset strains were 9.4% (average) and permanent strains were 9.2% (average) with very little test-to-test variation. At RT, the RCT ductility of high-burnup M5® was >9%. The results indicate that as-irradiated M5® has high RT ductility and very low strain-rate sensitivity. The low strain-rate sensitivity is consistent with data reported for irradiated Zry-4 [1].

RCTs were also conducted at 60°C and 90°C and the reference 5-mm/s displacement rate. These temperatures were chosen because RHT M5® showed a significant increase in ductility between 60°C and 90°C. As expected from the RT results, neither ring tested at higher temperature developed any cracks. The load results plotted in Fig. 11 were also normalized to 8-mm sample length. The maximum load decreased by <9%, with the increase in RCT temperature from 26°C to 90°C. Ductility values were 10% on the basis of average offset and permanent strains. Thus, at 5 mm/s, the ductility of high-burnup M5® is >10% for temperatures in the range of 26–90°C.

RCT results for as-irradiated M5® are summarized in Table 3. Baseline RCT load-displacement curves for high-burnup M5® are included in Appendix A.

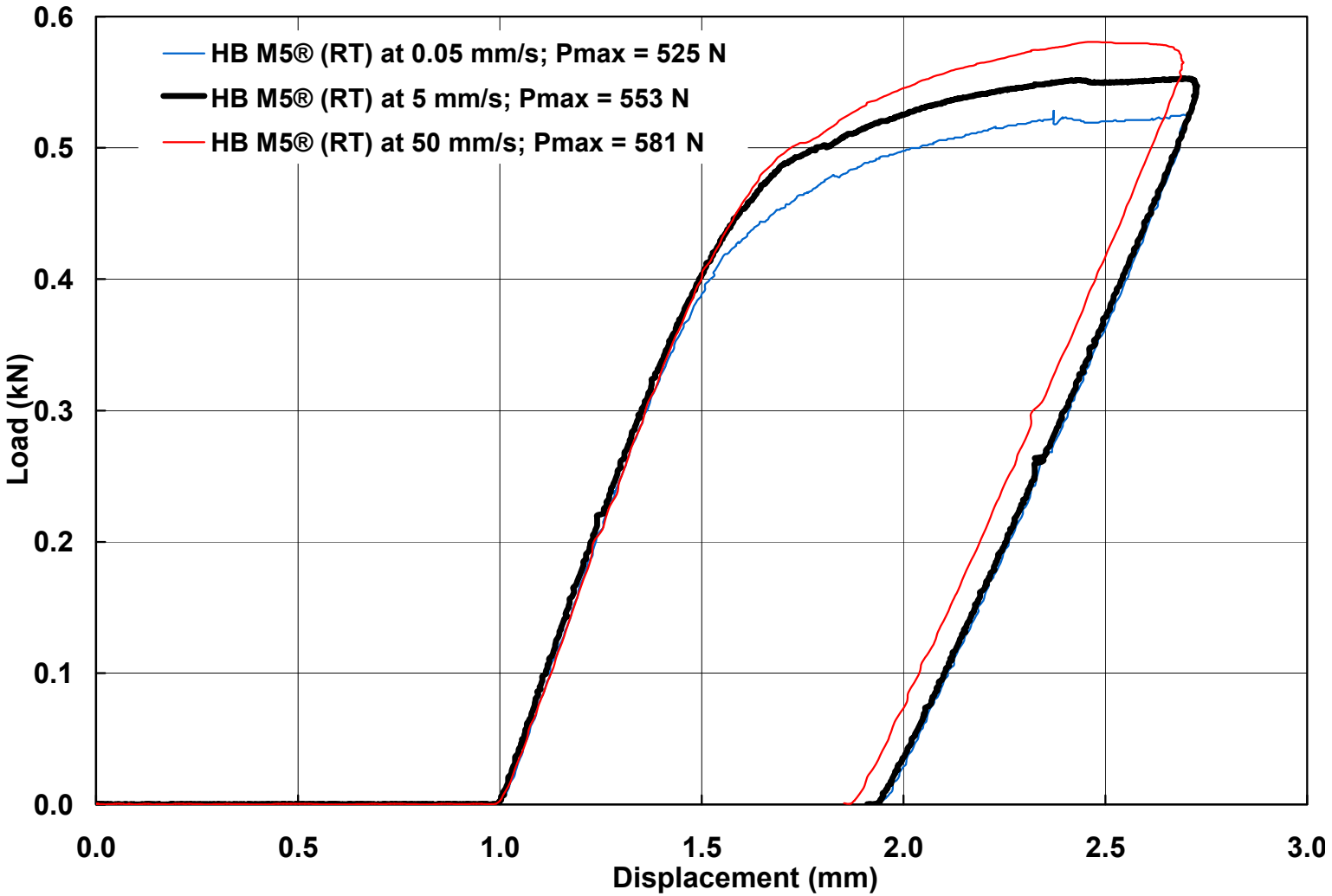

Figure 10. RCT load-displacement curves for as-irradiated, high-burnup M5® cladding samples tested at RT and displacement rates of 0.05, 5, and 50 mm/s. Loads were normalized to a sample length of 8.0 mm.

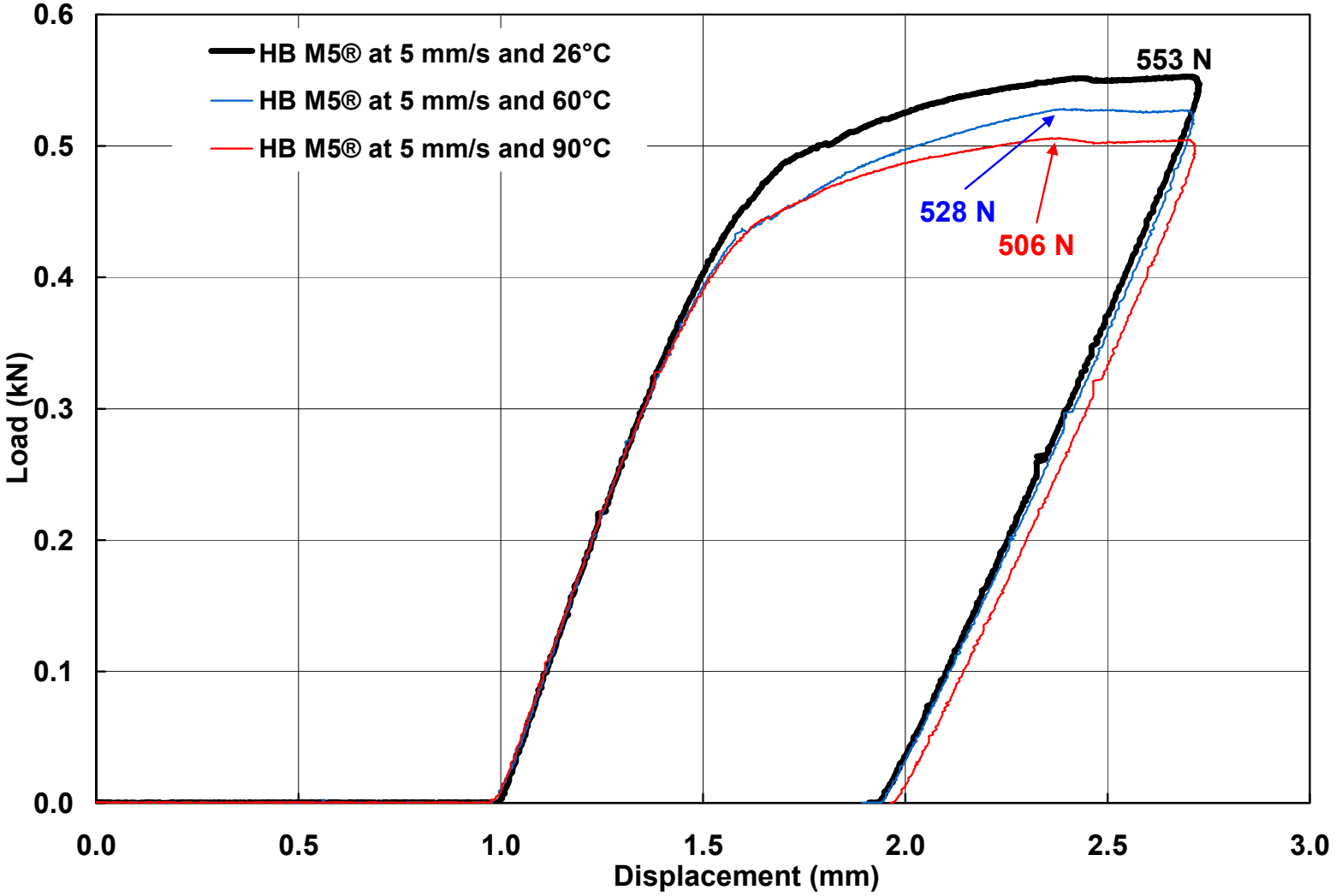

Figure 11. RCT load-displacement curves for as-irradiated, high-burnup M5® cladding samples tested at 5 mm/s displacement rate and RCT temperatures of 26°C, 60°C, and 90°C. Loads were normalized to a sample length of 8.0 mm.

Table 3. Summary of RCT results for as-irradiated, high-burnup M5® cladding samples. P_{max} was normalized to a sample length of 8.0 mm.

Sample ID	Length, mm	Displacement Rate, mm/s	RCT T, °C	Normalized Pmax, N	Offset Strain, %	Permanent Strain, %
652E6D	7.86	0.05	26	525	9.8	9.1
652E6E	8.02	5	26	553	9.8	9.6
652E6K	7.72	50	26	581	8.7	8.8
652E6C	7.66	5	60	528	9.7	9.5
652E6L	7.62	5	90	506	10.0	9.9

3.2 RCT Results for As-Irradiated High-Burnup ZIRLO™

For as-irradiated, high-burnup ZIRLO™, RCT data indicated a relatively high ductility prior to >25% load drop. Figure 12 shows RT RCT results for displacement rates of 0.05, 5.0, and 50 mm/s. Sample lengths were 7.90, 7.80, and 7.61 mm, respectively. Loads shown in Fig. 12 were normalized to a sample length of 7.80 mm. As with high-burnup M5® and Zry-4 [1], ZIRLO™ strength and ductility were relatively insensitive to the increase in displacement rate. P_{max} increased by 6% with the 1000-fold increase in displacement rate. Offset strains were 6.7%, 7.0%, and 5.5% for 0.05, 5.0, and 50 mm/s, respectively. Also, the first significant load drop was about 40% of P_{max} for all three cases.

To determine crack number and depth following ≈40% load drop, a fourth test was conducted at 0.05 mm/s with the test promptly terminated after the load drop. Figure 13 shows the load-displacement curve for the 7.1-mm-long ring tested under these conditions. The normalized (to 7.8 mm) P_{max} was 516 mm, the load drop was 37%, and the corrected offset strain was 8.8%. On the basis of post-RCT metallographic examination (Fig. 14), 15 cracks were observed, with two major cracks at the 3 and 9 o'clock orientations. All cracks originated at the cladding outer surface (oxide/hydride-rim interface). Cracks within the oxide layer that did not extend into the metal were not counted. The minor cracks were 10–16% of the metal wall thickness. The two major cracks extended into ≈50% of the cladding wall. Figure 14 shows the major crack at the 3 o'clock orientation. The crack path was radial through the brittle hydride rim, diagonal through the mixed metal-hydride region, and circumferential along a mid-radius circumferential hydride. The region from the mid-radius to the inner surface was relatively free of hydrides and no cracks were detected. This region is expected to have significantly higher RCT ductility than the outer half of the cladding wall.

RCTs were also conducted at the reference displacement rate (5 mm/s) and at elevated temperatures (90°C and 150°C). At 90°C, P_{max}, normalized to 7.8 mm, was 540 N, and significant cracking did not occur until 10.4% offset strain (see Fig. 15). There was a gradual decrease in load from P_{max} followed by an abrupt decrease of 17% in load. Post-RCT metallographic examination (see Fig. 16) revealed the presence of one major crack (extending through ≈60% of the wall) at the 9 o'clock orientation and 13 minor cracks through the hydride rim extending through 7–17% of the wall. Two of these minor cracks are observed in Fig. 16. All cracks initiated at the outer cladding surface.

The load-displacement curve for the 150°C RCT did not exhibit any abrupt load drops (see Fig. 17). P_{max} (normalized to 7.8 mm) was 512 N, and the ductility was 10.9% on the basis of offset displacement and 10.2% on the basis of permanent displacement. Post-RCT metallographic examination was performed to determine the cause of the gradual load drop from P_{max} to the end of the test. Seven minor cracks (five of which appear in Fig. 18) were observed to extend from the outer surface through 10–20% of the wall thickness through the hydride rim. These minor cracks appeared to have caused the gradual load drop.

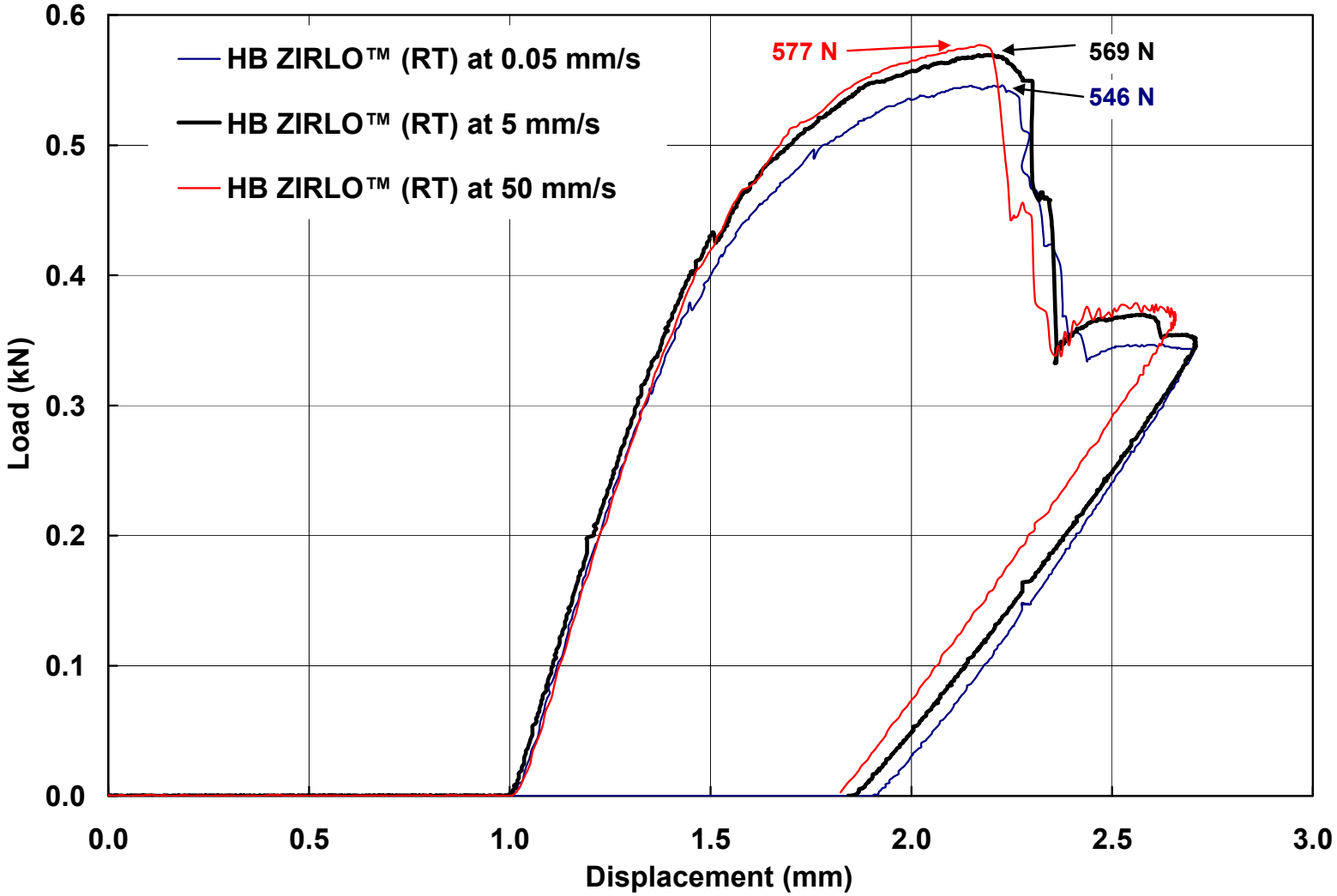

Figure 12. RCT load-displacement curves for as-irradiated, high-burnup ZIRLO™ cladding samples tested at RT and displacement rates of 0.05, 5, and 50 mm/s. Loads were normalized to a sample length of 7.8 mm.

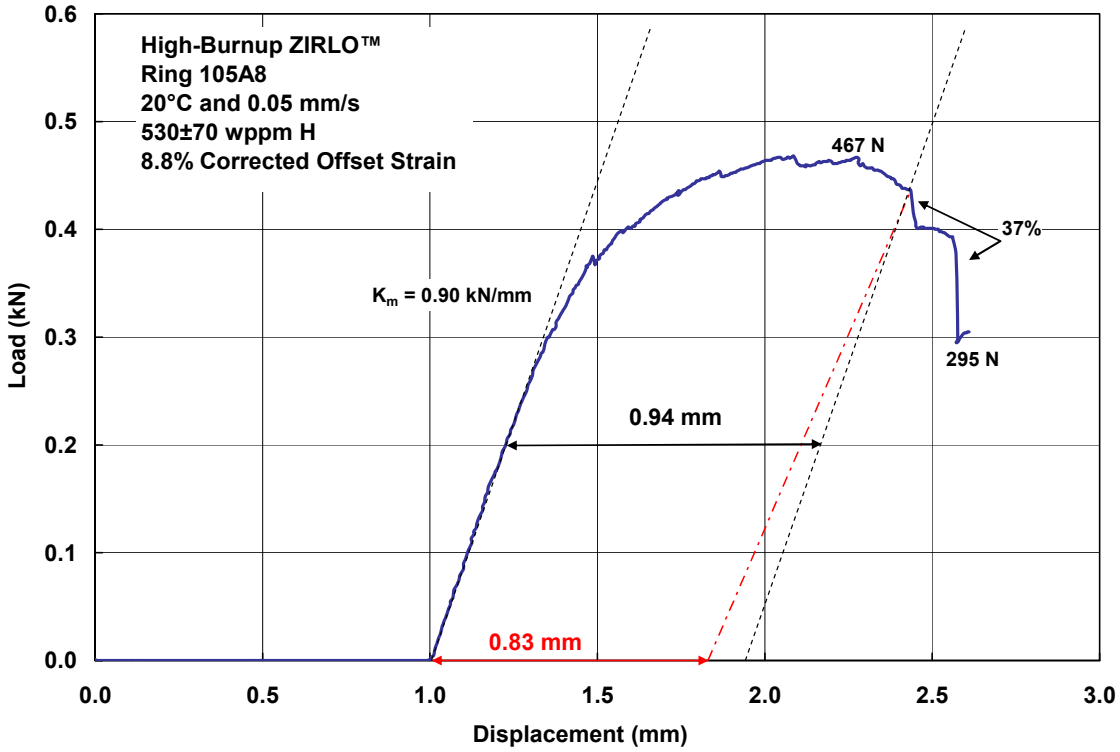

Figure 13. RCT load-displacement curve for as-irradiated, high-burnup ZIRLO™ cladding sample tested at RT and 0.05 mm/s. The test was stopped manually after the 37% load drop.

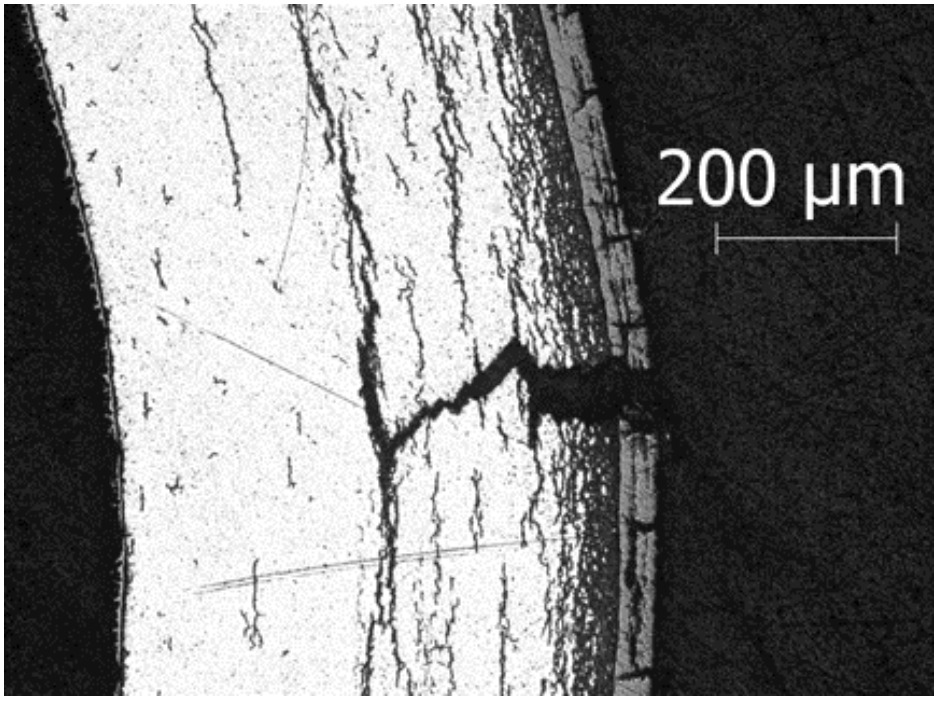

Figure 14. One of two cracks extending into 50% of the wall following the RCT described in Fig. 13. Thirteen minor cracks, extending into 10–16% of the wall, were observed at the cladding outer surface.

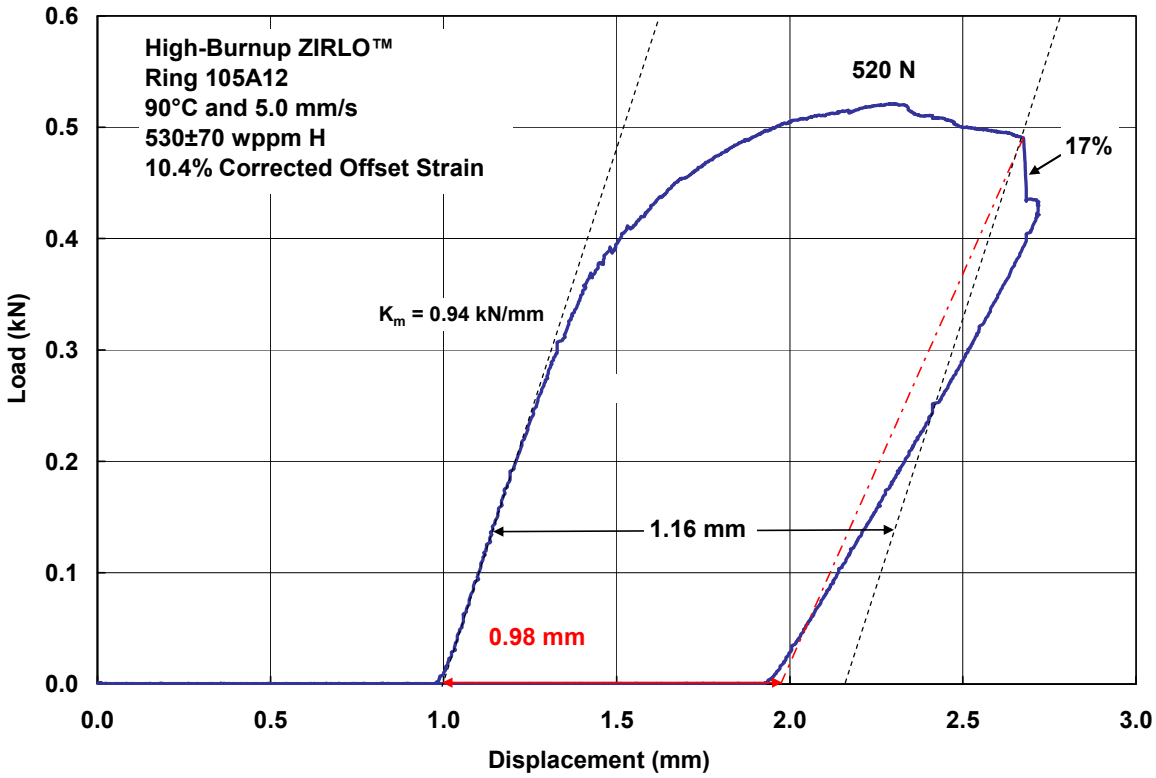

Figure 15. RCT load-displacement curve for as-irradiated, high-burnup ZIRLO™ cladding sample tested at 90°C and 5 mm/s.

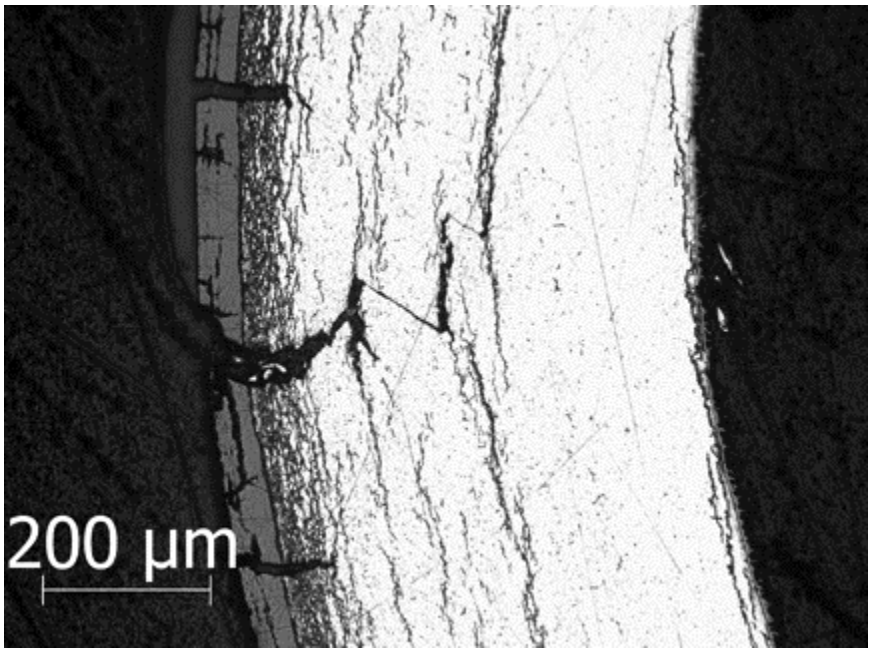

Figure 16. One major crack extending into >50% of the wall following the RCT described in Fig. 15. Thirteen minor cracks, extending into 7–17% of the wall, were also observed at the cladding outer surface. Two of these are present in this figure.

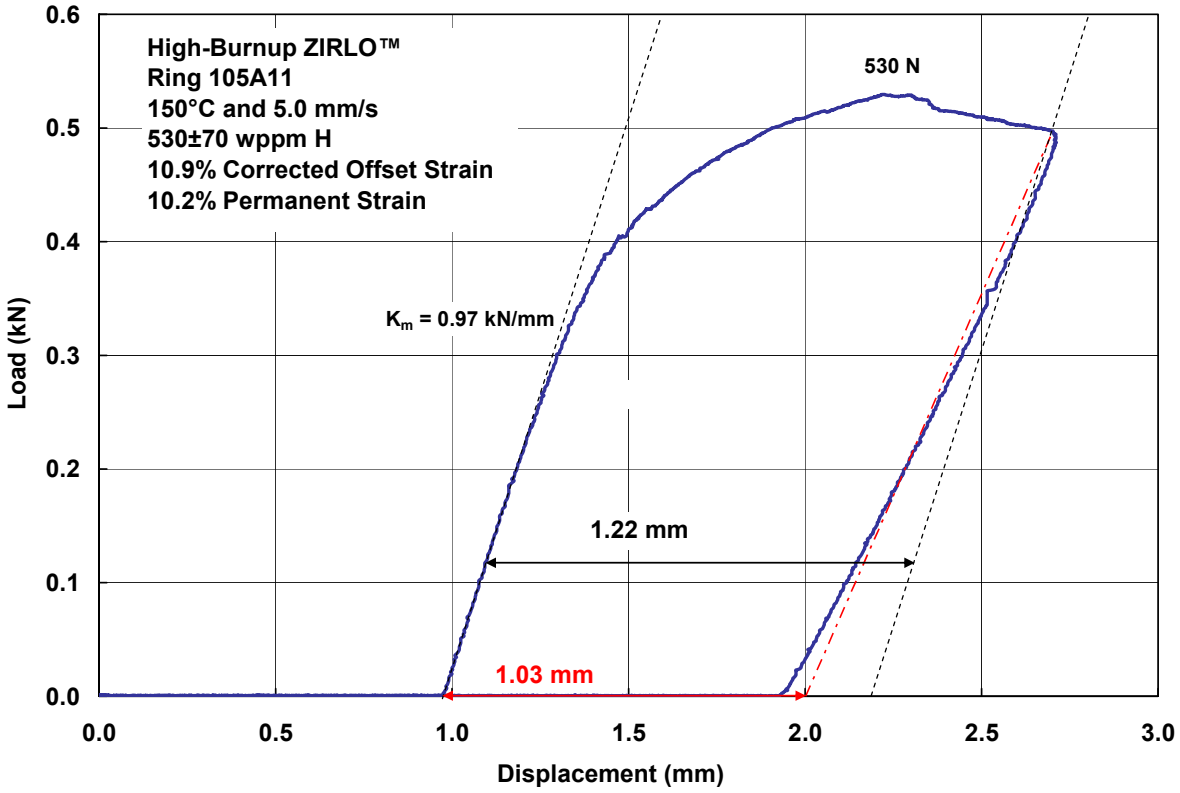

Figure 17. RCT load-displacement curve for as-irradiated, high-burnup ZIRLO™ cladding sample tested at 150°C and 5 mm/s.

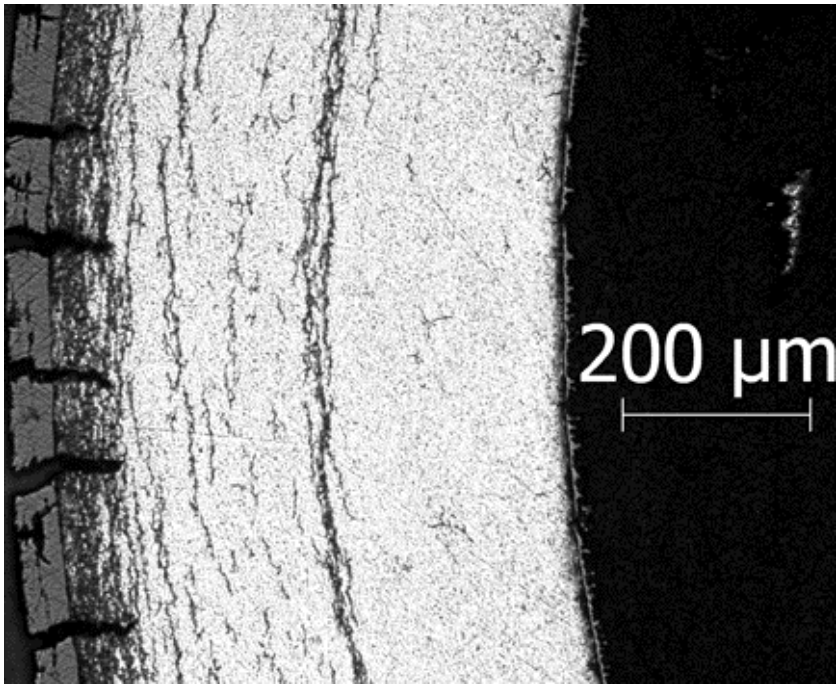

Figure 18. Five of seven minor cracks extending into 10–20% of the wall thickness following the RCT described in Fig. 17. The cracks in this figure extended into 10–14% of the cladding wall.

RCT results for as-irradiated, high-burnup ZIRLO™ are summarized in Table 4. Baseline RCT load-displacement curves for high-burnup ZIRLO™ are included in Appendix B.

Table 4. Summary of RCT results for as-irradiated, high-burnup ZIRLO™ cladding samples. P_{max} was normalized to a sample length of 8.0 mm to allow comparison with the M5® results in Table 3.

Sample ID	Length, mm	Displacement Rate, mm/s	RCT T, °C	Normalized P_{max}, N	Offset Strain, %	Permanent Strain, %
105A7	7.90	0.05	20	560	6.7	---
105A8	7.06	0.05	20	529	8.8	---
105A9	7.80	5	20	584	7.0	---
105A10	7.61	50	20	591	5.5	---
105A12	7.52	5	90	553	10.4	---
105A11	8.08	5	150	525	10.9	10.2

3.3 RCT Results for As-Irradiated High-Burnup Zry-4

The RT results for Zry-4 at 0.05, 5.0, and 50 mm/s were difficult to interpret because cracking and plastic flow occurred simultaneously after very low offset strains (≈1.5%). These results may have been caused by the thicker and more intact oxide layer (≈100 μm), the more diffuse hydride rim region, and the higher C_H in the outer half of the cladding wall. Figure 19 shows the load-displacement curves for the three strain rates. The load results were normalized to a sample length of 8.0 mm. P_{max} for the three strain rates was about 1000 N. The magnitude and number of load drops were comparable. The results were not conclusive regarding the strain-rate sensitivity of high-burnup Zry-4. Other samples with lower hydrogen content (300 wppm vs. 640 wppm) are available and could be used for more definitive determination of the strain-rate sensitivity of Zry-4, which is expected to be low on the basis of axial tensile data [1].

An additional RCT was conducted at RT and 0.05 mm/s. The test was promptly terminated after the first significant load drop (27%). Figure 20 shows the load-displacement curve for this RCT. The normalized value of P_{max} was 924 N, which was lower than the value (989 N) measured for the first RCT at 0.05 mm/s. A single crack, which extended from the outer cladding surface into about 40% of the wall, was observed at the 7 o'clock orientation. This orientation was unusual because the maximum outer-surface, hoop tensile stress occurred at the 3 and 9 o'clock orientations.

One RCT was conducted at 90°C, as shown in Fig. 22. P_{max}, normalized to 8.0 mm, was 958 N. The offset strain to the first significant load drop (28%) was 1.5%.

Table 5 summarizes the results of the RCT test for as-irradiated high-burnup Zry-4. Baseline RCT load-displacement curves for high-burnup Zry-4 are included in Appendix C.

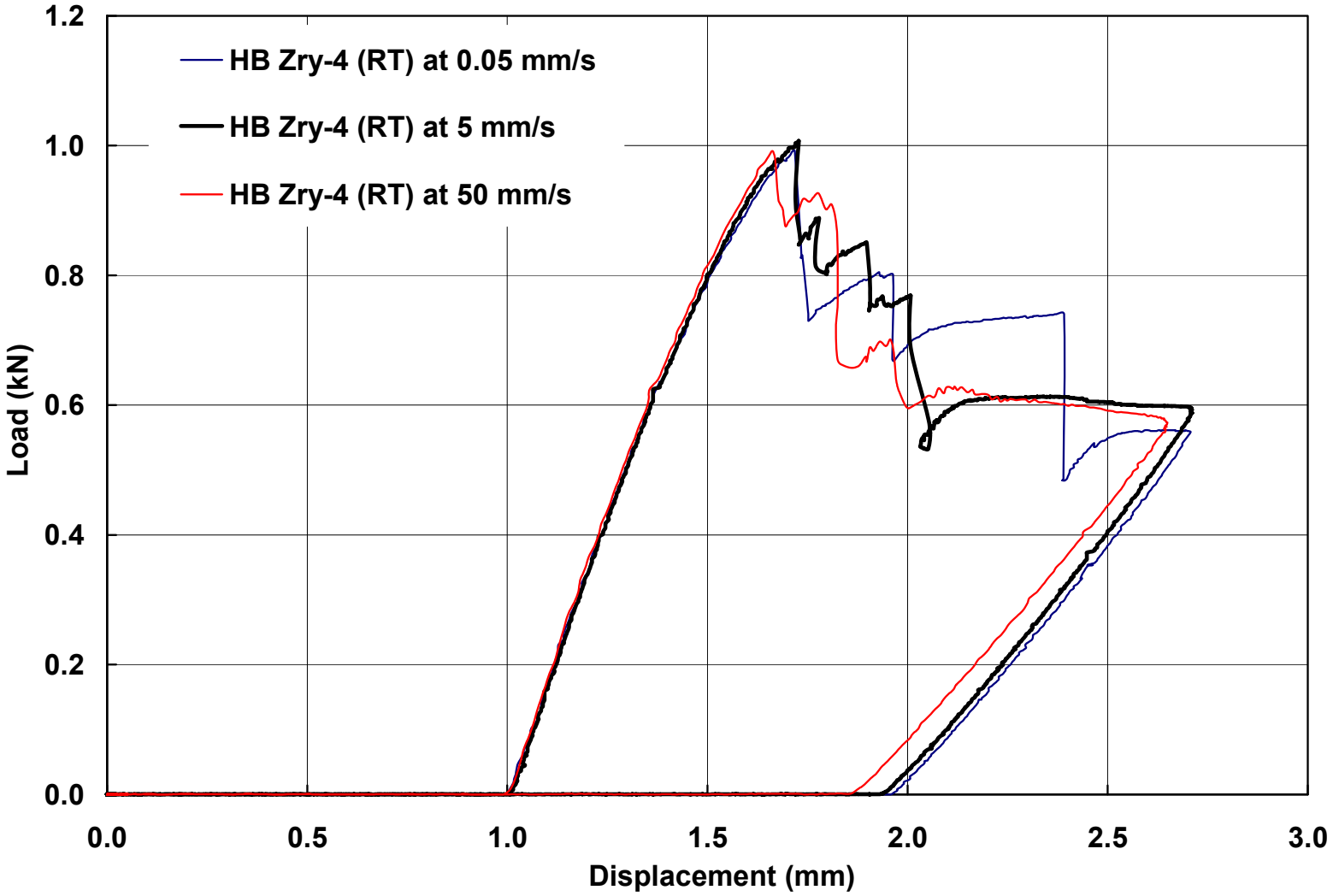

Figure 19. RCT load-displacement curves for as-irradiated, high-burnup Zry-4 cladding samples tested at RT and displacement rates of 0.05, 5, and 50 mm/s. Loads were normalized to a sample length of about 8.0 mm (7.97 mm).

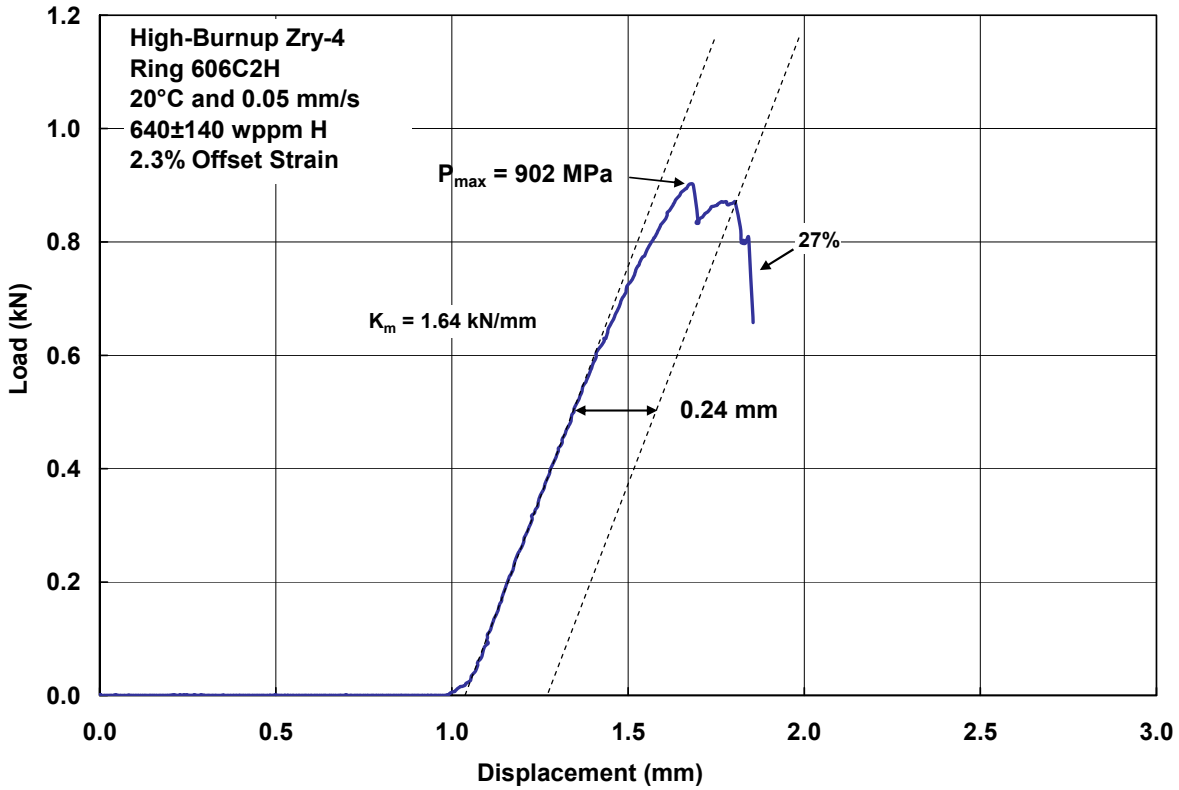

Figure 20. RCT load-displacement curve for as-irradiated, high-burnup Zry-4 cladding sample tested at RT and 0.05 mm/s. The test was stopped manually after the 27% load drop.

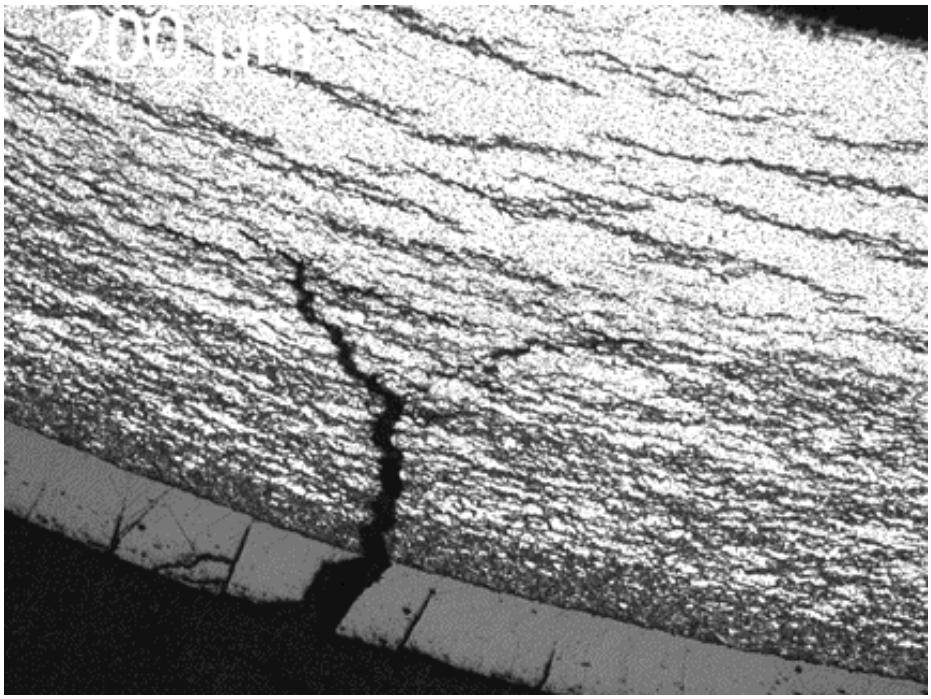

Figure 21. Single crack extending into 40% of the wall thickness following the RCT described in Fig. 20.

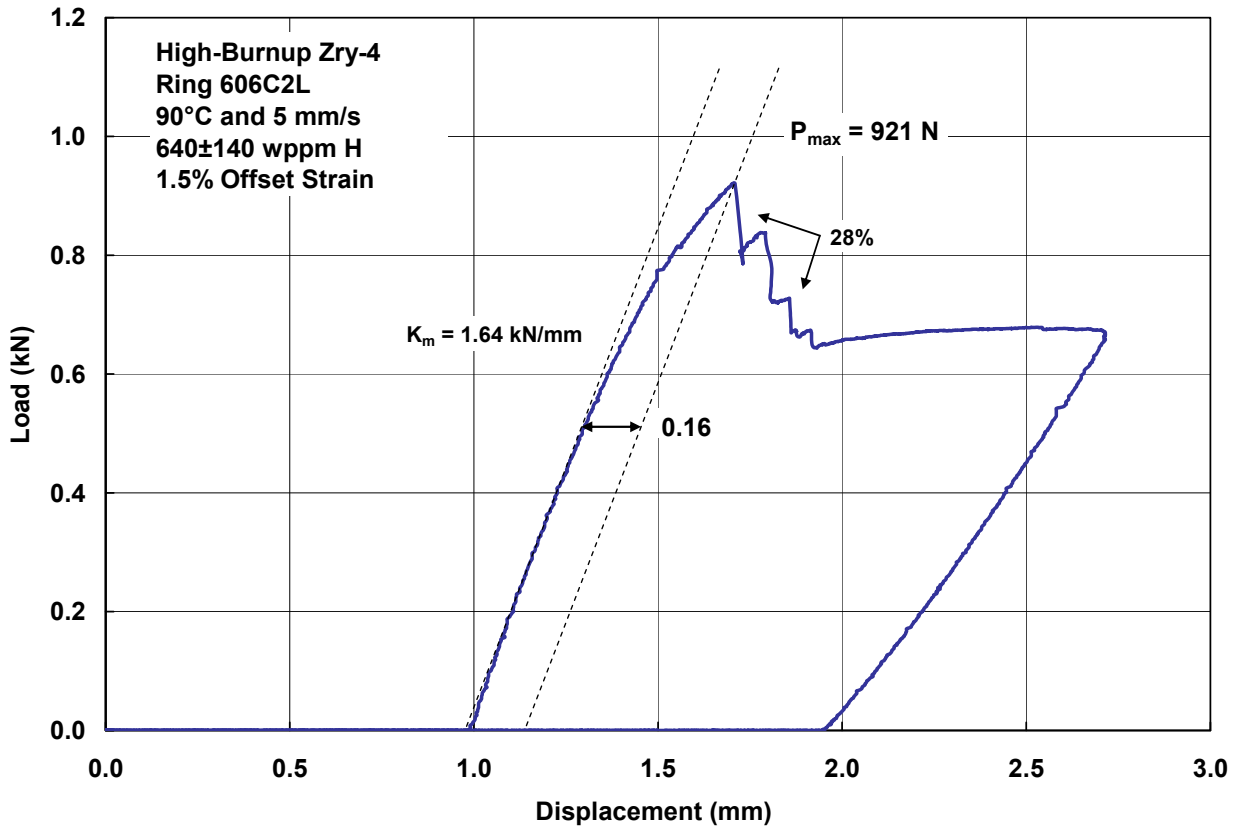

Figure 22. RCT load-displacement curve for as-irradiated, high-burnup Zry-4 cladding sample tested at 90°C and 5 mm/s.

Table 5. Summary of RCT results for as-irradiated, high-burnup Zry-4 cladding samples. P_{max} was normalized to a sample length of 8.0 mm.

Sample ID	Length, mm	Displacement Rate, mm/s	RCT T, °C	Normalized P_{max}, N	Offset Strain, %	Permanent Strain, %
606C2G	7.76	0.05	23	989	1.3	---
606C2H	7.81	0.05	20	924	2.3	---
606C2J	7.58	5	23	1010	1.5	---
606C2K	7.97	50	25	996	1.5	---
606C2L	7.69	5	90	958	1.5	---

4. CLADDING DEGRADATION DUE TO RHT

4.1 Comparison for As-Irradiated and RHT High-Burnup M5®

Load-displacement curves are given in Ref. 7 for high-burnup M5® following RHT at peak 400°C hoop stresses of 140 MPa and 110 MPa and slow cooling from 400°C at 5°C/h. Figure 23 shows offset strain vs. RCT test temperature for these two sets of RHT conditions. For both RHT stress conditions, RCT samples were classified as brittle (<2% offset strain) at RT and 60°C and ductile at T ≥90°C. The DBTT was estimated to be 80°C for the 140-MPa RHT and 70°C for the 110-MPa RHT.

Figure 24 compares the 60°C load-displacement curve for the 140-MPa RHT to the baseline results at 26°C for high-burnup M5®. The 140-MPa RHT loads (7.50-mm length) were normalized to 8.0 mm (baseline sample length). The first load drop for the RHT ring occurred during elastic loading at P = 267 N. After the load drop, loading increased at a linear rate to 324 N. On the basis of a >50% decrease in stiffness (i.e., loading slope), it was concluded that a crack had grown through >50% of the wall at the first load drop initiating from 267 N. Thus, P_{max} = 267 N and δ_p/D_{mo} = 0% for the RHT sample. By contrast, RT results for as-irradiated M5® were P_{max} = 553 N and δ_p/D_{mo} > 10%. Thus, the degradation in RCT properties due to RHT can be quantified as a 52% decrease in P_{max} and a ductility decrease from >10% to 0% for RCT temperatures below the DBTT. However, quantification of P_{max} for samples that fail within the elastic regime requires a large number of tests because of the expected variation in P_{max} for the brittle failure mode. As shown in Fig. 25, the brittle RHT sample tested at 30°C had a peak load of 368 N.

Figure 26 shows the hydride distribution and orientation in high-burnup M5® in the as-irradiated condition (Fig. 26a) and after RHT at 400°C and 140-MPa hoop stress (Fig. 26b). For the RHT M5®, primarily long radial hydrides precipitated during the 5°C/h cooling from 400°C. The longest radial hydride observed in Fig. 26b had a length that is 80% of the wall thickness. These radial hydrides provided pathways for crack initiation and propagation in response to hoop-stress loading. For the post-RHT RCT at 60°C, Fig. 24 shows three load drops. Although each load drop may represent simultaneous crack initiation and propagation through part of the wall, a simplistic interpretation would be that the first load drop in the elastic regime represents initiation of a single crack extending >50% of the wall thickness, the second load drop represents the same for a second crack, and the third load drop — which is large — represents initiation and propagation of two additional cracks. Following RCT, major cracks were observed at four locations: 12 o'clock (see Fig 27a), 3 o'clock, 6 o'clock (see Fig. 27b), and 9 o'clock. Metallographic examination was performed for a cross section at the sample mid-span. The 12 o'clock crack was partial-wall, but it extended through >50% of the wall. The other three cracks were essentially through-wall cracks, like the one imaged in Fig. 27b.

Strength and ductility results from RCTs for as-irradiated and RHT high-burnup M5® cladding are summarized in Table 6.

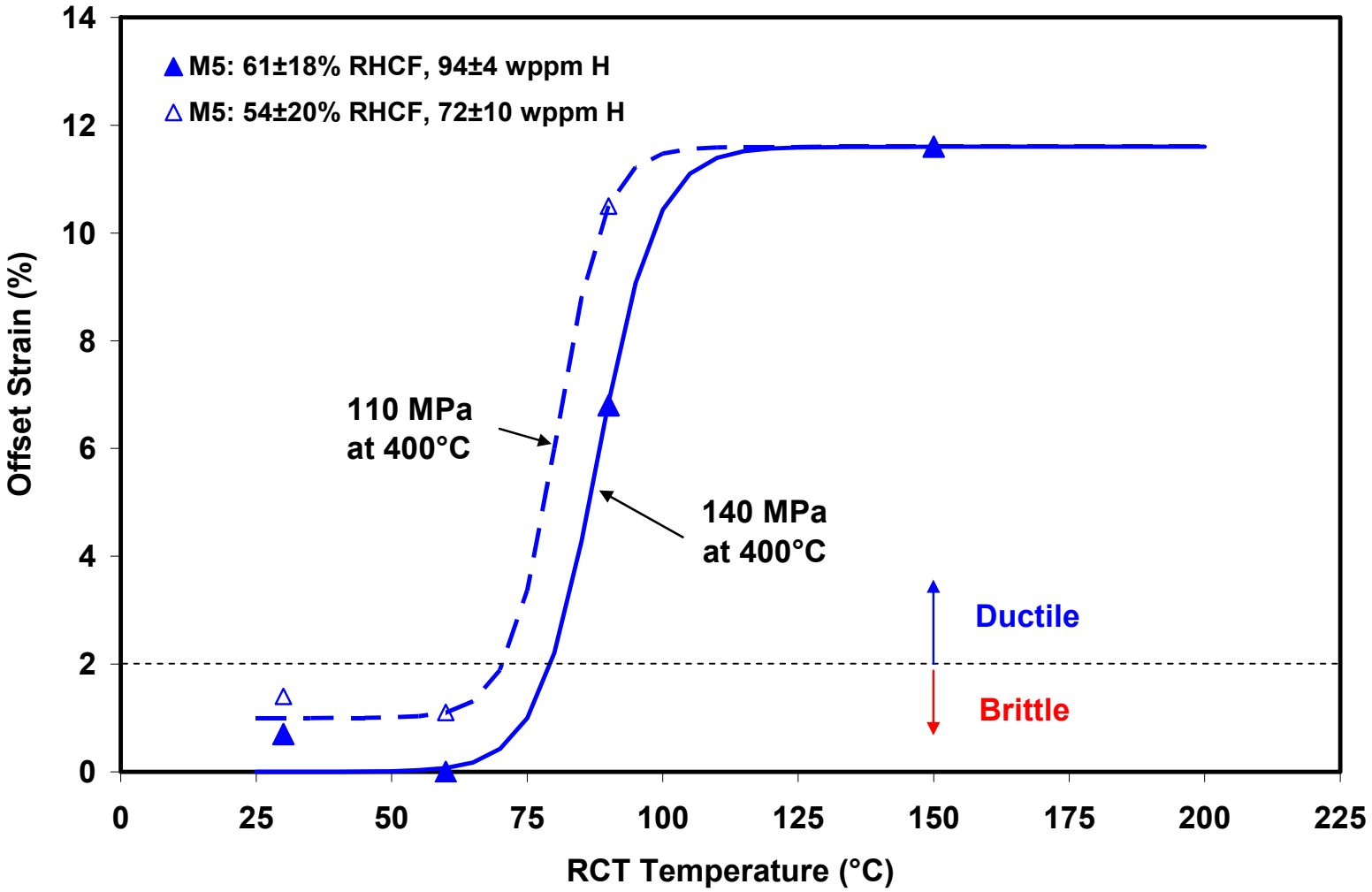

Figure 23. RCT offset strains vs. RCT temperature for high-burnup M5® following RHT at peak 400°C hoop stresses of 140 MPa and 110 MPa. RHCF is the radial-hydride-continuity factor, which increases with RHT hoop stress, and is defined in Ref. 7.

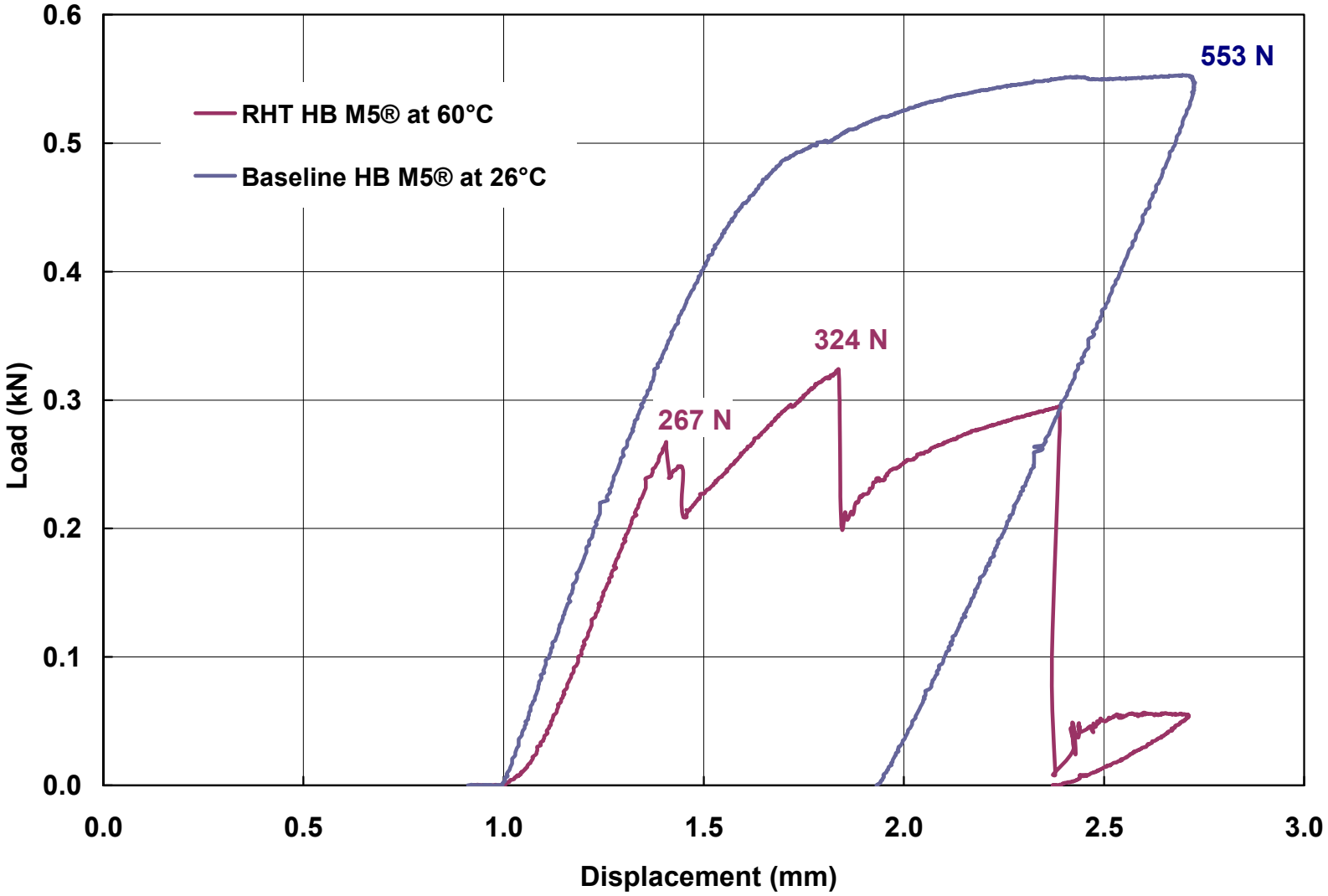

Figure 24. RCT load-displacement curves for high-burnup M5®: (a) as-irradiated (i.e., baseline) condition (see Fig. 26a) prior to drying-storage and tested at 26°C and (b) following RHT at 400°C and 140 MPa (see Fig. 26b) and tested at 60°C.

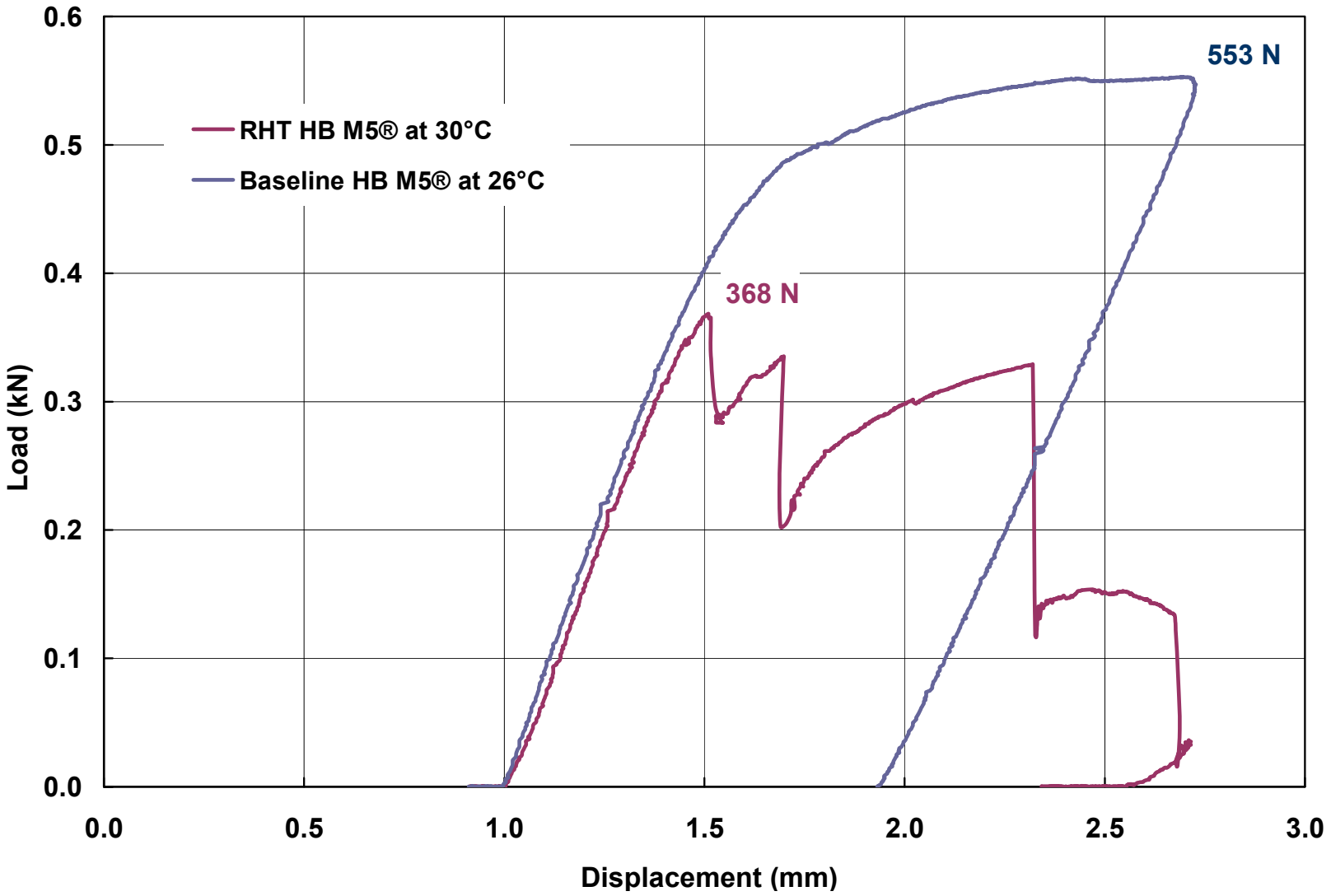

Figure 25. RCT load-displacement curves for high-burnup M5®: (a) as-irradiated (i.e., baseline) condition (see Fig. 26a) prior to drying-storage and tested at 26°C and (b) following RHT at 400°C and 140 MPa (see Fig. 26b) and tested at 30°C.

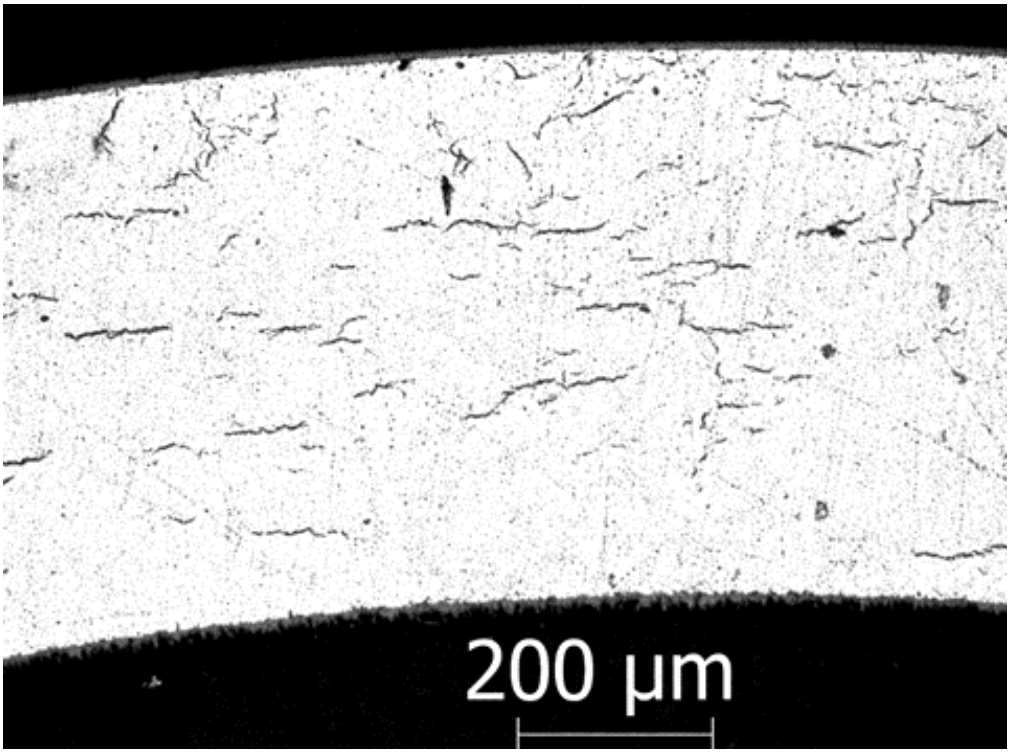

(a)

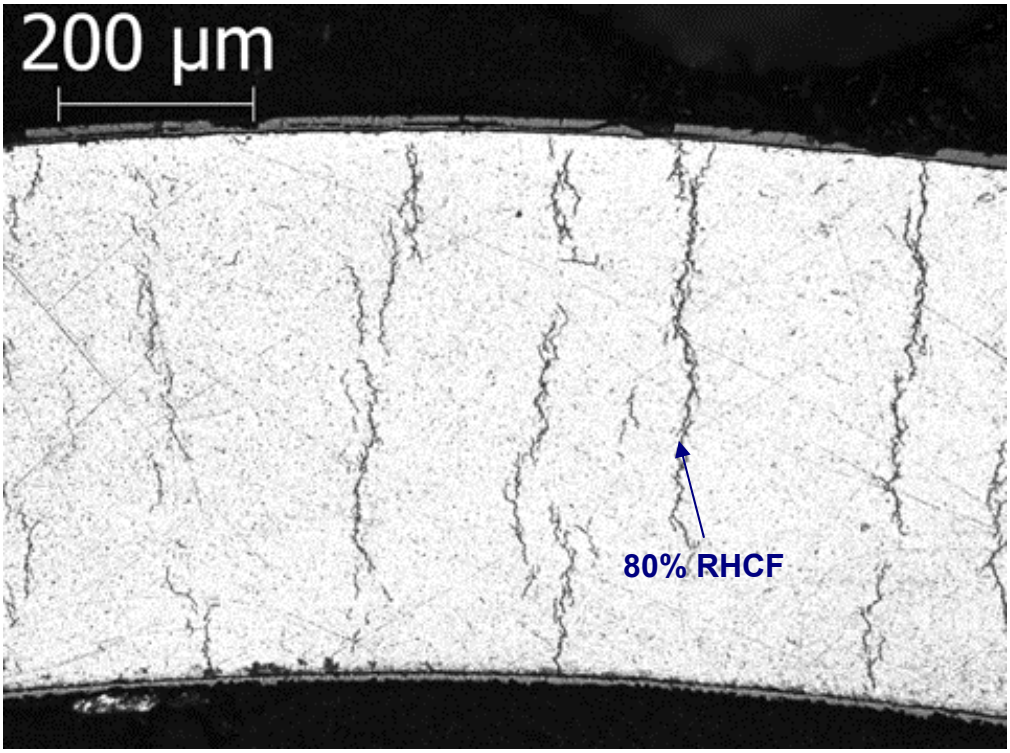

(b)

Figure 26. Hydride distribution and orientation in high-burnup M5®: (a) as-irradiated (baseline) with 76 wppm C_H and (b) after RHT at 400°C and 140 MPa with 94 wppm C_H.

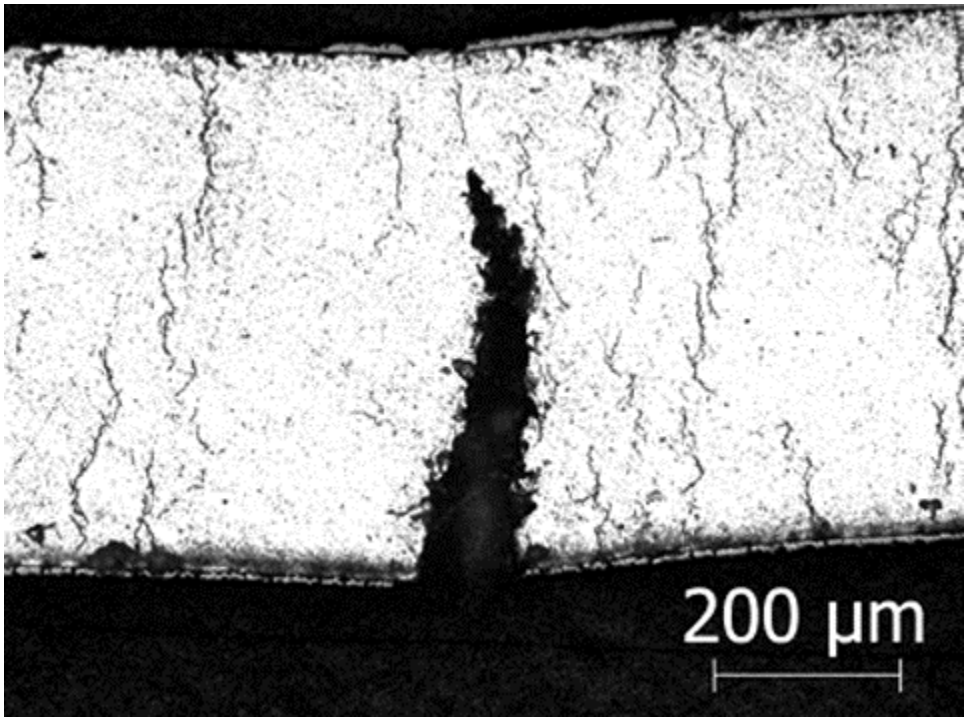

(a)

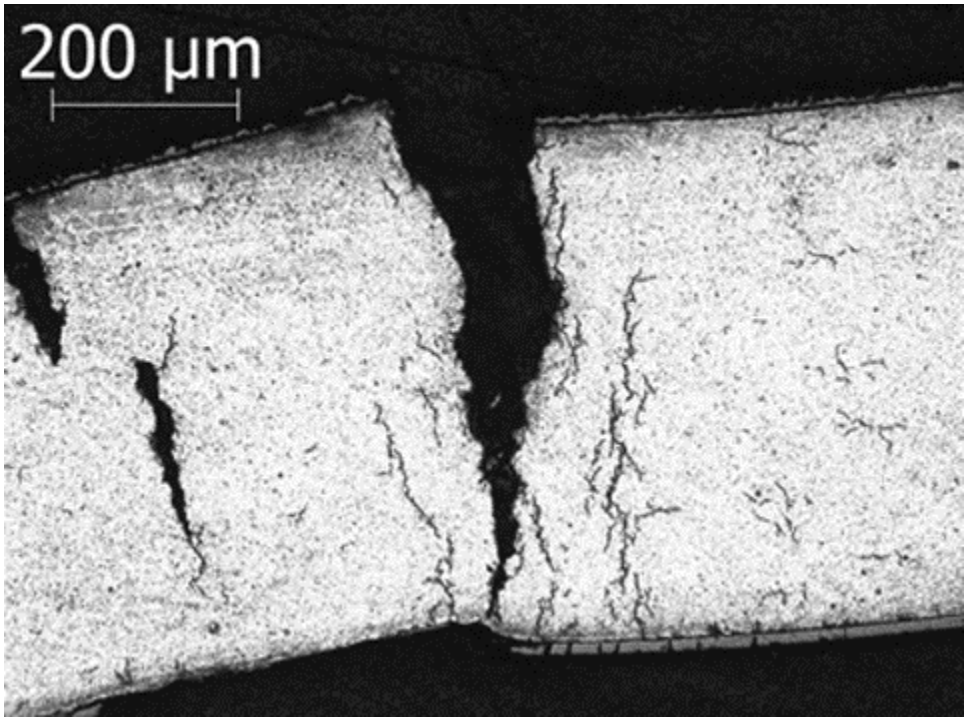

(b)

Figure 27. Two of four major cracks observed in the post-RCT metallographic images for RHT (400°C and 140 MPa) high-burnup M5® tested at 60°C: (a) 12 o'clock location (under the load) and (b) 6 o'clock location (above the support). Cracks similar to the one imaged in Fig. 27b were observed at the 3 and 9 o'clock orientations.

Table 6. Summary of strength (P_{max}) and ductility (δ_p/D_{mo}) results for high-burnup M5® in the as-irradiated condition (i.e., baseline results for 652E6E) and following RHT. P_{max} was normalized to 8-mm sample length to determine the percentage decrease in maximum load relative to the baseline result.

Sample ID	Peak RHT T, °C	Peak RHT σ_θ, MPa	RCT T, °C	Reduction in P_{max}, %	Ductility δ_p/D_{mo}, %
652E6E	---	---	26	0	>10
645D8	400	140	30	34	0.7
645D3	400	140	60	52	0
645D10	400	140	90	20	6.8
645D5	400	140	150	21	>12
651E5H	400	110	30	22	1.4
651E5C	400	110	60	28	1.1
651E5F	400	110	90	17	>11

4.2 Comparison for As-Irradiated and RHT High-Burnup ZIRLO™

Load-displacement curves are given in Refs. 4–6 for high-burnup ZIRLO™ following RHT at peak 400°C hoop stresses of 140 MPa and 110 MPa and slow cooling from 400°C at 5°C/h. Figure 28 shows offset strain vs. RCT test temperature for these two sets of RHT conditions. The DBTT decreased from ≈185°C to ≈125°C for a decrease in RHT hoop stress from 140 MPa to 110 MPa.

Figure 29 compares the load-displacement curve for as-irradiated, high-burnup ZIRLO™ tested at 30°C to the one for RHT (400°C and 140 MPa hoop stress) high-burnup ZIRLO™ tested at 150°C. The first load drop for the RHT ring occurred during elastic loading at P = 220 N. After the load drop, loading increased at a linear rate to 270 N. Based on the >50% decrease in stiffness (i.e., loading slope), it was concluded that a crack had grown through >50% of the wall at the first load drop from 220 N. Thus, P_{max} = 220 N and δ_p/D_{mo} = 0% for the RHT sample. By contrast, RT results for as-irradiated ZIRLO™ were P_{max} = 570 N and δ_p/D_{mo} = 7.0%. The degradation in RCT properties due to RHT can be quantified as a 61% decrease in P_{max} and a ductility decrease from 7% to 0% for RCT temperatures below the DBTT. As with high-burnup M5®, quantification of P_{max} for samples that fail within the elastic regime requires a large number of tests because of the expected variation in P_{max} for the brittle failure mode. Figure 30 shows the load-displacement curve comparison for a second RHT ZIRLO™ ring tested at 150°C. The peak load for the RHT ring was 471 N (17% decrease) and the offset strain was 1.4%. For both RHT rings, post-RCT examination indicted through-wall cracks at the 12 and 6 o'clock orientations. These cracks initiated at the cladding inner surface at the maximum tensile hoop stress locations.

Figure 31 shows the hydride distribution and orientation in high-burnup ZIRLO™ in the as-irradiated condition (Fig. 31a) and after RHT at a peak 400°C hoop stress of 140 MPa (Fig. 31b). For RHT ZIRLO™, continuous radial-circumferential hydrides precipitated during the 5°C/h cooling from 400°C. The longest pathway for continuous crack growth across the cladding wall was ≈80% of the wall thickness (see Fig. 31b), and the shortest pathway was 40% of the cladding wall at the thickness (at the 4:30 o'clock orientation). Also, because these long radial hydrides extended to the cladding inner surface, they would be subjected to the maximum tensile hoop stress if they were located below the applied load or above the support.

Strength and ductility results from RCTs for as-irradiated and RHT high-burnup ZIRLO™ cladding are summarized in Table 7.

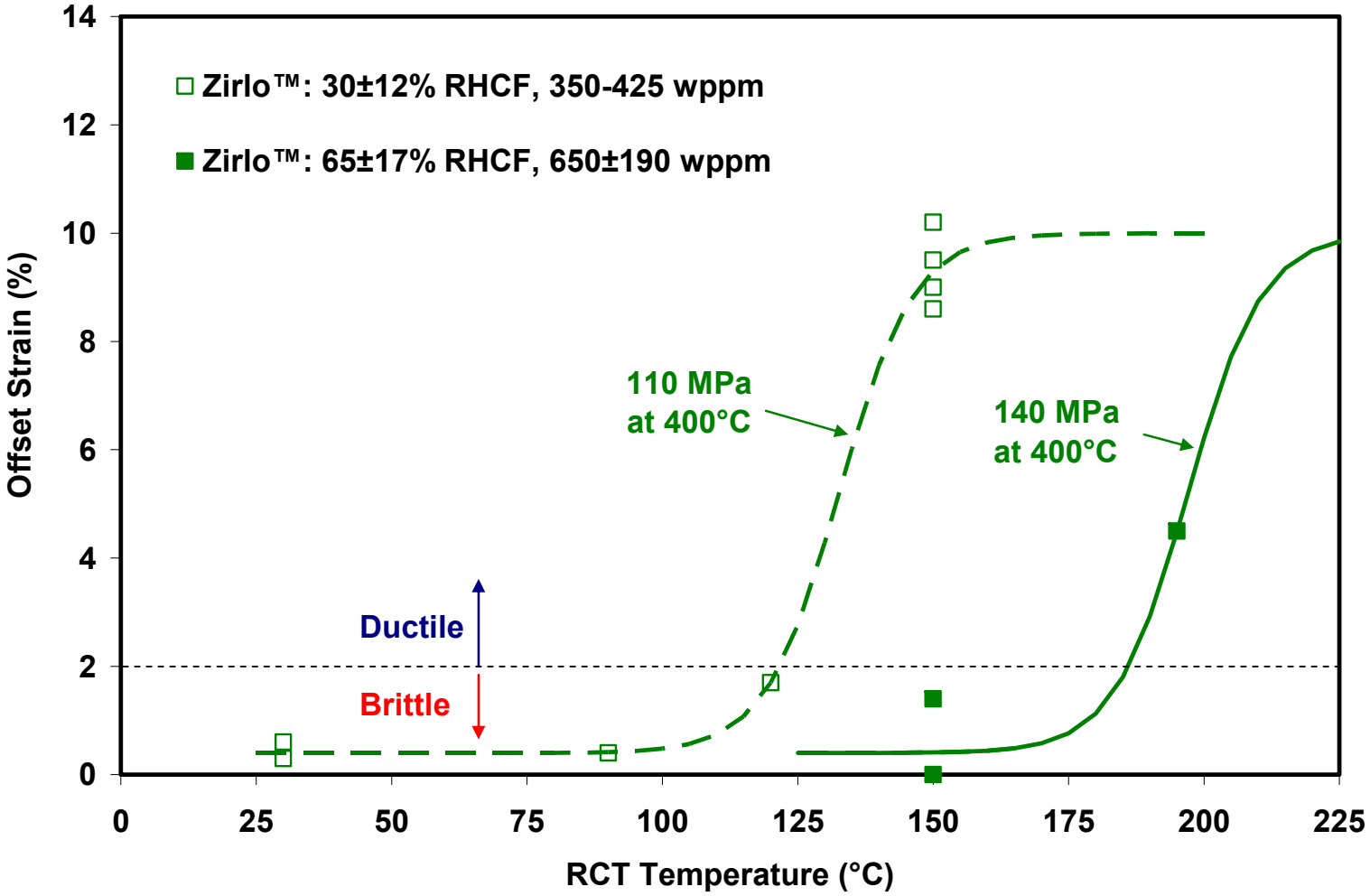

Figure 28. RCT offset strains vs. RCT temperature for high-burnup ZIRLO™ following RHT at peak 400°C hoop stresses of 140 MPa and 110 MPa. RHCF is the radial-hydride-continuity factor, which increases with RHT hoop stress, and is defined in Refs. 4–7.

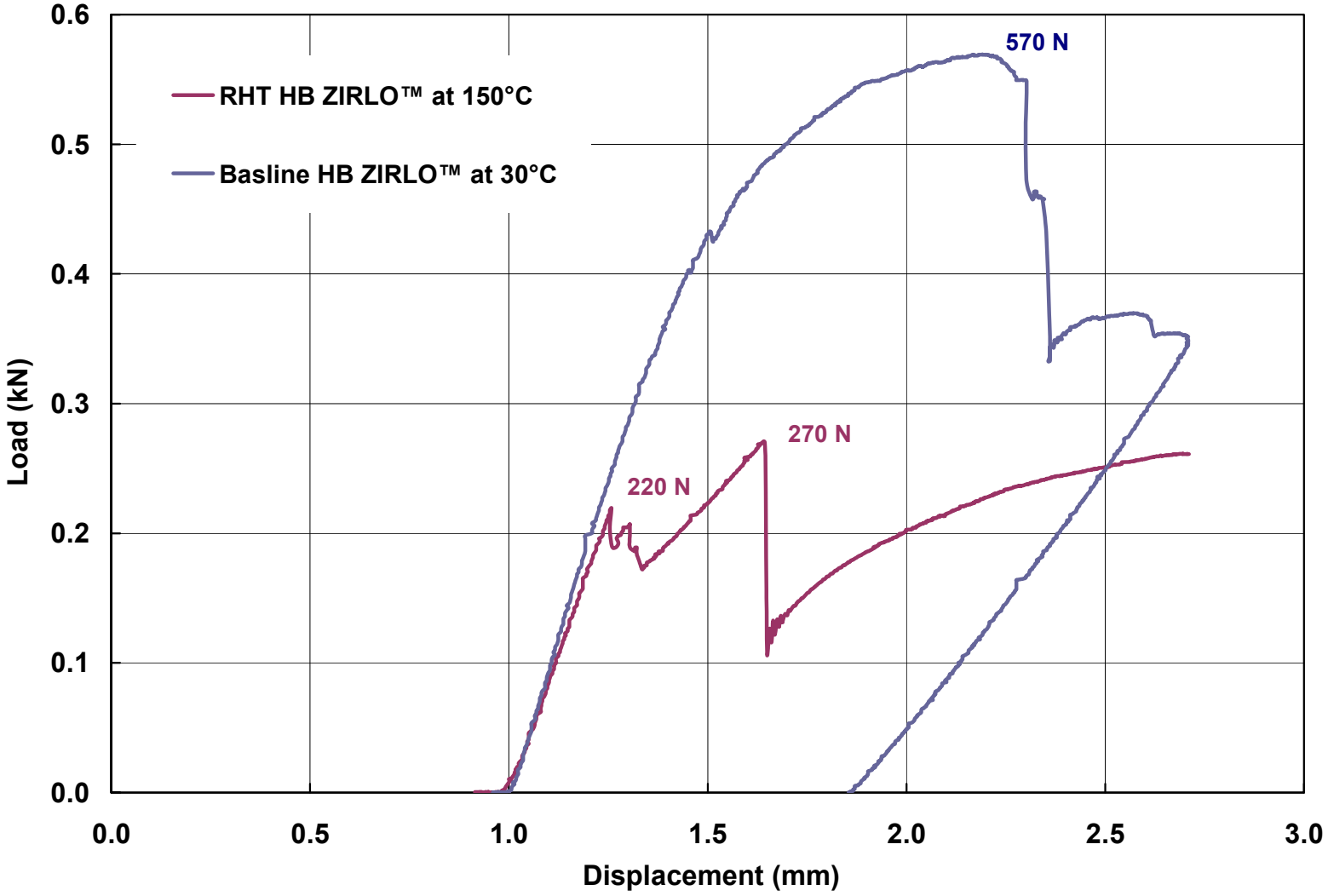

Figure 29. RCT load-displacement curves for high-burnup ZIRLO™: (a) as-irradiated (i.e., baseline) condition (see Fig. 31a) prior to drying-storage and tested at 30°C and (b) following RHT at 400°C and 140 MPa (see Fig. 31b) and tested at 150°C (1st ring).

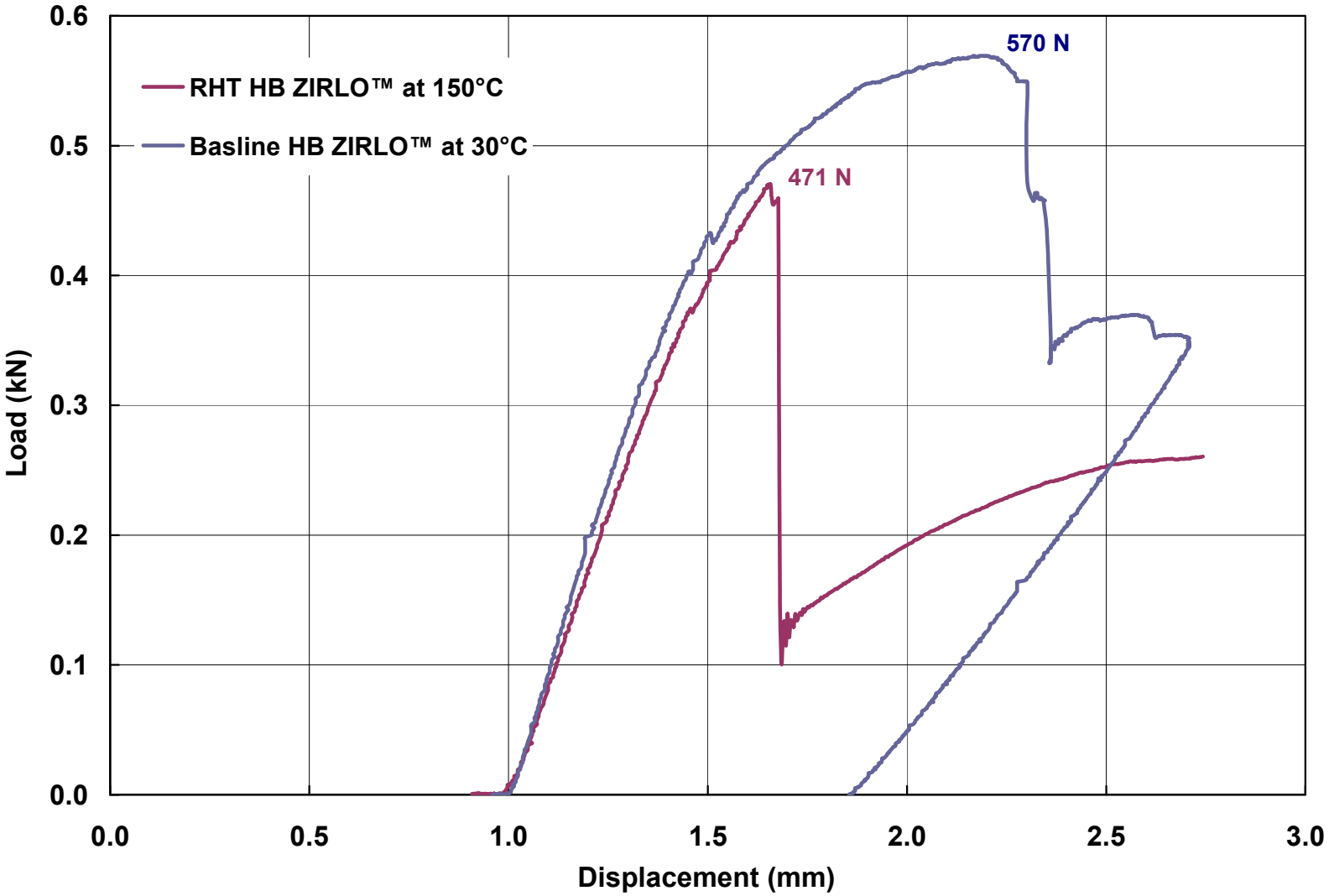

Figure 30. RCT load-displacement curves for high-burnup ZIRLO™: (a) as-irradiated (i.e., baseline) condition (see Fig. 31a) prior to drying-storage and tested at 30°C and (b) following RHT at 400°C and 140 MPa (see Fig. 31b) and tested at 150°C (2nd ring).

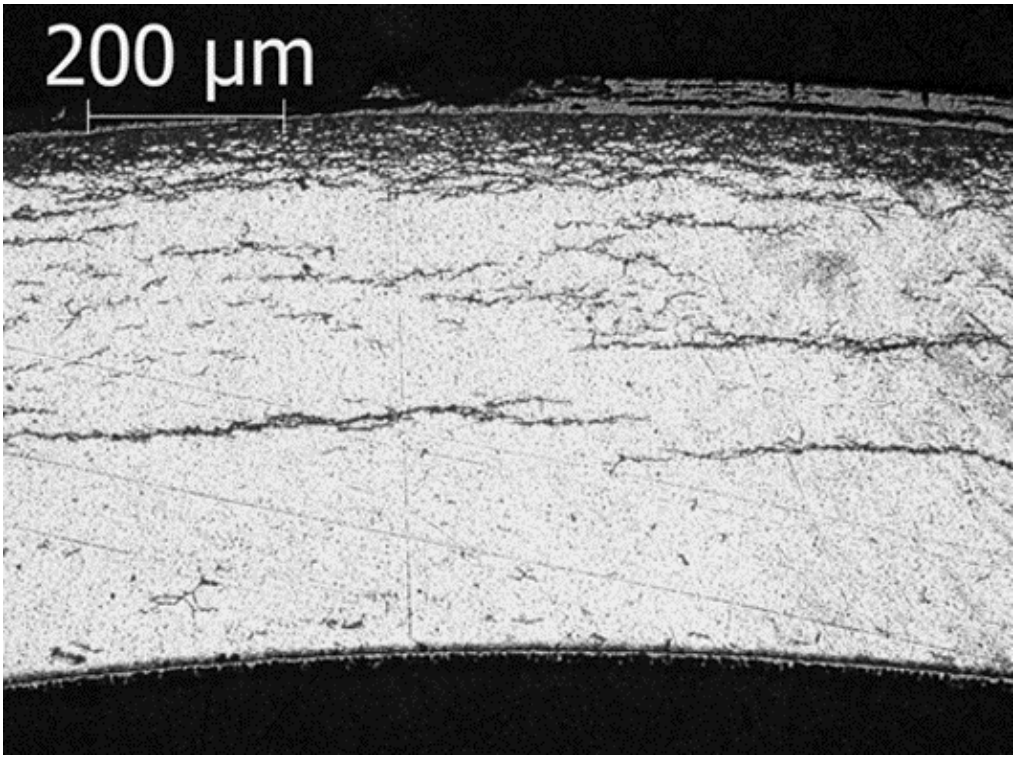

(a)

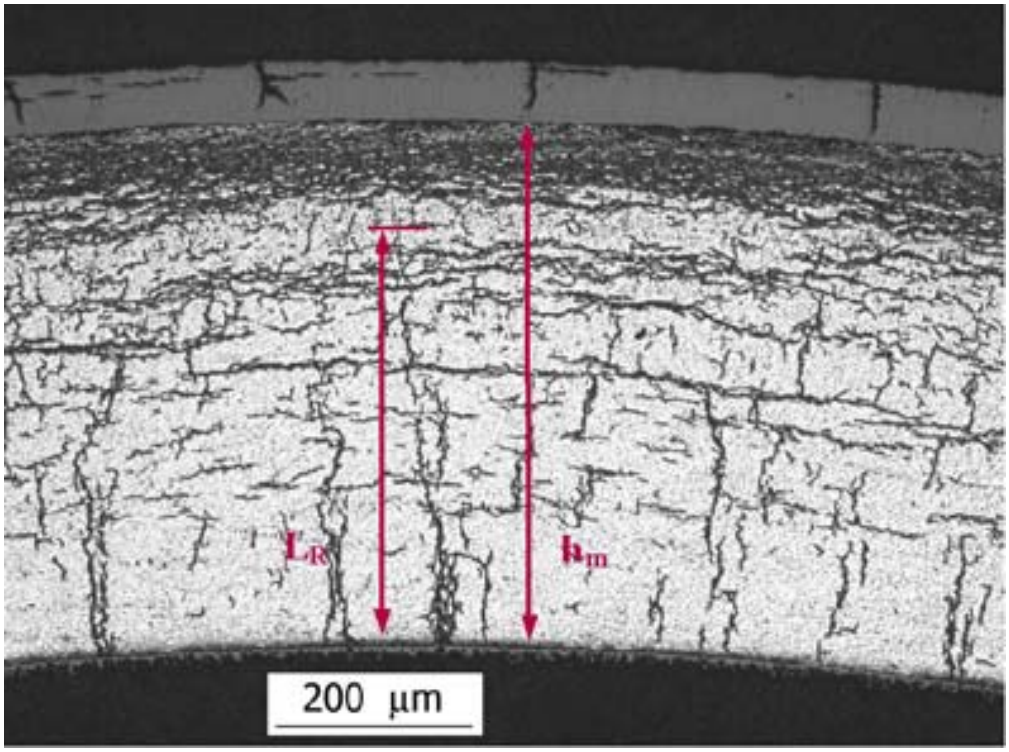

(b)

Figure 31. Hydride distribution and orientation in high-burnup ZIRLO™: (a) as-irradiated baseline with 530 wppm C_H and (b) after RHT at 400°C and 140 MPa with 650 wppm C_H.

Table 7. Summary of strength (P_{max}) and ductility (δ_p/D_{mo}) results for high-burnup ZIRLO™ in the as-irradiated condition (i.e., baseline results) and following RHT. P_{max} was normalized to 8-mm sample length to determine the percentage decrease in maximum load relative to the baseline result (105A9).

Sample ID	Peak RHT T, °C	Peak RHT σ_θ, MPa	RCT T, °C	Reduction in P_{max}, %	Ductility δ_p/D_{mo}, %
105A9	---	---	20	0	7.0
648G5	400	140	150	61	0
648G10	400	140	150	17	1.4
648D3	400	110	30	40	0.6
648D5	400	110	150	9	>9.5
648D8	400	110	150	5	8.6
648D10	400	110	150	6	>9.0

4.3 Comparison for As-Irradiated and RHT High-Burnup Zry-4

Load-displacement curves are given in Refs. 5–6 for high-burnup ZIRLO™ following RHT at peak 400°C hoop stresses of 140 MPa and 110 MPa and slow cooling from 400°C at 5°C/h. Figure 32 shows offset strain vs. RCT test temperature for these two sets of RHT conditions. The DBTT decreased from ≈55°C to <24°C for a decrease in RHT hoop stress from 140 MPa to 110 MPa. However, the gradual increase in ductility with increasing RCT temperature is not typical of a material that undergoes a ductile-to-brittle transition.

Figure 33 compares the load-displacement curve for as-irradiated, high-burnup Zry-4 tested at 23°C to the one for RHT (400°C and 140 MPa hoop stress) high-burnup Zry-4 tested at 30°C. The offset strains and maximum loads are comparable, but the extent of cracking is quite different following the first significant load drop. As shown in Fig. 21, a crack extending ≈40% through the wall was observed after a 27% load drop for as-irradiated, high-burnup Zry-4. Following the 47% load drop shown in Fig. 33, deep cracks (≈90% of the wall) were observed at the 3 and 9 o'clock orientations at the ends of the as-irradiated ring. For the RHT ring, a 90% load drop is indicated in Fig. 33, and deep cracks were observed at the 3 (90%), 6 (50%), and 9 (70%) o'clock orientations at the ring ends.

Figure 34 shows the hydride distribution and orientation in high-burnup Zry-4 in the as-irradiated condition (Fig. 34a) and after RHT at a peak 400°C hoop stress of 140 MPa (Fig. 34b). For radial hydrides in Fig. 34b, they are relatively short and located in positions across the wall such that they may participate in crack propagation but not crack initiation.

Strength and ductility results from RCTs for as-irradiated and RHT high-burnup ZIRLO™ cladding are summarized in Table 8.

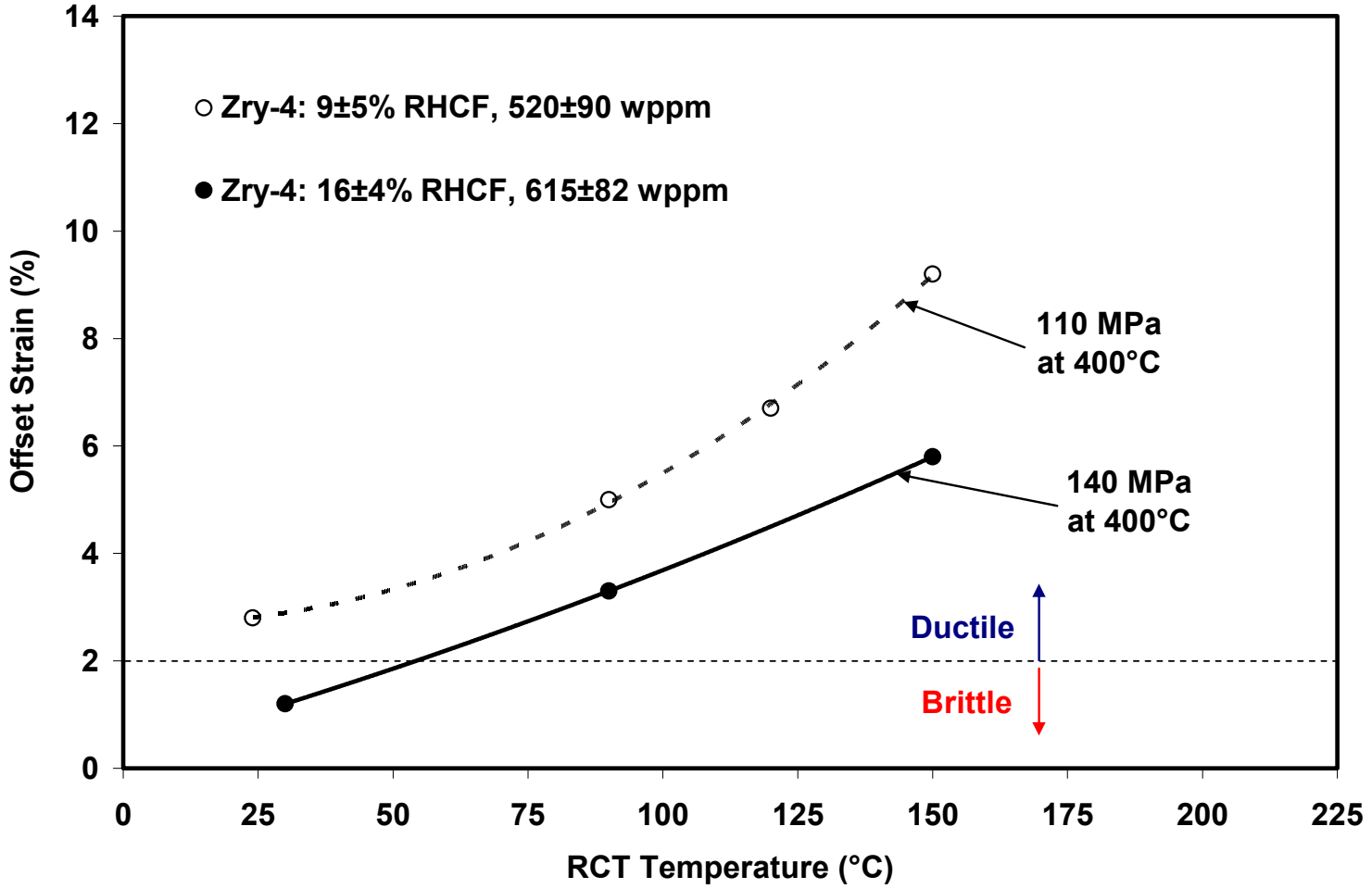

Figure 32. RCT offset strains vs. RCT temperature for high-burnup Zry-4 following RHT at peak 400°C hoop stresses of 140 MPa and 110 MPa. RHCF is the radial-hydride-continuity factor, which increases with RHT hoop stress, and is defined in Refs. 4–7.

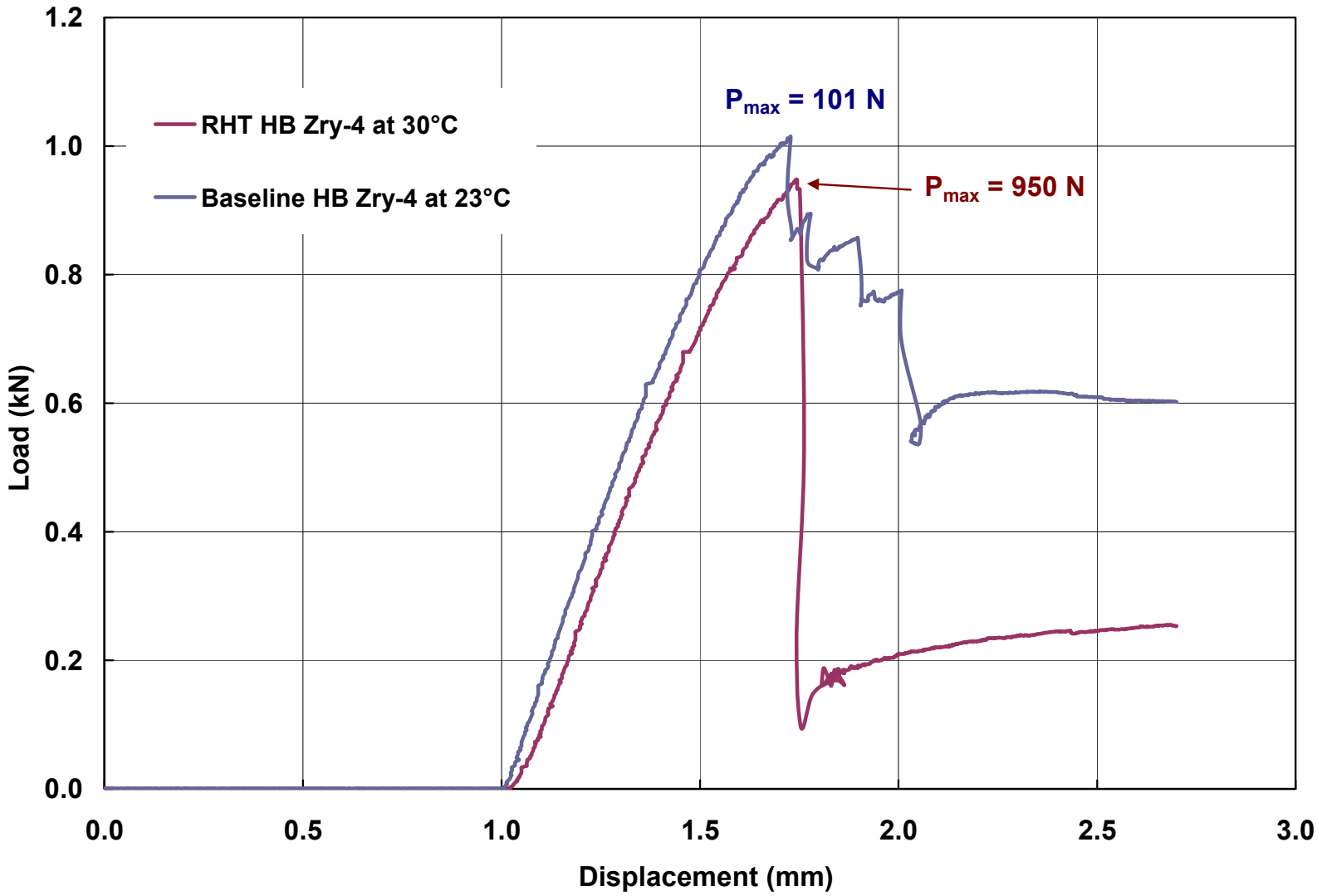

Figure 33. RCT load-displacement curves for high-burnup Zry-4: (a) as-irradiated (i.e., baseline) condition (see Fig. 34a) before drying-storage and tested at 23°C and (b) following RHT at 400°C and 140 MPa (see Fig. 34b) and tested at 30°C.

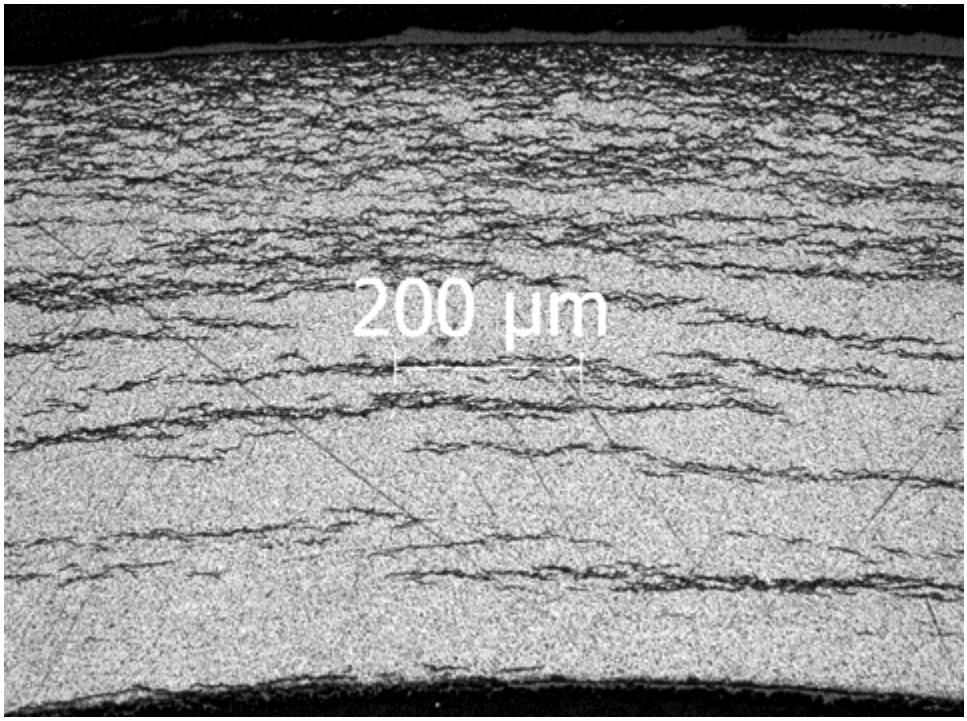

(a)

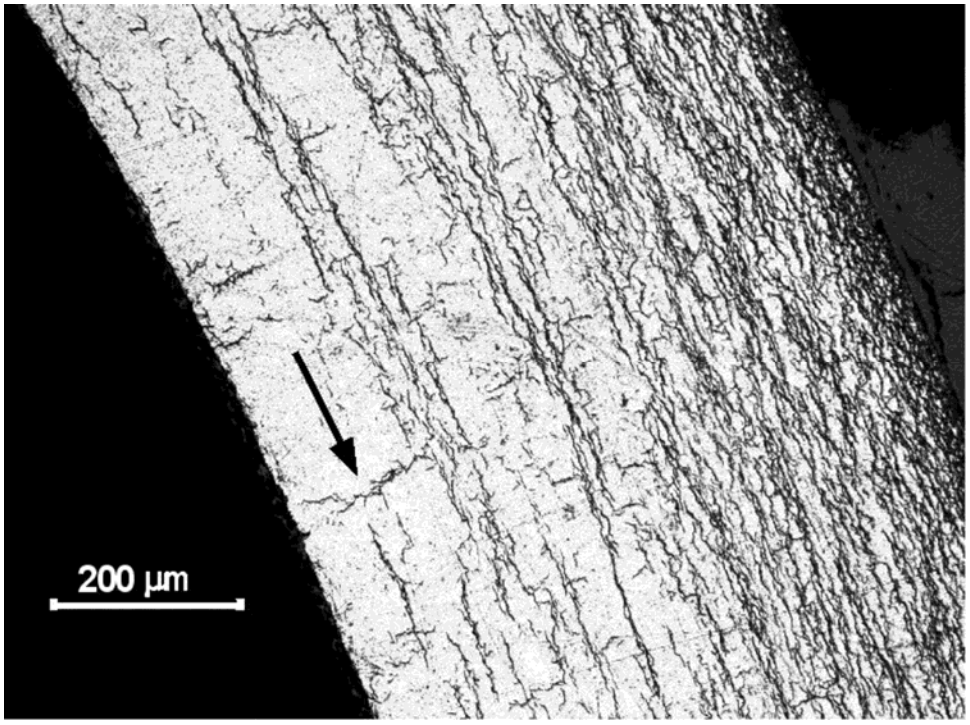

(b)

Figure 34. Hydride distribution and orientation in high-burnup Zry-4: (a) as-irradiated baseline with 640 wppm C_H and (b) after RHT at 400°C and 140 MPa with 615 wppm C_H.

Table 8. Summary of strength (P_{max}) and ductility (δ_p/D_{mo}) results for high-burnup Zry-4 in the as-irradiated condition (i.e., baseline results) and following RHT. P_{max} was normalized to 8-mm sample length to determine the percentage decrease in maximum load relative to the baseline result (606C2J).

Sample ID	Peak RHT T, °C	Peak RHT σ_θ, MPa	RCT T, °C	Reduction in P_{max}, %	Ductility δ_p/D_{mo}, %
606C2J	---	---	23	0	1.5
605C2G	400	140	30	0.9	1.2
605C2F	400	140	90	14	3.3
605C2C	400	140	150	19	5.8
605C6E	400	110	24	6	2.8
605C6C	400	110	90	9	5.0
605C6J	400	110	120	22	6.7
605C6H	400	110	150	14	>9.2

5. DISCUSSION

Baseline characterization and RCT data for as-irradiated, high-burnup M5® indicate high ductility and strength at RT, relatively low strain-rate sensitivity over 1000-fold increase in displacement and elastic strain rates, and low temperature sensitivity within RT to 90°C. The low temperature sensitivity determination was based on strength comparisons of results at RT, 60°C, and 90°C. As none of the as-irradiated M5® rings tested developed cracks, the sensitivity of ductility (i.e., strain before failure) to strain-rate and temperature could not be fully quantified. Relative to high-burnup ZIRLO™ and Zry-4, higher ductility was anticipated for high-burnup M5® because of its lower hydrogen content (<100 wppm) and the sparse distribution of short hydrides. However, quantification of the RT ductility is important because axial and hoop tensile properties and failure limits are not publically available for M5®. Hoop tensile properties and failure limits have been generated for irradiated M5® and documented within the PROMETRA program [12] and other test campaigns. Because the PROMETRA data were generated specifically for Reactivity Insertion Accident (RIA) testing and analysis, emphasis was placed on RIA-relevant temperatures (280–800°C), which are not relevant for longer-term dry-cask storage (RT to <200°C). Also, distribution of documentation is restricted to partners of these programs. AREVA has accumulated a large company-proprietary database for irradiated M5® with testing performed by Argonne, CEA-Saclay, and other labs. If hoop tensile properties and failure limits were available publicly for irradiated M5®, it would be straightforward to incorporate the properties into an FEA or other advanced code. The results of the RCTs could then be used to determine axial tensile properties and degree of anisotropy, as well as to benchmark models in codes for the biaxial stress state in RCT samples. Although primarily hoop stresses are induced by RCT loading, the large ratio of sample length to cladding wall thickness results in axial stresses, which are about 0.37 times the hoop stresses at RT within the elastic deformation regime.

Baseline characterization and RCT data for as-irradiated, high-burnup ZIRLO™ indicate relatively low sensitivity of strength to increasing strain rate and temperature. Ductility exhibited low sensitivity to strain rate over the 1000-fold increase in displacement rate. For the three displacement rates used, the ductility was within the range of 6.5±1.0%. The spread in data was comparable to data scatter for the two tests conducted at 0.05 mm/s (6.7% and 8.8%). Ductility increased with temperature to 10% at 90°C and >11% at 150°C. The ZIRLO™ tested had 530±70 wppm total hydrogen, a well-developed dense hydride rim, and about 140-wppm hydrogen within the inner two-thirds of the cladding. This distribution of hydrogen and hydrides across the cladding wall is very important in anticipating the susceptibility of high-burnup cladding to radial-hydride precipitation and in modeling the behavior and failure limits for high-burnup ZIRLO™. However, as with irradiated M5®, the database for ZIRLO™ is restricted to program participants (e.g., hoop tensile properties in Ref. 12), and test temperatures are generally higher than are relevant for dry-cask storage and transport. The extent of Westinghouse-proprietary mechanical-properties data for ZIRLO™ is unknown.

Baseline characterization and RCT data for as-irradiated, high-burnup Zry-4 revealed a more diffuse hydride rim, a higher concentration of hydrogen (about 250 wppm) within the inner two-thirds of the cladding wall, and relatively low sensitivity of strength to a 1000-fold increase in strain rate and an increase in test temperature from RT to 90°C. The degree of cracking, as determined by number and extent of load-drops, was also insensitive to strain rate and temperature within the range of conditions tested. However, ductility values were too low to assess strain-rate and temperature sensitivity. On the basis of published data for irradiated Zry-4 [1,13], irradiated Zry-4 is expected to be relatively strain-rate insensitive within the range of rates investigated in the current work. However, the high hydrogen content (640±140 wppm) and the more diffuse hydride rim led to simultaneous cracking and plastic flow within the outer half of the cladding wall at low offset strain values. The sensitivity of ductility to strain-rate and temperature could not be assessed from the baseline RCT data generated in the current work.

Baseline RCT properties for as-irradiated, high-burnup M5®, ZIRLO™, and Zry-4 were compared to those generated previously for these alloys following RHT (140 and 110 MPa at 400°C and 5°C/h cooling) to assess degradation in strength and ductility resulting from drying-storage. The degradation is due to the embrittling effects of radial-hydride precipitation during cooling under tensile hoop stresses. It can be severe for test temperatures below the DBTT.

Figures 35 and 36 summarize the status of the RCT databases for RHT high-burnup PWR cladding alloys subjected to a peak drying-storage temperature of 400°C and peak hoop stresses of 140 MPa (Fig. 35) and 110 MPa (Fig. 36). The most extensive data set shown in these figures is for high-burnup ZIRLO™ subjected to a peak 400°C hoop stress of 110 MPa. Tests should be repeated for all other cases to assess data scatter and to better determine the DBTT for these alloys. In particular, the sharp increase in RHT M5® ductility from 60°C to 90°C needs to be verified by future confirmatory tests in this temperature regime. For the RCT, the maximum elastic tensile stresses are concentrated under the load and above the support for the initial point loading. As the displacement increases, the shape of the ring cross section changes from circular to elliptical to elliptical with flattened contact areas below the loading platen and above the support plate. Under point-loading conditions, the maximum tensile hoop stress decreases by 16% at locations ±0.5 mm from the point load. If a crack initiated at the inner-surface location of a shorter radial hydride (e.g., 40% of the wall), it would reduce the stresses in the surrounding areas as it propagated. The load-displacement curve might indicate ductile behavior for such a case. If a crack initiated at the inner-surface location of a longer radial hydride (e.g., 80% of the wall), it would propagate through >50% of the wall. The load-displacement curve might indicate brittle behavior for such a case. Thus, the observed difference in results for the 60°C and 90°C RCTs may be due to sample orientation rather than the 30°C increase in RCT temperature. Figure 37 shows the post-RCT metallographic image for RHT (400°C and 140 MPa) high-burnup M5® ring 645D10. The load-displacement curve for this 90°C RCT exhibited a small load drop (11%) at low offset displacement and a 36% load drop at 6.8% offset strain. Figure 37a shows a low-magnification image of the 60% wall crack and the regions to the left and right of the crack. Although the crack initiated at a particular radial hydride that extended about 60% into the wall, longer radial hydrides were present in the surrounding cladding. If the crack initiated at one of the longer radial hydrides emanating from the inner cladding surface, crack initiation may have occurred at <2% offset strain, and crack growth may have extended through >60% of the wall.

However, before repeat tests are conducted, the effects of lower peak drying-storage temperatures and hoop stresses should be determined. High-burnup ZIRLO™ showed a significant improvement (60°C decrease in DBTT) with the decrease in 400°C hoop stress from 140 MPa to 110 MPa. As indicated in the Argonne Test Plan [7], tests are planned for high-burnup M5® and ZIRLO™ at a peak 400°C hoop stress of 80 MPa, as well as at a peak 400°C hoop stress of 160 MPa for high-burnup Zry-4. Decreasing the peak RHT temperature will result in less dissolved hydrogen available for radial-hydride precipitation. Tests are also planned at a peak drying-storage temperature of 350°C (more realistic than NRC-recommended limit of 400°C) and hoop stresses in the range of 80 to 160 MPa for PWR cladding. Similar testing of BWR cladding (Zry-2) is planned at 400°C and 350°C and hoop stresses in the range of 60–120 MPa. It is more important to conduct these new tests to map out DBTT as a function of drying conditions before repeating tests to more sharply determine DBTT.

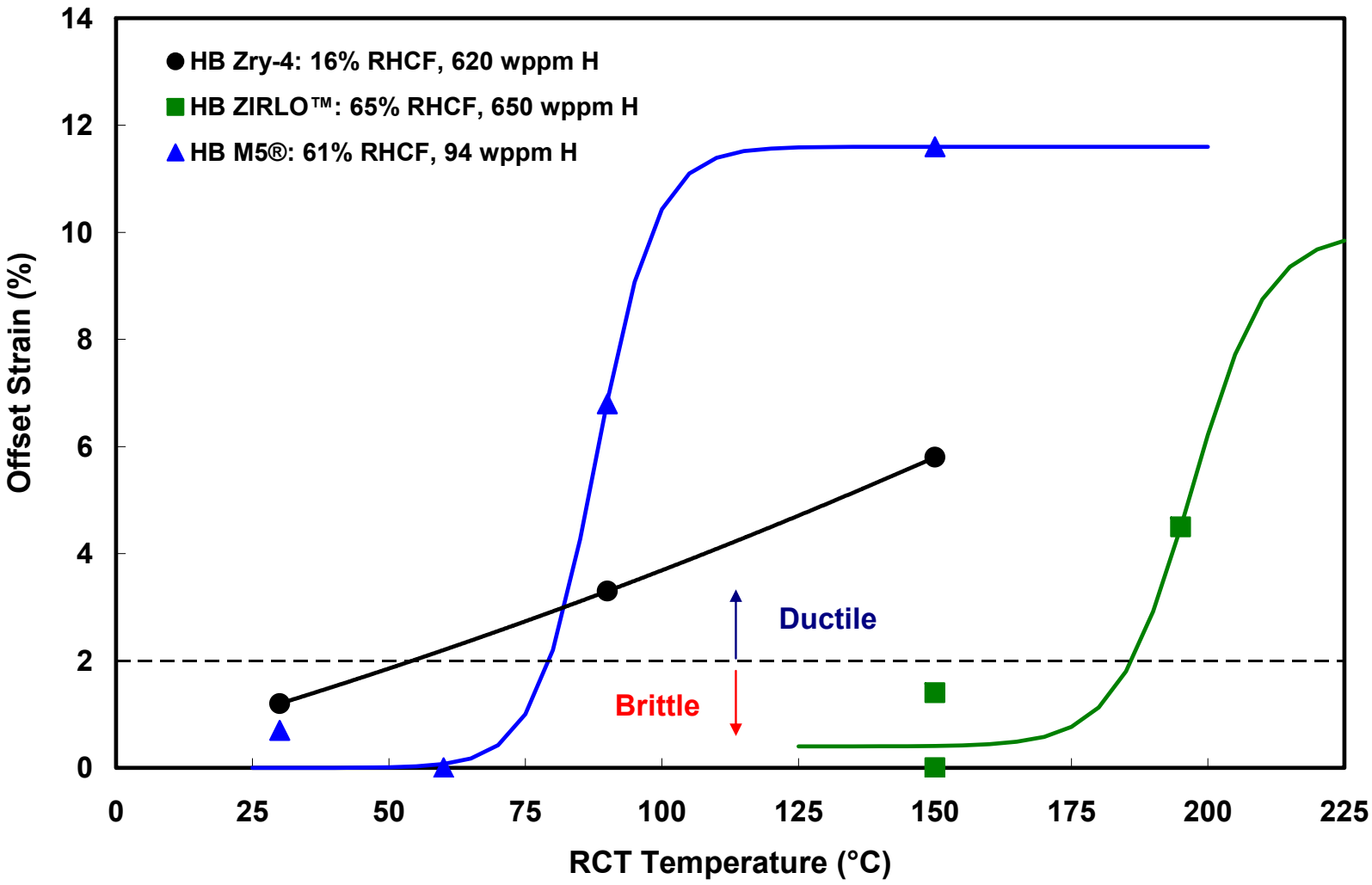

Figure 35. RCT ductility data vs. test temperature for high-burnup (HB) PWR cladding alloys following slow cooling at 5°C/h from 400°C and 140-MPa hoop stress. RHCF is the radial hydride continuity factor.

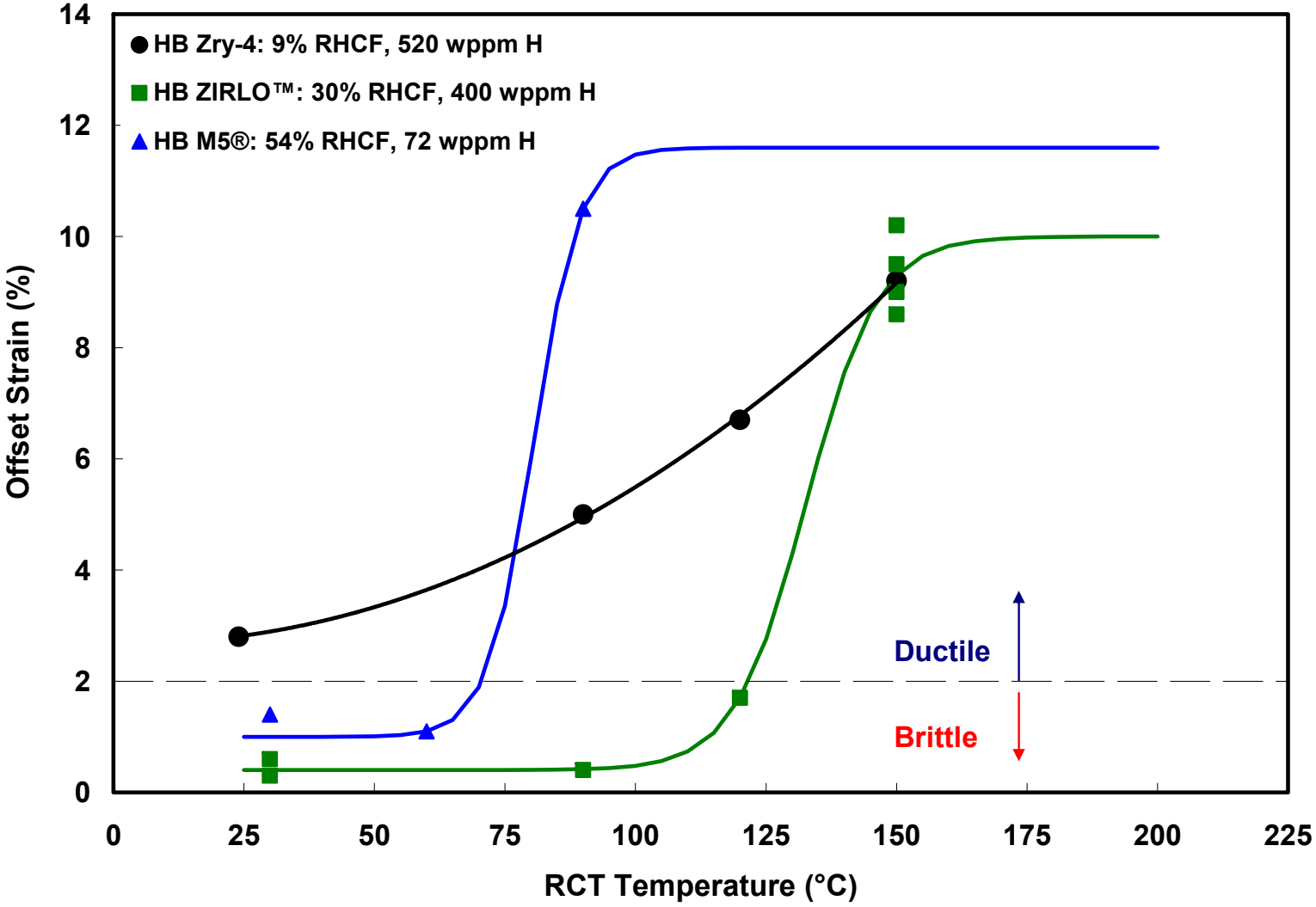

Figure 36. RCT ductility data vs. test temperature for high-burnup (HB) PWR cladding alloys following slow cooling at 5°C/h from 400°C and 110-MPa hoop stress. RHCF is the radial hydride continuity factor.

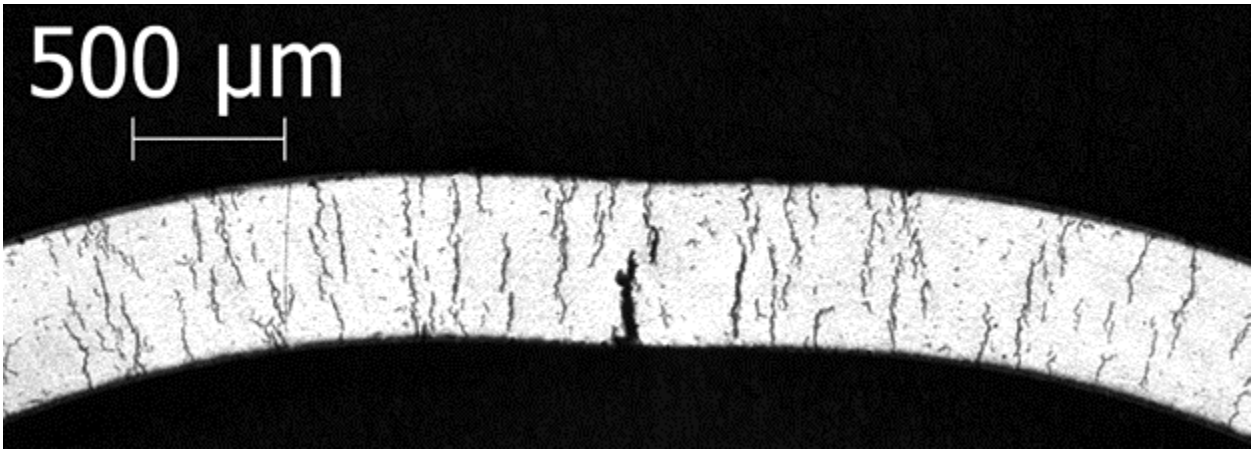

(a)

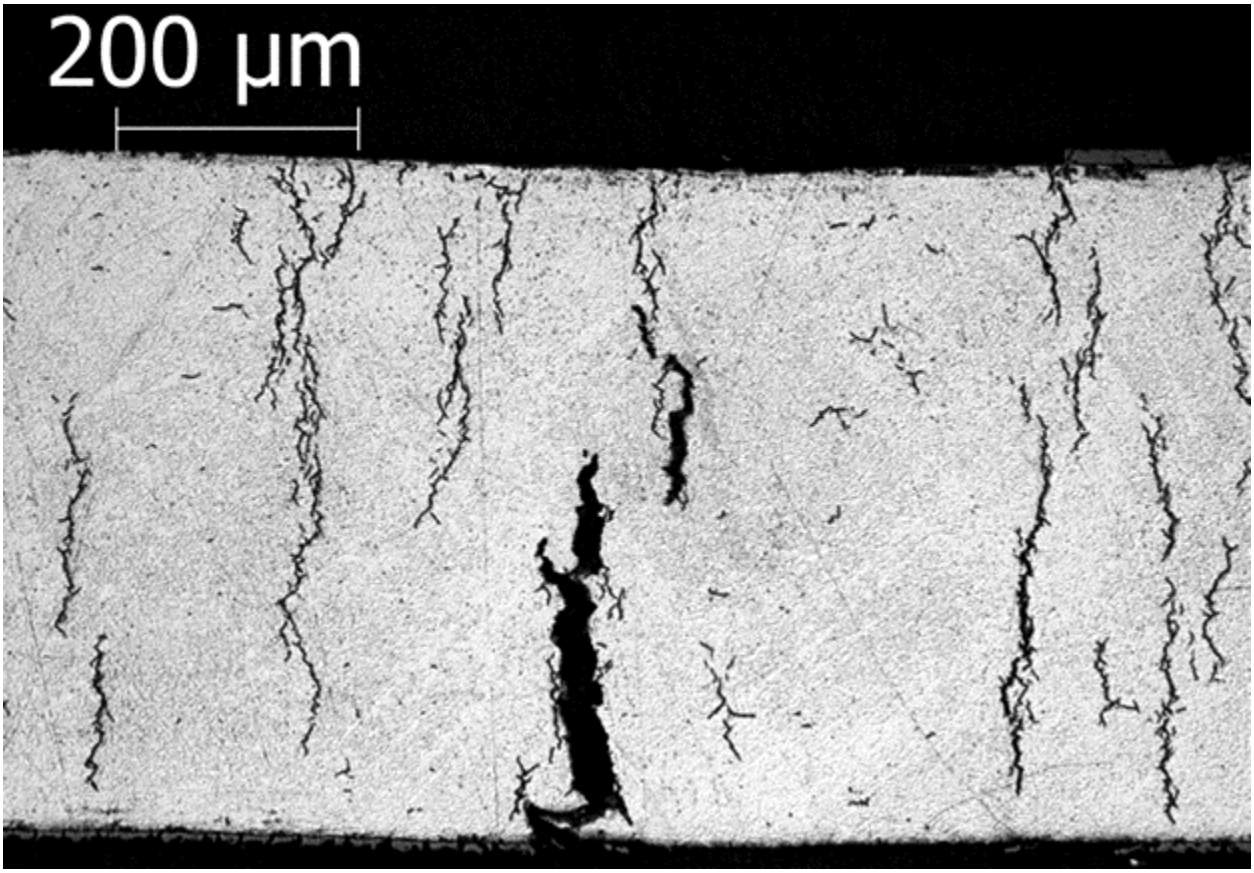

(b)

Figure 37. Post-RCT metallographic images of cracks in RHT (400°C and 140 MPa) high-burnup M5® ring 645D10 tested at 90°C and 5 mm/s: (a) from low-magnification (25X) image and (b) from higher-magnification image (100X).

REFERENCES

[1] K.J. Geelhood, W.G. Lusher, and C.E. Beyer, *PNNL Stress/Strain Correlation for Zircaloy*, PNNL-17700, July 2008.

[2] Nuclear Regulatory Commission 2003 Interim Staff Guidance (ISG)-11, Revision 3, "Cladding Considerations for the Transportation and Storage of Spent Fuel," November 2003. [ML033230335 at http://www.nrc.gov/reading-rm/adams.html]

[3] NRC Public Meeting to Obtain Stakeholder Feedback on Enhancements to the Licensing and Inspection Programs for Spent Fuel Storage and Transportation under 10 CFR Parts 71 and 72, August 16–17, 2012, Rockville, MD. [http://www.nrc.gov/public-involve/conference-symposia/2012-sfst-lic-process-conf.html]

[4] T.A. Burtseva, Y. Yan, and M.C. Billone, "Radial-Hydride-Induced Embrittlement of High-Burnup ZIRLO Cladding Exposed to Simulated Drying Conditions," ANL letter report to NRC, June 20, 2010. [ML101620301 at http://www.nrc.gov/reading-rm/adams/web-based.html]

[5] M.C. Billone, T.A. Burtseva, and Y. Yan, "Ductile-to-Brittle Transition Temperature for High-Burnup Zircaloy-4 and ZIRLO™ Exposed to Simulated Drying-Storage Conditions," ANL Letter Report to NRC, Sept. 28, 2012. Internal ADAMS document ML12181A238 (to be made publically available after NRC review).

[6] M.C. Billone, T.A. Burtseva, and R.E. Einziger, "Ductile-to-brittle transition temperature for high-burnup cladding alloys exposed to simulated drying-storage conditions," J. Nucl. Mat. 433 (2013) 431-448. Available at http://dx.doi.org/10.1016/j.jnucmat.2012.10.002.

[7] M.C. Billone, T.A. Burtseva, J.P. Dobrzynski, D.P. McGann, K. Byrne, Z. Han, and Y.Y. Liu, *Phase I Ring Compression Testing of High-Burnup Cladding*, FCRD-USED-2012-000039, Dec. 31, 2011.

[8] M. Aomi, T. Baba, T. Miyashita, K. Kaminura, T. Yasuda, Y. Shinohara, and T. Takeda, "Evaluation of Hydride Reorientation and Mechanical Properties for High-Burnup Fuel-Cladding Tubes in Interim Dry Storage," J of ASTM Intl, JAI101262 (2008). [Available online at www.astm.org]

[9] M. Billone, Y. Yan, T. Burtseva, and R. Daum, *Cladding Embrittlement during Postulated Loss-of-Coolant Accidents*. NUREG/CR-6967 (2008). [ML082130389 at http://www.nrc.gov/reading-rm/adams.html]

[10] Y. Yan, T.A. Burtseva, and M.C. Billone, "Post-quench Ductility Results for North Anna High-burnup 17×17 ZIRLO Cladding with Intermediate Hydrogen Content," ANL letter Report to NRC, April 17, 2009. [ML091200702 at http://www.nrc.gov/reading-rm/adams.html]

[11] M.C. Billone, *Assessment of Current Test Methods for Post-LOCA Cladding Behavior*, NUREG/CR-7139 (2012). [ML12226A182 at http://www.nrc.gov/reading-rm/adams.html]

[12] J. Desquines, *Release of the PROMETRA V2.5 material database (Zircaloy-4, ZIRLO, M5)*, CABRI Water Loop IRSN 2007-95, SEMCA-2007-318 (2007). In NRC non-public ADAMS as ML073540348.

[13] J. Desquines, B. Cazalis, C. Poussard, X. Averty, and P. Yvon, "Mechanical Properties of Zircaloy-4 PWR Fuel Cladding with Burnup 54-64MWd/kgU and Implications for RIA Behavior," J. ASTM Intl., Paper ID JAI112465 (2005). Available online at www.astm.org.

Appendix A

Load-Displacement Curves for As-Irradiated, High-Burnup M5®

This page intentionally blank.

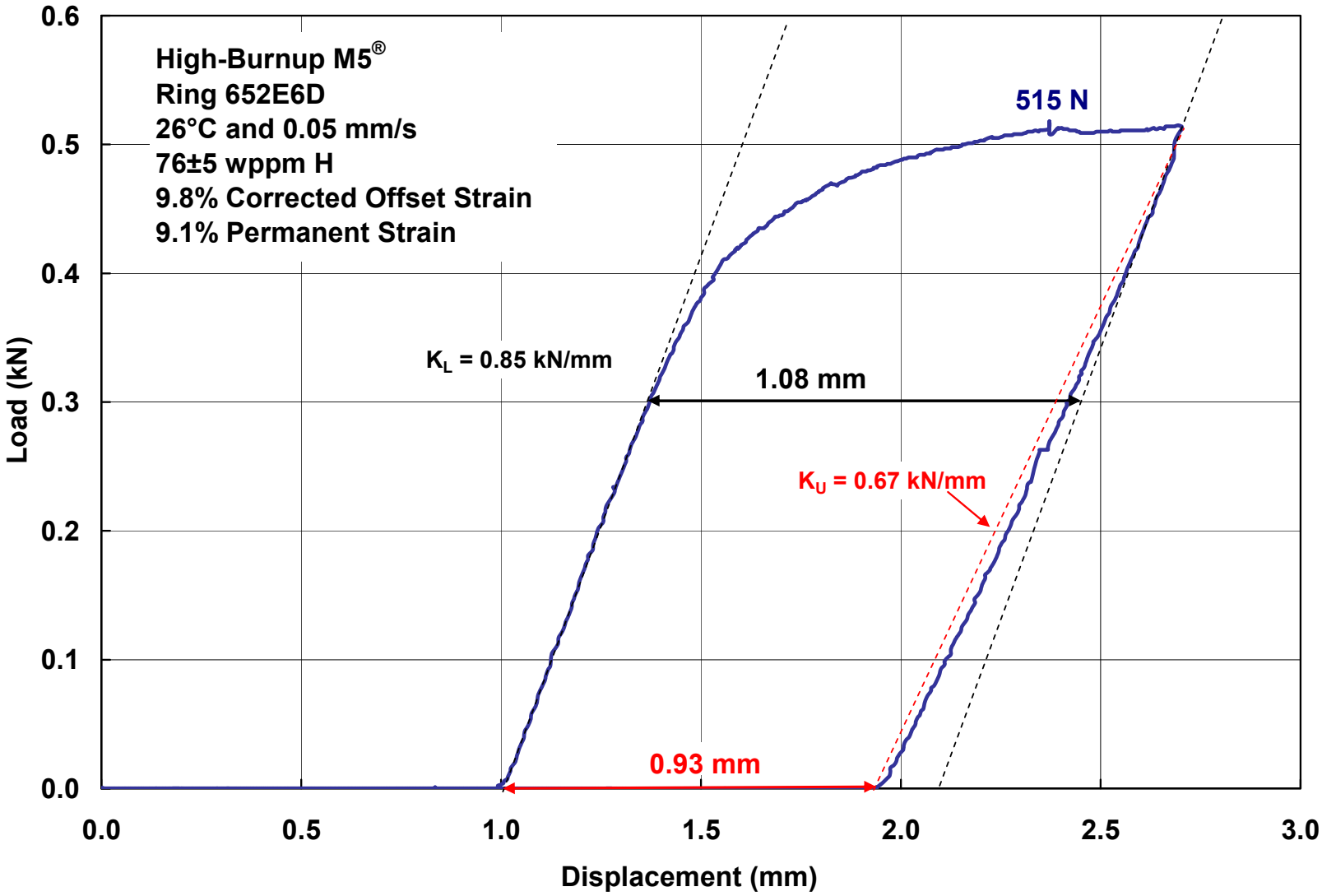

Figure A.1. RCT load-displacement curve for as-irradiated, high-burnup M5® ring 652E6D tested at 26°C and 0.05-mm/s displacement rate.

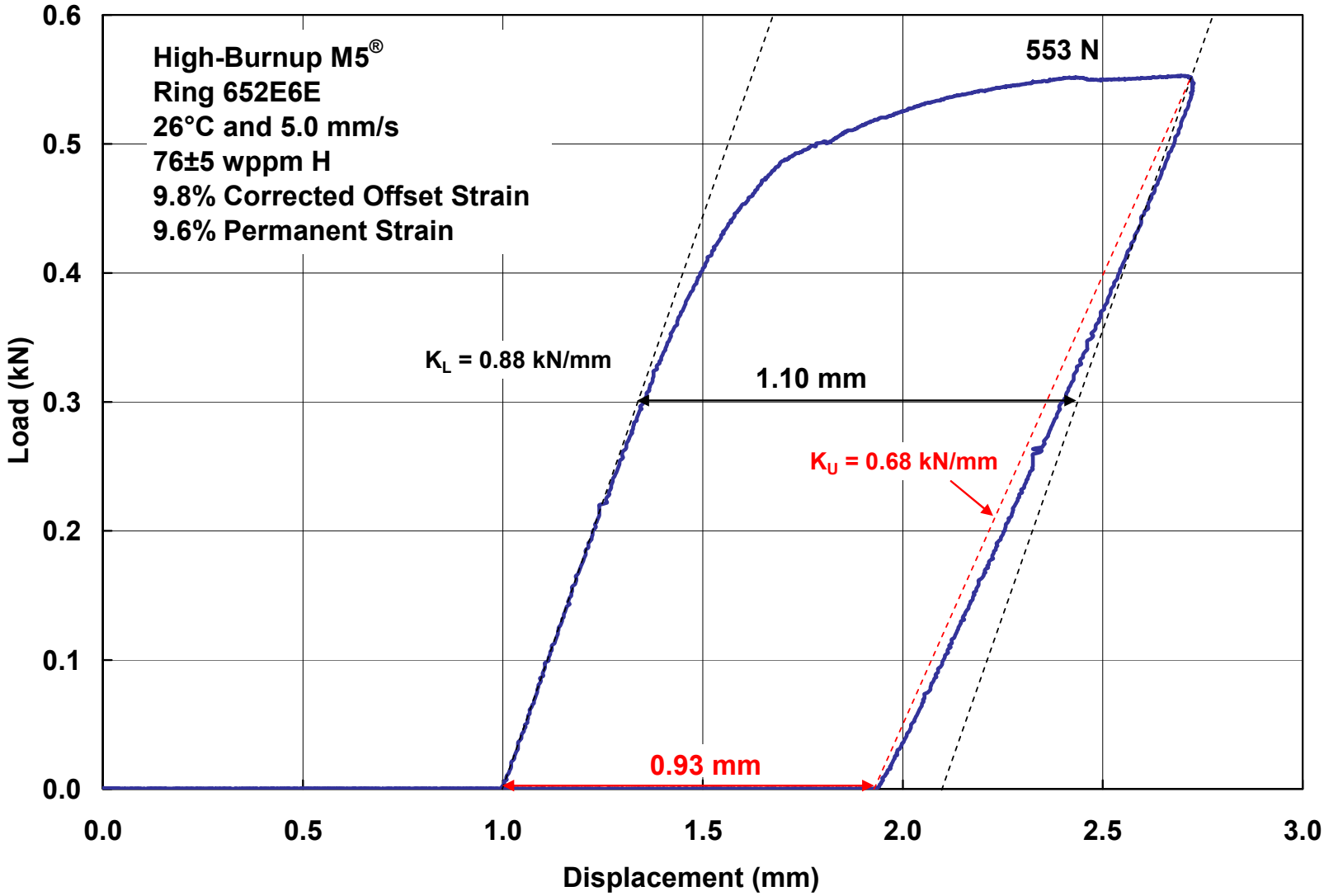

Figure A.2. RCT load-displacement curve for as-irradiated, high-burnup M5® ring 652E6E tested at 26°C and 5-mm/s displacement rate.

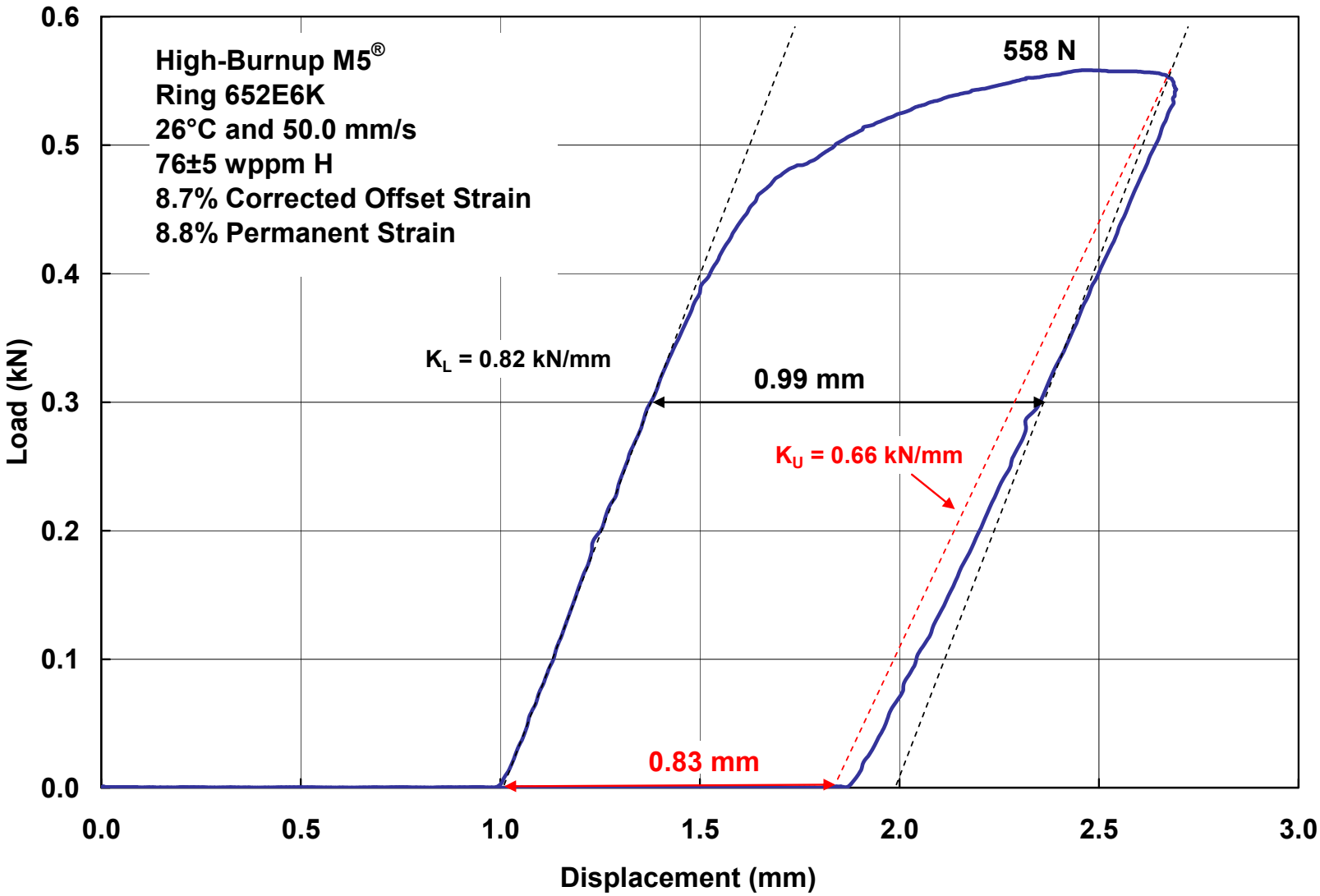

Figure A.3. RCT load-displacement curve for as-irradiated, high-burnup M5® ring 652E6K tested at 26°C and 50-mm/s displacement rate.

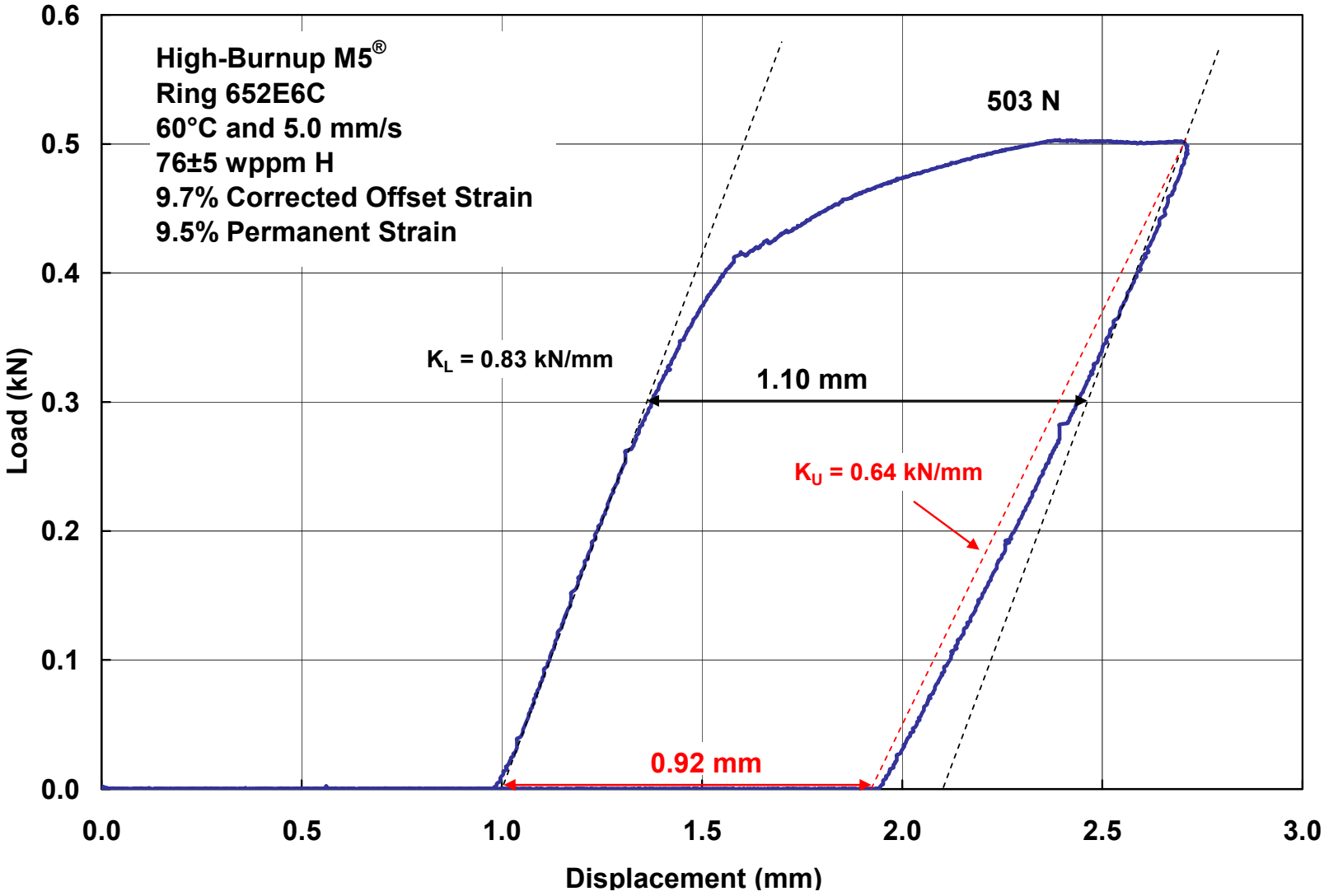

Figure A.4. RCT load-displacement curve for as-irradiated, high-burnup M5® ring 652E6C tested at 60°C and 5-mm/s displacement rate.

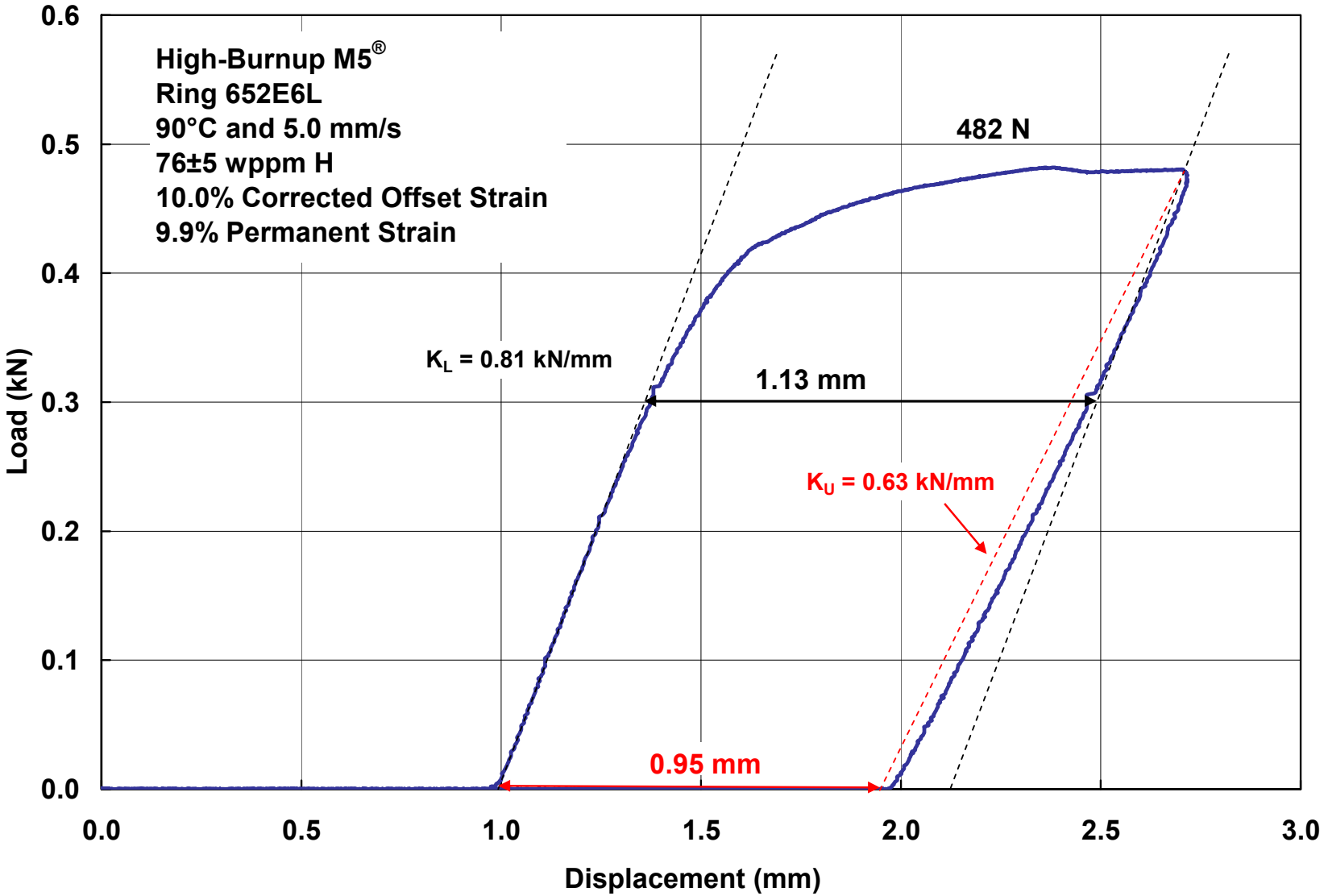

Figure A.5. RCT load-displacement curve for as-irradiated, high-burnup M5® ring 652E6L tested at 90°C and 5-mm/s displacement rate.

This page intentionally blank.

Appendix B

Load-Displacement Curves for As-Irradiated, High-Burnup ZIRLO™

This page intentionally left blank.

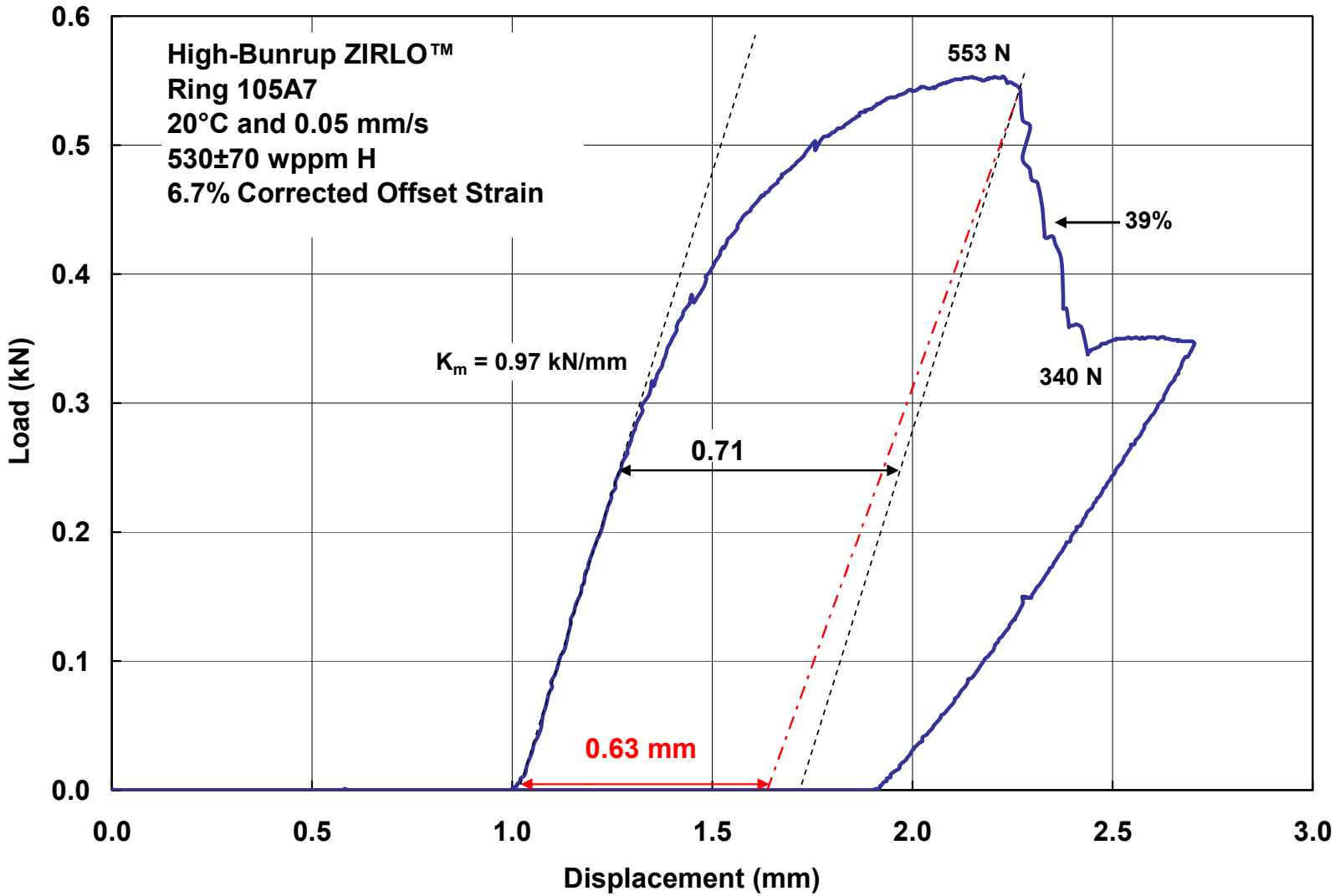

Figure B.1. RCT load-displacement curve for as-irradiated, high-burnup ZIRLO™ ring 105A7 tested at 20°C and 0.05-mm/s displacement rate.

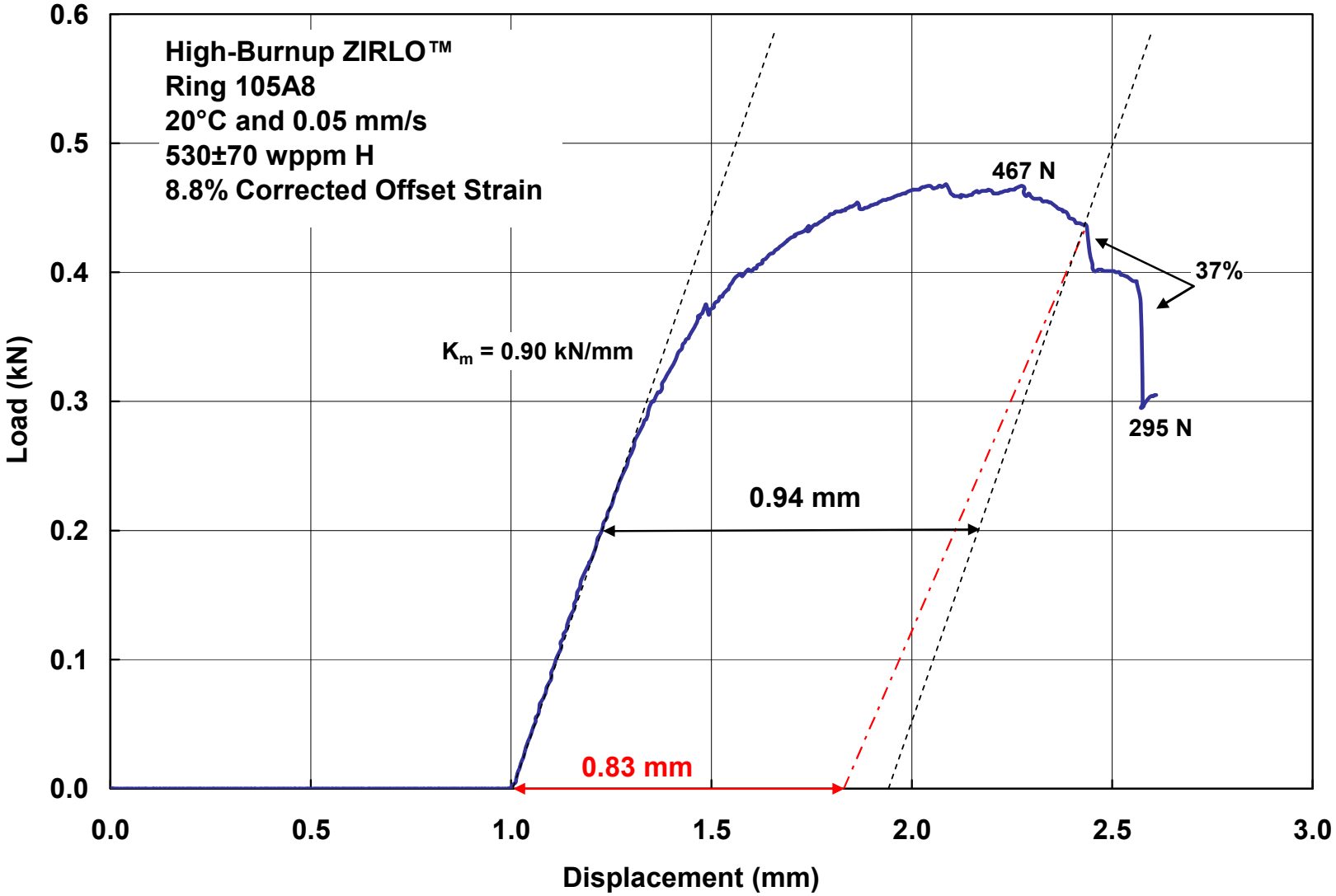

Figure B.2. RCT load-displacement curve for as-irradiated, high-burnup ZIRLO™ ring 105A8 tested at 20°C and 0.05-mm/s displacement rate. The test was terminated after the first significant load drop.

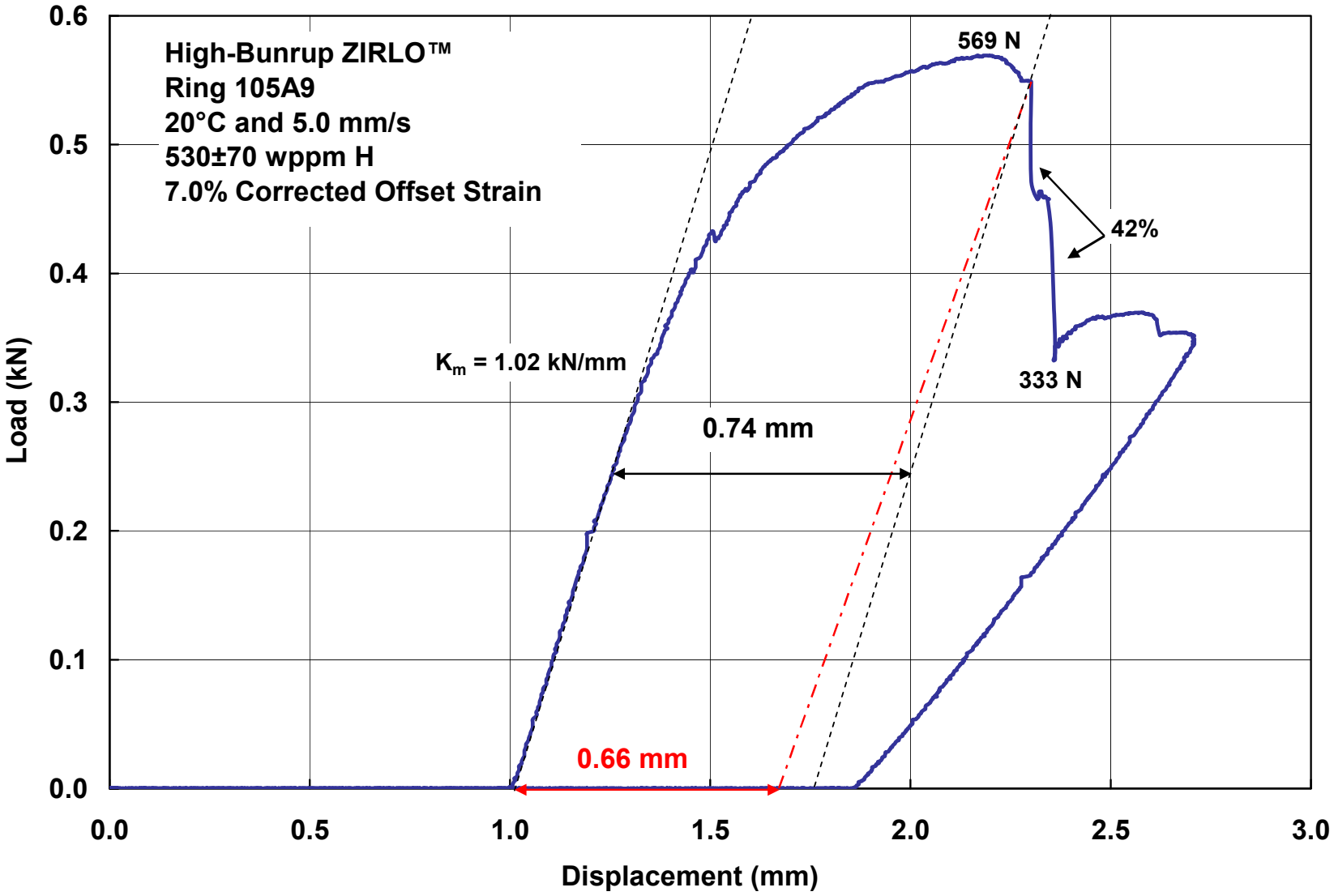

Figure B.3. RCT load-displacement curve for as-irradiated, high-burnup ZIRLO™ ring 105A9 tested at 20°C and 5-mm/s displacement rate.

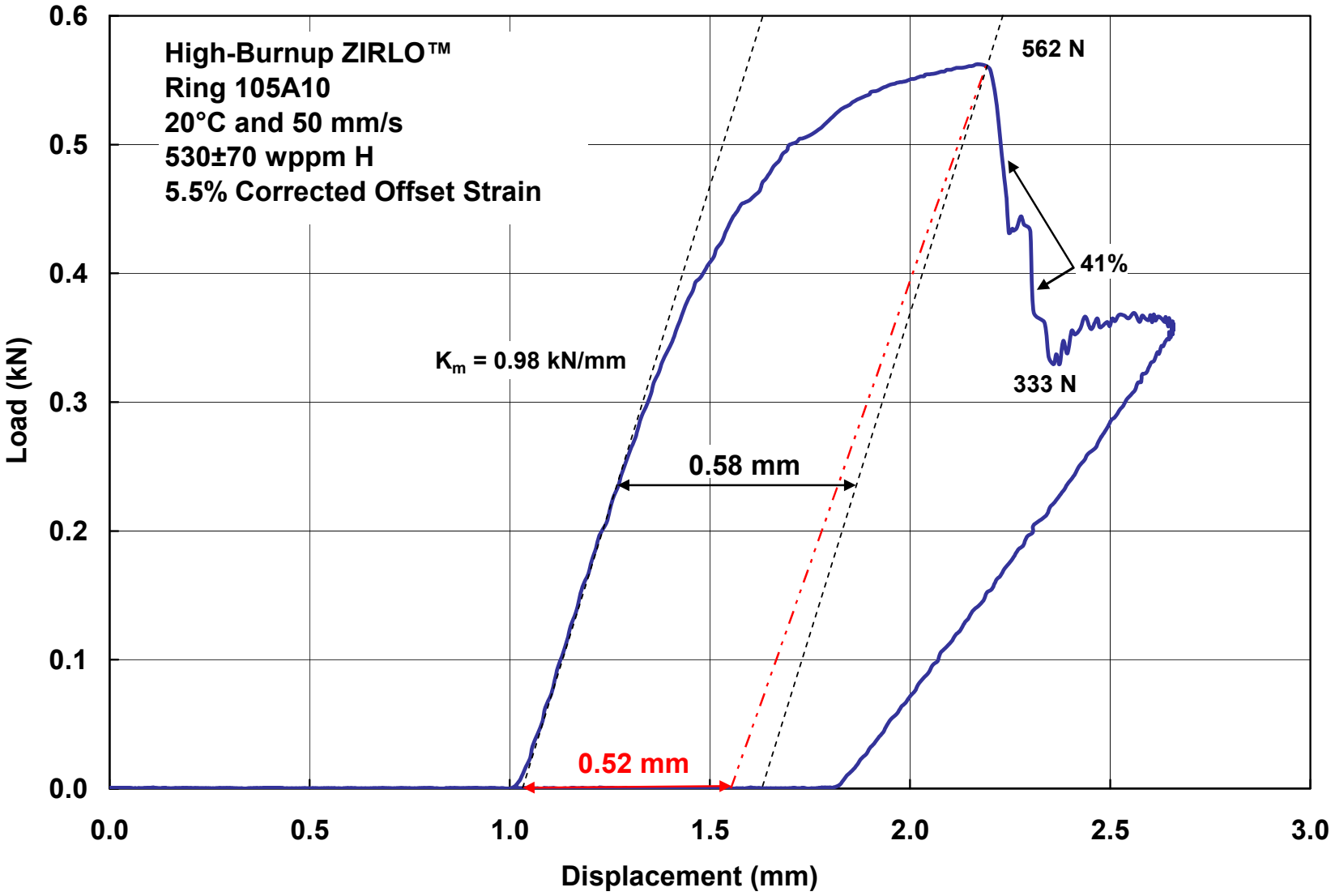

Figure B.4. RCT load-displacement curve for as-irradiated, high-burnup ZIRLO™ ring 105A10 tested at 20°C and 50-mm/s displacement rate.

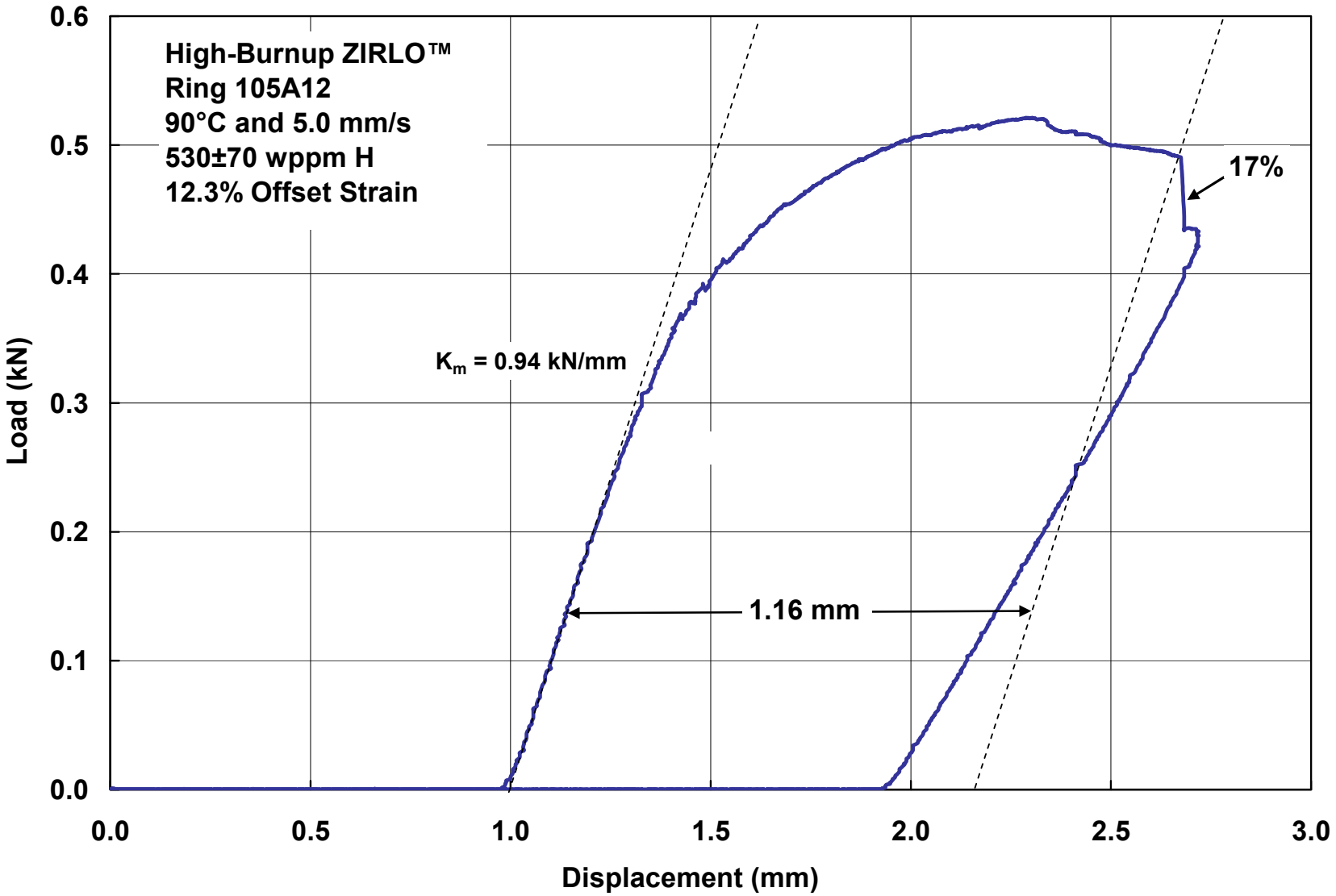

Figure B.5. RCT load-displacement curve for as-irradiated, high-burnup ZIRLO™ ring 105A12 tested at 90°C and 5-mm/s displacement rate.

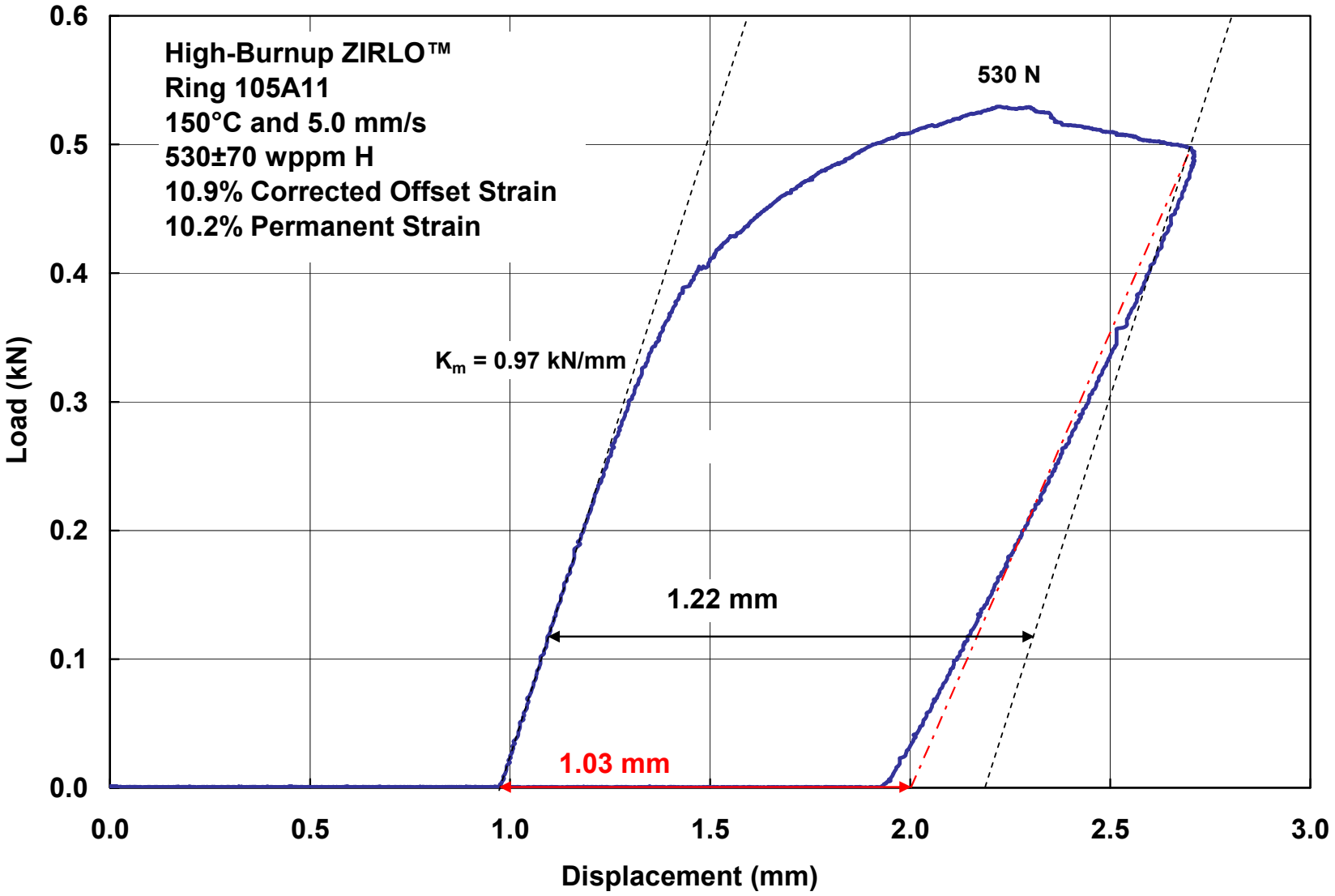

Figure B.6. RCT load-displacement curve for as-irradiated, high-burnup ZIRLO™ ring 105A11 tested at 150°C and 5-mm/s displacement rate.

Appendix C

Load-Displacement Curves for As-Irradiated, High-Burnup Zry-4

This page intentionally blank.

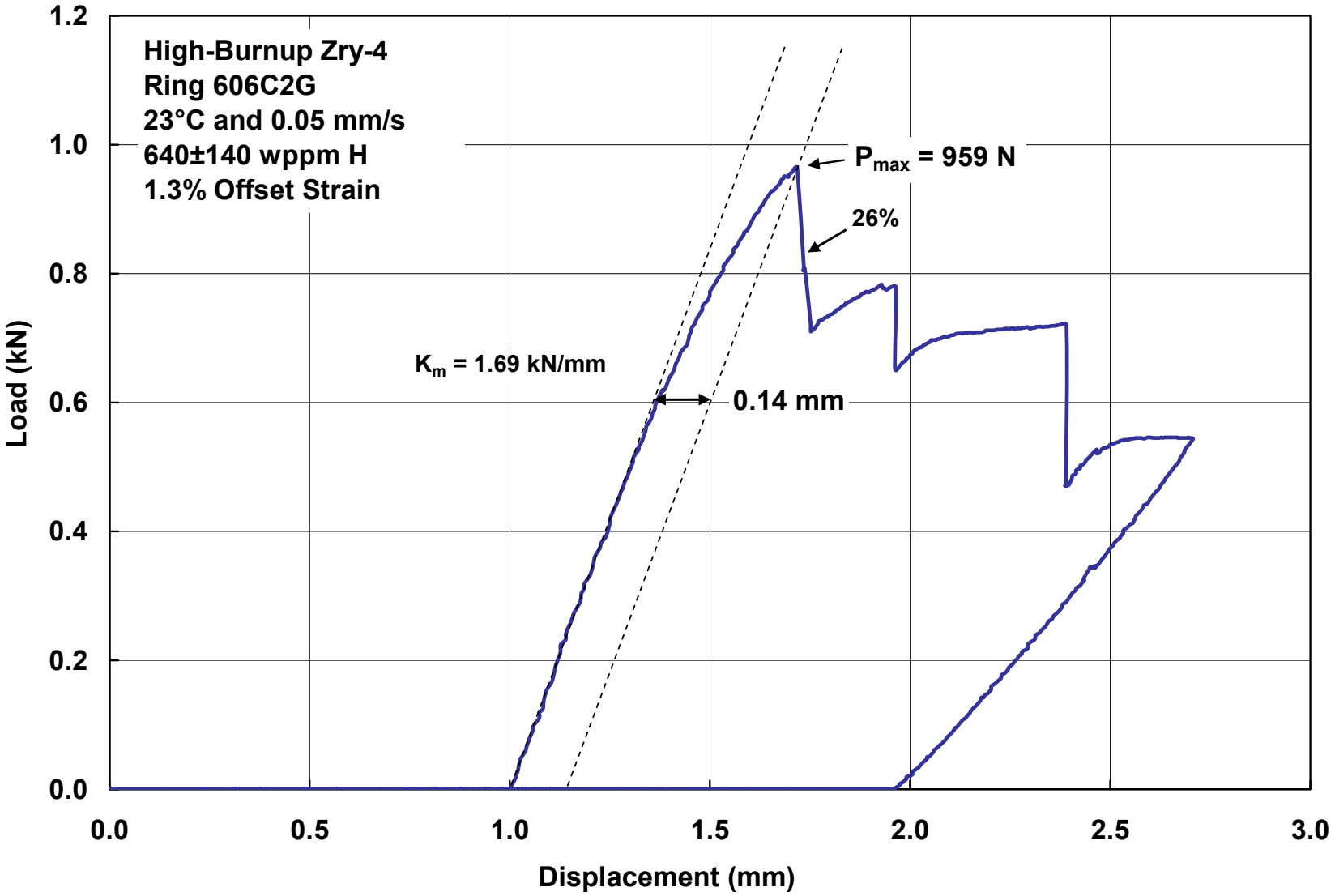

Figure C.1. RCT load-displacement curve for as-irradiated, high-burnup Zry-4 ring 606C2G tested at 23°C and 0.05-mm/s displacement rate.

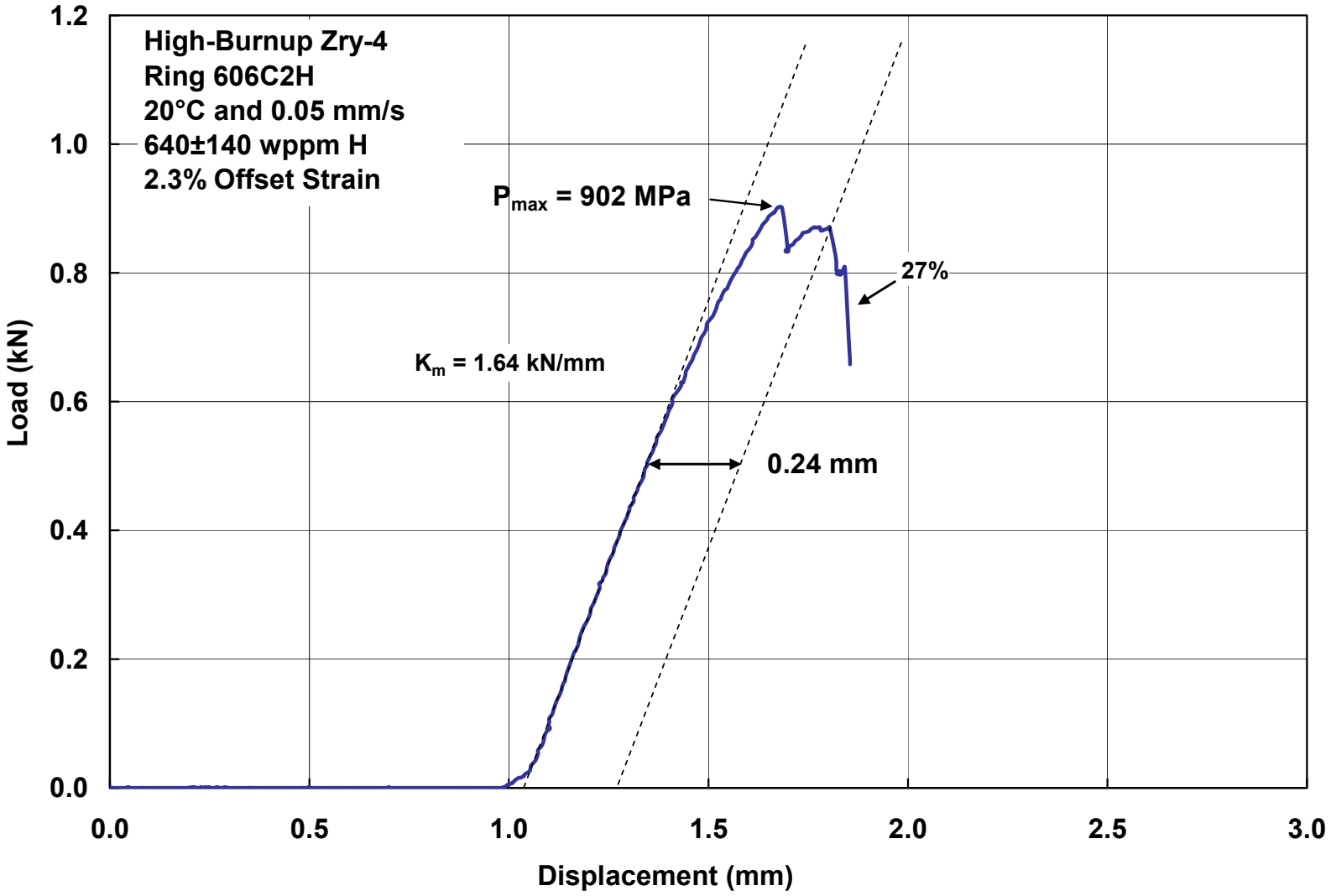

Figure C.2. RCT load-displacement curve for as-irradiated, high-burnup Zry-4 ring 606C2H tested at 20°C and 0.05-mm/s displacement rate. Test was terminated after the first significant load drop.

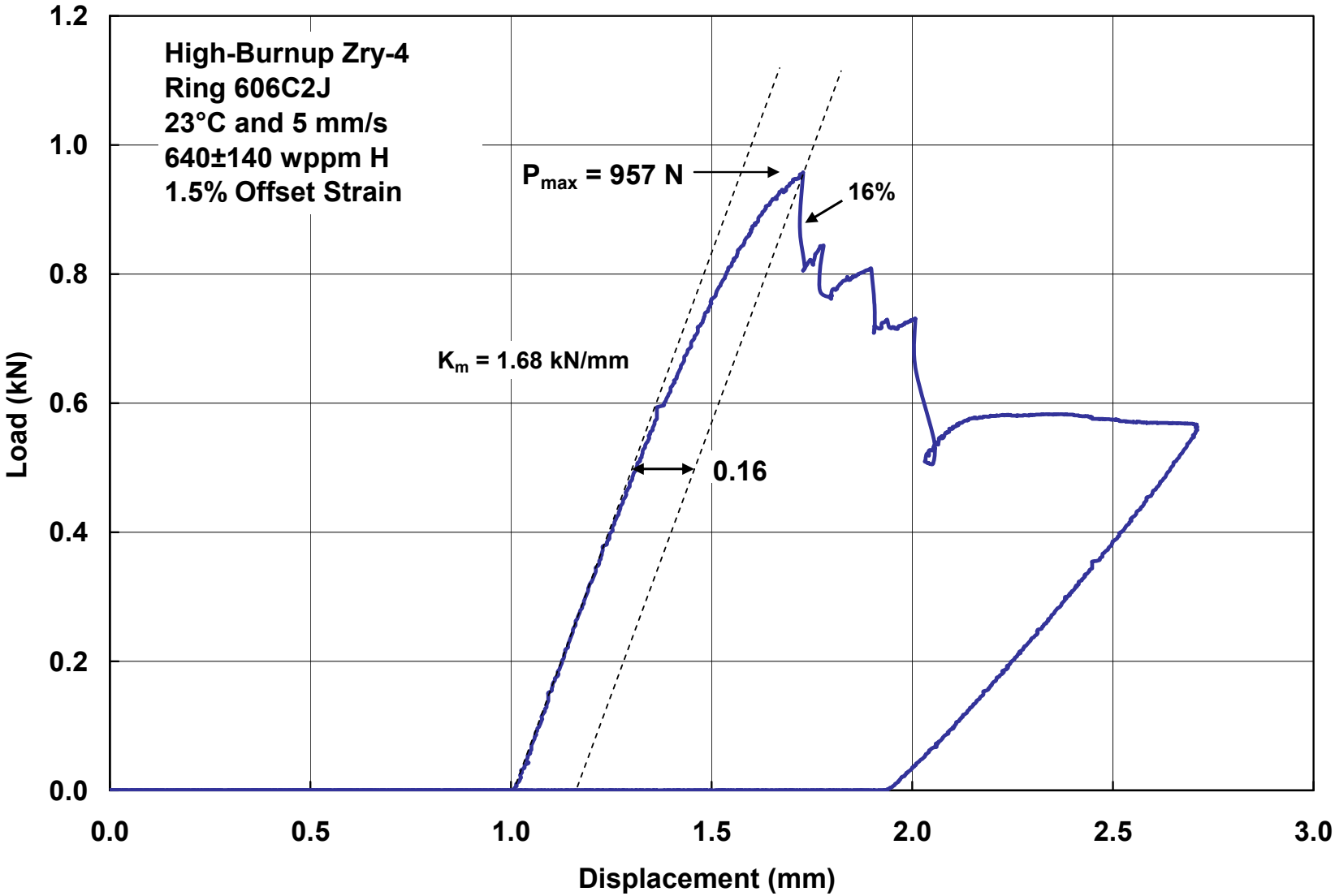

Figure C.3. RCT load-displacement curve for as-irradiated, high-burnup Zry-4 ring 606C2J tested at 23°C and 5-mm/s displacement rate.

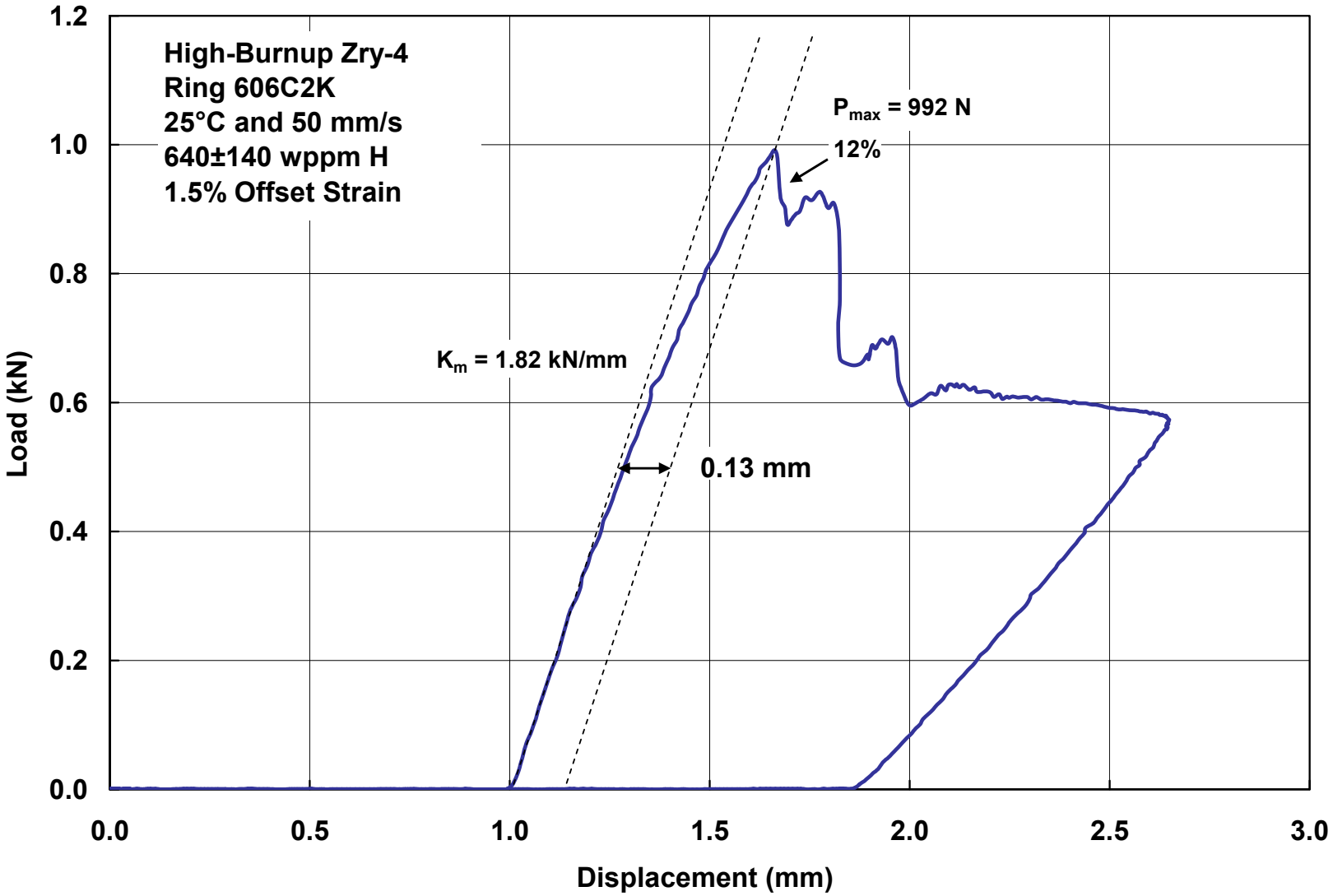

Figure C.4. RCT load-displacement curve for as-irradiated, high-burnup Zry-4 ring 606C2K tested at 25°C and 50-mm/s displacement rate.

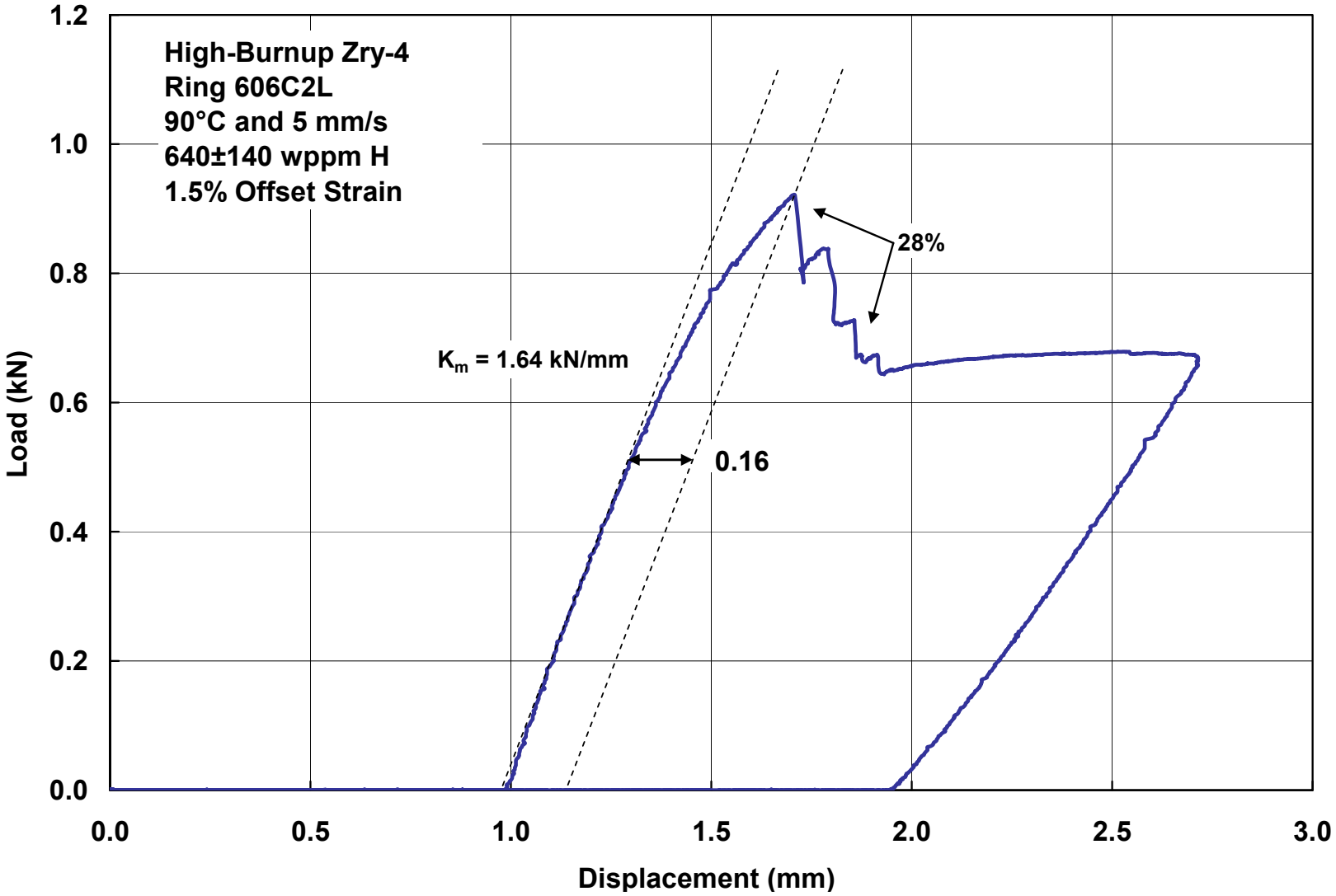

Figure C.5. RCT load-displacement curve for as-irradiated, high-burnup Zry-4 ring 606C2L tested at 90°C and 5-mm/s displacement rate.

Appendix E
FCT Document Cover Sheet

Name/Title of Deliverable/Milestone	*Baseline Studies for Ring Compression Testing of High-Burnup Fuel Cladding*
Work Package Title and Number	ST Storage and Transportation Experiments - ANL
Work Package WBS Number	FT-13AN0805011
Responsible Work Package Manager	Yung Liu (Name/Signature)

Date Submitted 12/07/2012

Quality Rigor Level for Deliverable/Milestone	☐ QRL-3	☒ QRL-2	☐ QRL-1 ☐ Nuclear Data	☐ N/A*

This deliverable was prepared in accordance with Argonne National Laboratory
(Participant/National Laboratory Name)

QA program which meets the requirements of
☒ DOE Order 414.1 ☐ NQA-1-2000

This Deliverable was subjected to:

☒ Technical Review ☐ Peer Review

Technical Review (TR)
Review Documentation Provided
☐ Signed TR Report or,
☐ Signed TR Concurrence Sheet or,
☒ Signature of TR Reviewer(s) below

Peer Review (PR)
Review Documentation Provided
☐ Signed PR Report or,
☐ Signed PR Concurrence Sheet or,
☐ Signature of PR Reviewer(s) below

Name and Signature of Reviewers
Hanchung Tsai

*Note: In some cases there may be a milestone where an item is being fabricated, maintenance is being performed on a facility, or a document is being issued through a formal document control process where it specifically calls out a formal review of the document. In these cases, documentation (e.g., inspection report, maintenance request, work planning package documentation or the documented review of the issued document through the document control process) of the completion of the activity along with the Document Cover Sheet is sufficient to demonstrate achieving the milestone. QRL for such milestones may be also be marked N/A in the work package provided the work package clearly specifies the requirement to use the Document Cover Sheet and provide supporting documentation.